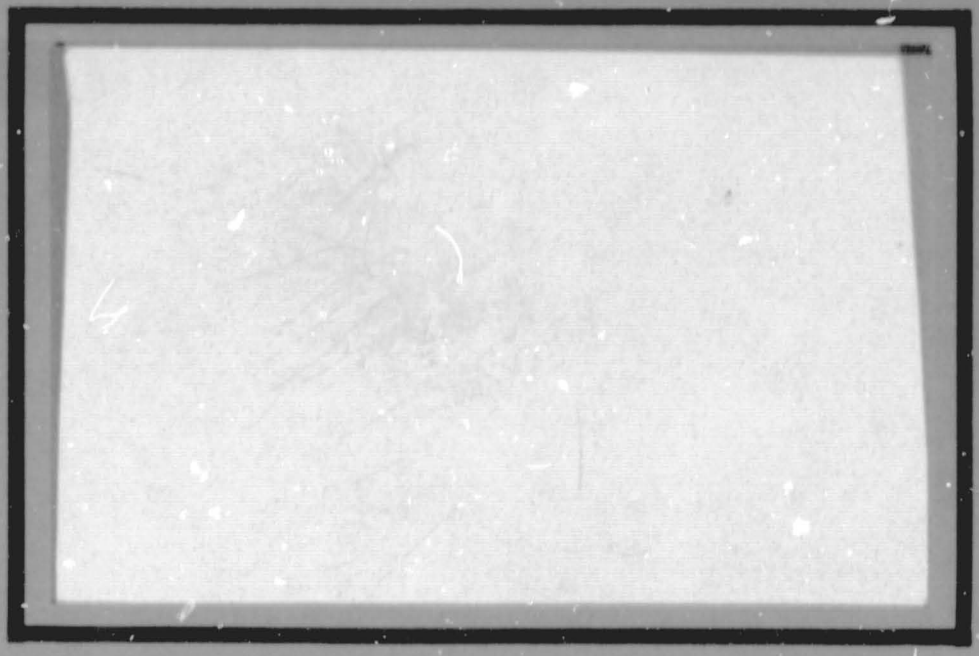

Virginia Polytechnic Institute and State University

Electrical Engineering

BLACKSBURG, VIRGINIA 24061

FINAL REPORT

"Optical Fiber Interferometer for the Study of Ultrasonic Waves in Composite Materials"

NASA Grant NAG-1-68

October 1981

Prepared for: Dr. John H. Cantrell
Grant Monitor
NASA Langley Research Center
Hampton, VA 23665

Prepared by: R. O. Claus
P. S. Zerwekh
T. M. Turner
J. C. Wade
R. T. Rogers
A. O. Garg
Electrical Engineering Department
Virginia Tech
Blacksburg, VA 24061

TABLE OF CONTENTS

SUMMARY

This summary is submitted as the final report for NASA Research Grant NAG-1-68 titled "Optical Fiber Interferometer for the Study of Ultrasonic Waves in Composite Materials." The major part of this report is a collection of published technical articles based upon work supported by this Grant. These articles are divided into sections by topic and included as Appendices.

The primary objective of this Grant, from October 1, 1980 to September 30, 1981, was to investigate the possibility of acoustic emission detection in composites using embedded optical fibers as sensing elements. Optical fiber interferometry, fiber acoustic sensitivity, fiber interferometer calibration, and acoustic emission detection have been reported [1-3, Appendix A]. Additional experimental and analytical research related to this problem are being partially supported by current NASA Grant funding [4].

Related secondary objectives during this grant have included the investigation of adhesive bond layer dynamical properties using ultrasonic interface waves [5-9, Appendix B], the design and construction of an ultrasonic transducer with a two-dimensional Gaussian pressure profile [10, Appendix C], and the development of an optical differential technique for the measurement of surface acoustic wave particle displacements and propagation direction [11-15, Appendix D]. Additional work continues in these areas also.

DISCUSSION

The stated objective of this project has been to study ultrasonic waves in composite materials using optical fiber waveguide as the detecting device. Because we have detected ultrasonic waves inside solids and the bulk modes induced by acoustic emission events in composites, this objective has been attained. The fundamental unstated purpose of this project, however, has been to investigate the possibility of using embedded probes in composites for nondestructive evaluation; this project has clearly not developed a technique for this attractive application. Our current optical interferometric system is sensitive but requires accurate optical positioning at both fiber input and output not easily obtainable in practical field use. Additionally, the frequency response of the fiber geometry including core and cladding center, coating, and jacketing is not known because fiber manufacturers have not measured the bulk properties of these materials.

To take advantage of the positive preliminary results obtained, additional work is required in several areas. Specific recommended projects, grouped according to the topics corresponding to Appendices A through D, are listed below.

OPTICAL FIBER INTERFEROMETRY

1. Fiber frequency response. An analytical model of fiber frequency response based on measurements of fiber material elastic contants should be compared to experimental frequency response results.

2. High frequency acoustic emission data. Useful measurements of acoustic emission cannot be made without the proper equipment. Additional measurements of acoustic emission in composites by fiber interferometry

should be made using a high frequency data acquisition device capable of pre-triggering to capture the entire single shot acoustic event pulses.

3. Optical fiber modulator. It may be possible to modulate transmitted light in an optical fiber by placing two stripped fibers close to each other in a liquid bath and launching ultrasonic waves in the liquid. If the liquid index of refraction varies, the amount of light transmitted from one fiber to the other via crosstalk will change. This may provide a simple method for fiber modulation.

4. Fiber in a differential interferometer. Optical fiber could be used to transmit the light from source to specimen surface in a differential interferometer, thus eliminating the need for a large optical system next to the specimen.

ULTRASONIC INTERFACE WAVES

1. Nonlinear hysteresis theory. Murty has recently developed a model for the nonlinear hysteresis of interface wave velocity during cyclic boundary loading. This theory may be used to predict the velocity behavior noted during measurements performed at NASA/LRC during August 1980. This qualitative agreement should be studied.

2. Embedded interface wave transducer. An interdigital transducer embedded at the boundary between two solid substrates could be theoretically analyzed and experimentally constructed to optimize interface wave generation.

3. Interface wave delay line device. Using embedded IDTs, an interface wave delay line could be modeled and constructed. Such a delay line could be used for the nondestructive evaluation of the boundary between the substrate materials.

GAUSSIAN PROFILE TRANSDUCER

1. Focussing Gaussian transducer. An ultrasonic transducer which focuses to a Gaussian profile spot could be analyzed and constructed.

2. Variable transducer. Using the concentric ring electrode concept, a transducer having a number of electrodes and capable of being switched to obtain different far field patterns could be developed for applications in NDE.

3. Surface inspection using Gaussian profile ultrasonic beams. The far field pattern of a Gaussian field profile transducer is also Gaussian because a transform relationship exists via Fresnel theory between the near and far fields. If the propagating Gaussian field is incident upon a surface which has a reflection coefficient that is a function of position, the received far field pattern will contain the reflection coefficient information. Since the theoretical output field is Gaussian, deconvolution to determine surface structure in NDE applications is straightforward. Such a system for surface analysis could be modeled using operator theory and experimentally investigated.

DUAL DIFFERENTIAL INTERFEROMETER

1. Internal measurements. A dual differential interferometric optical system could be applied to the measurement of 3D acoustic wave fields in transparent solids and liquids.

2. Reconstruction techniques. Computer methods for the reconstruction of 3D fields from differential measurements are necessary.

3. Improved dual channel timing. To improve the dual channel resolution of wave direction and point displacement determination, a sensitive high speed differential timer interfaced directly to the dual channel data acquisition system is necessary.

References

[1] R. O. Claus and J. H. Cantrell, "Detection of Ultrasonic Waves in Solids by an Optical Fiber Interferometer," Proc. 1980 IEEE Ultrasonics Symposium (Boston, MA), Nov. 1980.

[2] R. O. Claus and J. H. Cantrell, "DC Calibration of the Strain Sensitivity of a Single Mode Optical Fiber Interferometer," Proc. 1981 IEEE Region 3 Conf. (Huntsville, AL), April 1981.

[3] J. C. Wade, P. S. Zerwekh, and R. O. Claus, "Detection of Acoustic Emission in Composites by Optical Fiber Inteferometry," Proc. 1981 IEEE Ultrasonics Symposium (Chicago, IL), Oct. 1981.

[4] NASA Grant NAG-1-192, "Acoustooptical Techniques in Ultrasonic Transducer Calibration for Materials Inspection."

[5] R. O. Claus and R. A. Kline, "Pulsed Ultrasonic Leaky Waves on a Titanium-Aluminum Boundary," Acoust. Soc. Am. Annual Meeting (Los Angeles, CA), Nov. 1980; also in J. Acoust. Soc. Am 68, S107 (1980).

[6] T. M. Turner and R. O. Claus, "Pulse-Echo Interface Wave Characterization of Bolted Plates," Proc. 1981 IEEE Region 3 Conf. (Huntsville, AL), April 1981.

[7] R. O. Claus, "Attenuation of Ultrasonic Interface Waves on Metal-Polymer-Metal Boundaries," Seventh International Conference on Internal Friction and Ultrasonic Attenuation in Solids (Lausanne, Switzerland), July 1981.

[8] R. O. Claus, "Characterization of Metal-Polymer Boundaries using Stoneley and Leaky Interface Waves," International Symposium on Physicochemical Aspects of Polymer Surfaces (New York, NY), Aug. 1981.

[9] R. O. Claus and R. T. Rogers, "Waves Guided by a Thim Viscoelastic Layer Between Elastic Solids," Proc. 1981 IEEE Ultrasonics Symposium (Chicago, IL), Oct. 1981.

[10] P. S. Zerwekh and R. O. Claus, "Ultrasonic Transducer with Gaussian Radial Velocity Distribution," Proc. 1981 IEEE Ultrasonics Symposium (Chicago, IL), Oct. 1981.

[11] R. O. Claus and J. H. Cantrell, "Rayleigh Wave Detection by Wideband Differential Interferometry," Acoust. Soc. Am. Annual Meeting (Los Angeles, CA), Nov. 1980; J. Acoust. Soc. Am., 68, S108 (1980).

[12] P. S. Zerwekh and R. O. Claus, "Optical Detection of Pulsed Surface Particle Displacements," Proc. 1981 IEEE Region 3 Conf. (Huntsville, AL), April 1981.

[13] R. O. Claus and J. H. Cantrell, "Wideband Optical Measurements of Ultrasonic Pulses," Ultrasonics International 81 (Brighton, UK), June 1981.

[14] T. M. Turner and R. O. Claus, "Dual Differential Interferometer for Measurements of Broadband Surface Acoustic Waves," Proc. 1981 IEEE Ultrasonics Symposium (Chicago, IL), Oct. 1981.

[15] R. O. Claus and J. H. Cantrell, "Optical Probing of Pulsed Acoustic Surface Waves Using Wideband Differential Interferometry," Acoustics Letters, in press.

APPENDIX A

Optical Fiber Techniques for Ultrasonic Wave Detection

R. O. Claus and J. H. Cantrell, "Detection of Ultrasonic Waves in Solids by an Optical Fiber Interferometer," Proc. 1980 IEEE Ultrasonics Symposium (Boston, MA), Nov. 1980.

DETECTION OF ULTRASONIC WAVES IN SOLIDS BY AN OPTICAL FIBER INTERFEROMETER

Richard O. Claus
Department of Electrical Engineering
Virginia Polytechnic Institute and State University
Blacksburg, Virginia 24061

John H. Cantrell, Jr.
NASA Langley Research Center
Hampton, Virginia 23665

Abstract

An optical fiber interferometer has been developed for the detection of ultrasonic waves in solids. The optical paths in both the signal and reference arms of the Mach-Zehnder interferometer are through the cores of similar lengths of single mode fiber mode stripped at both input and output. Light emerging from the output ends of the reference fiber and a signal fiber which was embedded in a 2.54-cm disc of plastic resin 1.1-cm thick was superimposed to form a straight line interference pattern. Instantaneous translation of the pattern is proportional to the localized strain produced by ultrasonic bulk waves generated in the disc and integrated along the fiber path. By spatially filtering the moving fringe pattern and synchronously demodulating the filtered optical intensity distribution, a signal proportional to the integrated strain is obtained. Direct calibration at dc indicates a minimum theoretical detectable strain of less than 10^{-10}.

1. Introduction

A differential optical interferometer may be constructed using similar lengths of fiber waveguide as the propagation paths in both the reference and sample arms. Such a modified Mach-Zehnder system may be used to measure changes in the difference in phase delay between the two paths. Several authors have investigated potential phase modulation mechanisms in optical fibers. Schlosser analyzed the change in phase delay distortion for a single mode fiber of circular cross section as a function of static elliptical deformation.[1] Davies, Kingsley, and Culshaw later considered phase modulation due to changes in the length, diameter, and refractive index of a fiber subjected to longitudinal mechanical tension,[2] demonstrated a low frequency piezoelectric modulator using a heterodyne optical receiver,[3] and predicted the acoustic sensitivity of both single mode and multimode fiber sensors.[4] In 1977, several authors reported the detection of low frequency acoustic waves in liquids using similarly designed differential fiber interferometers and homodyne optical detection.[5-8]

Since 1977, such interferometers have been developed for use in hydrophones having low noise and high sensitivity. Acoustic sensitivity of typical coiled fiber toroids used in the hydrophones has been calculated for several modeled cases of applied mechanical deformation and has been experimentally measured.[9,10] Recently, increased sensitivity has been obtained by optimally orienting the hydrophone fiber array axis with respect to the direction of propagation of incident longitudinal acoustic waves[11] and by embedding the fiber in a jacket of material with a modulus lower than that of the bare fiber itself.[12-15] Concurrent studies of fiber birefringence modulation effects and multimode fiber interferometer performance suggest additional improvements in acoustic sensitivity.[16-18]

This paper reports the detection of longitudinal and shear ultrasonic waves in solids by fiber interferometry. Increases in sensitivity due to elastic material jacketing, spatial optical filter demodulation, and synchronous heterodyne rf detection have been observed.

2. Fiber Interferometer System

The basic optical system of the fiber interferometer is shown in figure 1. Light from an

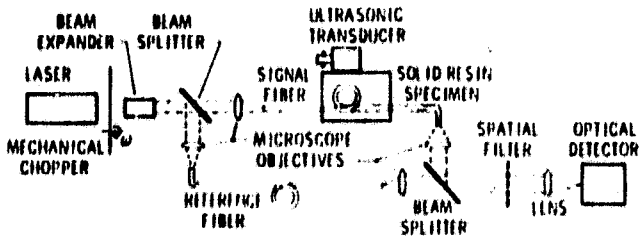

Figure 1 - Basic optical system of single mode fiber interferometer. Interference fringe pattern at output is optically demodulated using a ruled spatial filter, then optically detected and electronically synchronously demodulated using a low frequency reference signal from the rotating chopper.

adaptively stabilized 0.5 mW helium-neon laser source is square wave modulated by a rotating mechanical chopper, expanded, and divided into two beams of equal intensity which are focused using standard 20x microscope objectives onto the input

0090-5607/80/0000-0719 $00.75 © 1980 IEEE

ends of two ITT-110 single mode fibers having nominal 4.5-micron-diameter cores. The exterior fiber jacketing and inner plastic sleeving were removed from the first several centimeters at both ends of both fibers and the exposed cladding was painted with index matching mode stripping fluid. Approximately 0.5 cm of fiber at the ends of the fibers was not painted.

Both optical fibers were nominally 2-m long. The sample fiber was wound into a 100 turn 6-layer toroid having an average diameter of 3.5 cm and embedded in a plastic resin disc 5.1 cm in diameter and 1.4-cm thick. Light from the output of both this sample fiber and the reference fiber was collimated by a second set of identical microscope objectives and superimposed using a second beamsplitter. The resulting straight line interference pattern was spatially filtered with a Ronchi ruling having a periodicity equal to that of the fringe pattern. Finally, the filtered optical signal was focused and synchronously detected.

The amplitude of the ac component of the detected signal is proportional to the instantaneous changes in the difference in phase along the reference and signal fiber paths. Let the laser light have a free space propagation constant k_0 and a single mode propagation constant k inside the fibers of length L, core diameter D, and index of refraction n. The optical phase delay or relative retardation of the light that propagates through both fibers without modulation is

$$\phi_{sample} - \phi_{reference} = kL, \qquad (1)$$

so the resulting output signal is zero.

If the fiber in the sample arm is deformed due to applied stress, the resulting total sample phase delay is

$$\phi_s = kL + k\Delta L + L\Delta k, \qquad (2)$$

and the output signal is proportional to the phase difference

$$\Delta\phi = \phi_s - \phi_r$$

$$= k\Delta L + L\Delta k, \qquad (3)$$

If the applied stress is small,

Equation (3) may be evaluated as

$$\Delta\phi = \frac{P}{E} kL(2\nu - 1) + L\frac{\Delta k}{\Delta n}\Delta n \qquad (4)$$

$$+ L\frac{k}{D}\Delta D,$$

where P is the pressure, E is Young's modulus and ν is Poisson's ratio.[19] For ITT-110 fiber, the change in phase per unit pressure per unit fiber length may be approximated as[19]

$$\left|\frac{\Delta\phi}{PL}\right| = 4 \times 10^{-5} \frac{\text{radians}}{\text{Pa} - \text{m}} \qquad (5)$$

Changes in $\Delta\phi$ cause the fringes at the output of the interferometer to shift. Several authors have measured this fringe shift by scanning the optical intensity distribution using a photomultiplier with a pinhole aperture.[7,9] If instead the interference pattern is interrogated with a straight line spatial filter as shown in figure 1, sensitivity is increased.[20] For example, if the size of the pinhole is one-fourth the width of one fringe in a square pattern of 10 fringes, spatial filtering increases total sensitivity by approximately three orders of magnitude.

To calibrate the interferometer, the differential system shown in figure 2 was used. The

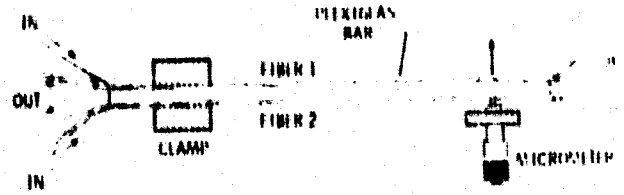

Figure 2 - Cantilever bar geometry used to calibrate dc strain sensitivity. The two fibers are the arms of a differential optical interferometer.[20]

two interferometer layers were doubled back on themselves and glued to opposite sides of a 0.1-cm thick plexiglass bar 6-cm wide and 35-cm long. Clamping one end of the bar and bending it as a cantilever produces tension in one fiber, compression in the other, and a fringe shift at the output. Figure 3 shows the dc strain sensitivity calibration

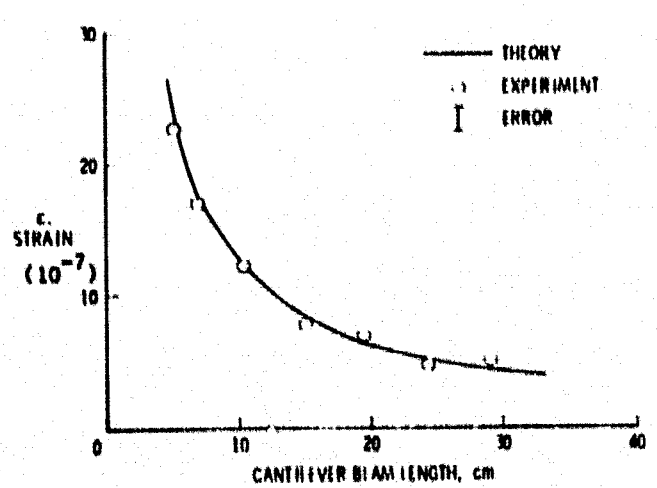

Figure 3 - Differential strain in cantilever bar measured using fiber geometry shown in figure 2.

for this system as a function of bar length. Strain is calculated as $\varepsilon = 3ad/4L^2$, where d is the displacement of the free end of the bar, and a and L are the thickness and length of the bar, respectively. Average experimental strain data agree within 8 percent to the theoretical value in equation (5) and indicate an improvement in the minimum detectable strain to approximately 10^{-10} by spatial filtering.[7,9]

3. Experiment

Pulsed ultrasonic waves were mechanically generated in the solid resin specimen shown in figure 1 using an automatic spring-loaded center-punch. The centerpunch was manually operated; the point being positioned on the flat surface of the disc directly above the center of the embedded fiber toroid. Figure 4 shows the detected optical signal corresponding to a typical pulse broadened due to pathlength integration in the fiber.

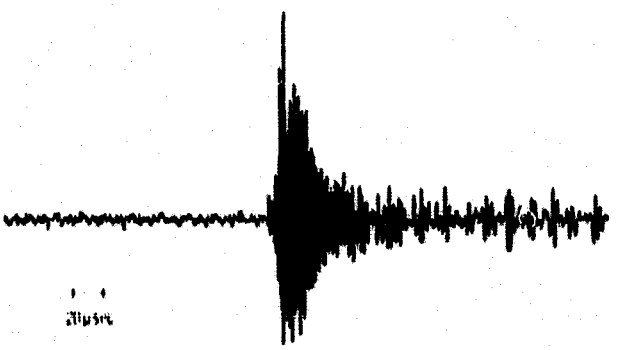

Figure 4 - Ultrasonic wave pulse detected by a coiled optical fiber embedded in a plastic resin disc.

Fourier analysis of the pulse indicates a bandwidth from 29 kHz to 53 kHz and that signal components with frequencies higher than 200 kHz are present. Total bandwidth is limited by the mechanical response of the punch and the coupling characteristic of the fiber-resin boundary. Recent results indicate that similar low frequency ultrasonic pulses may be detected using a single straight birefringent fiber embedded in a low modulus solid. Calibration using a wideband non-contacting technique and use of the fiber interferometer for the detection of acoustic emission in solids is suggested.

4. Acknowledgements

When part of this research was performed, R. O. Claus was a Visiting Scientist at the NASA Langley Research Center. Part of this research has been supported by NASA Grant No. NAG-1-68. The authors thank A. Inge, T. Clark, and M. Terry for their assistance and the ITT Electro-Optics Division for donating fiber.

5. References

1. W. O. Schlosser: "Delay Distortion in Weakly Guiding Optical Fibers Due to Elliptic Deformation at the Boundary," Bell Sys. Tech. J. 51, 487 (1972).
2. D. K. N. Davies and S. Kingsley: "Method of Phase-Modulating Signals in Optical Fibres: Applications to Optical-Telemetry Systems," Elect. Lett. 10, 21 (1974).
3. S. A. Kingsley: "Optical-Fibre Phase Modulator," Elect. Lett. 11, 453 (1975).
4. B. Culshaw, D. K. N. Davies, and S. A. Kingsley: "Acoustic Sensitivity of Optical-Fibre Waveguides," Elect. Lett. 13, 760 (1977).
5. J. H. Cole, R. L. Johnson, and P. G. Bhuta: "Fiber-Optic Detection of Sound," J. Acoust. Soc. Am. 62, 1136 (1977).
6. J. A. Bucaro, H. D. Dardy, and E. F. Carome: "Optical Fiber Acoustic Sensor," Appl. Opt. 16, 1961 (1977).
7. J. A. Bucaro, H. D. Dardy, and E. F. Carome: "Fiber-Optic Hydrophone," J. Acoust. Soc. Am. 62, 1302 (1977).
8. J. A. Bucaro and E. F. Carome: "Single Fiber Interferometric Acoustic Sensor," Appl. Opt. 17, 330 (1978).
9. P. Shajenko, J. P. Flatley and M. B. Moffett: "On Fiber-Optic Hydrophone Sensitivity," J. Acoust. Soc. Am. 64, 1286 (1978).
10. J. A. Bucaro and T. R. Hickman: "Measurement of Sensitivity of Optical Fibers for Acoustic Detection," Appl. Opt. 18, 938 (1979).
11. P. G. Cielo: "Fiber Optic Hydrophone Improved Strain Configuration and Environmental Noise Protection," Appl. Opt. 18, 2933 (1979).
12. G. B. Hocker: "Fiber-Optic Acoustic Sensors with Increased Sensitivity by use of Composite Structures," Opt. Lett. 4, 320 (1979).
13. G. B. Hocker: "Fiber Optic Acoustic Sensors with Composite Structure: An Analysis," Appl. Opt. 18, 3679 (1979).
14. B. Budiansky, D. C. Drucker, G. S. Kino, and J. R. Rice: "Pressure Sensitivity of a Clad Optical Fiber," Appl. Opt. 18, 4085 (1979).
15. R. Hughes and J. Jarzynski: "Static Pressure Sensitivity Amplification in Interferometric Fiber-Optic Hydrophones," Appl. Opt. 19, 98 (1
16. F. P. Kapron, N. F. Borelli, and D. B. Keck: "Birefringence in Dielectric Optical Waveguides," IEEE J. Quant. Elect. QE-8, 222 (1972).
17. A. M. Smith: "Birefringence Induced by Bends and Twists in Single-Mode Optical Fiber," Appl. Opt. 19, 2606 (1980).
18. G. Roychoudhuri: "Multimode Fiber-Optic Interferometry," Appl. Opt. 19, 1901 (1980).
19. G. B. Hocker: "Fiber-Optic Sensing of Pressure and Temperature," Appl. Opt. 18, 1445 (1979).
20. C. B. Palmer, R. O. Claus, and S. L. Fick: "Ultrasonic Wave Measurement by Differential Interferometry," Appl. Opt. 16, 1849 (1977).

R. O. Claus and J. H. Cantrell, "DC Calibration of the Strain Sensitivity of a Single Mode Optical Fiber Interferometer," Proc. 1981 IEEE Region 3 Conf. (Huntsville, AL), April 1981.

DC CALIBRATION OF THE STRAIN SENSITIVITY OF A SINGLE MODE OPTICAL FIBER INTERFEROMETER

RICHARD O. CLAUS
Department of Electrical Engineering
Virginia Polytechnic Institute and State University
Blacksburg, VA 24061

JOHN H. CANTRELL, JR.
NASA Langley Research Center
Hampton, VA 23665

Abstract

The strain sensitivity of an optical fiber interferometer developed for the detection of pulsed ultrasonic waves in solids has been calibrated. The optical paths in both signal and reference arms of the interferometer are through similar 2 m lengths of ITT-110 single mode fibers mode stripped by index matching at both ends and attached to opposite sides of a 30 cm plexiglas bar 0.3 cm thick. Light from the output ends of both fibers was superimposed to form an interference fringe pattern that was interrogated in the far field to give a signal proportional to the differential optical fiber path length. Strain sensitivity was determined by comparing data obtained by clamping and bending the bar at different lengths to simple cantilever beam theory. Calibration indicates a minimum theoretical detectable strain of less than 10^{-10}.

Introduction

A differential optical interferometer may be constructed using similar lengths of fiber waveguide as the propagation paths in both the reference and sample arms. Such a modified Mach-Zehnder system may be used to measure changes in the difference in phase delay distortion for a single mode fiber of circular cross section as a function of static elliptical deformation [1]. Davies, Kingsley, and Culshaw later considered phase modulation due to changes in the length, diameter, and refractive index of a fiber subjected to longitudinal mechanical tension, demonstrated a low frequency piezoelectric modulator using a heterodyne optical receiver, and predicted the acoustic sensitivity of both single mode and multimode fiber sensors [2-4]. In 1977, several authors reported the detection of low frequency acoustic waves in liquids using similarly designed differential fiber interferometers and homodyne optical detection [5-8].

Since 1977, such interferometers have been developed for use in hydrophones having low noise and high sensitivity. Acoustic sensitivity of typical coiled fiber toroids used in the hydrophones has been calculated for several modeled cases of applied mechanical deformation and has been experimentally measured [9,10]. Recently, increased sensitivity has been obtained by optimally orienting the hydrophone fiber array axis with respect to the direction of propagation of incident longitudinal acoustic waves and by embedding the fiber in a jacket of material with a modulus lower than that of the bare fiber itself [11-15]. Concurrent studies of fiber birefringence modulation effects and multimode fiber interferometer performance suggest additional improvements in acoustic sensitivity [16-18].

Experiment

The basic optical system of the fiber interferometer is shown in Figure 1. Light from an adaptively stabilized 0.5 mW helium-neon laser source is square wave modulated by a rotating mechanical chopper, expanded, and divided into two beams of equal intensity which are focused using standard 20x microscope objectives into the input ends of two ITT-110 single mode fibers having nominal 4.5-micron-diameter cores. The exterior fiber jacketing and inner plastic sleeving were removed from the first several centimeters of both ends of both fibers and the exposed cladding was painted with index matching mode stripping fluid. Approximately 0.5 cm of fiber at the ends of the fibers was not painted.

Both optical fibers were nominally 2 m long. The sample fiber was wound into a 100 turn 6-layer toroid having an average diameter of 3.5 cm and embedded in a plastic resin disc 5.1 cm in diameter and 1.4 cm thick. Light from the output of both this sample fiber and the reference fiber was collimated by a second set of identical microscope objectives and superimposed using a second beam-splitter. The resulting straight line interference pattern was spatially filtered with a Ronchi ruling having a periodicity equal to that of the fringe pattern. Finally, the filtered optical signal was focused and synchronously detected.

The amplitude of the ac component of the detected signal is proportional to the instantaneous changes in the difference in phase along the reference and signal fiber paths. Let the laser

IEEE Region 3 Conf. (Huntsville, AL), April, 1981.

light have a free space propagation constant k_o and a single mode propagation constant k inside the fibers of length L, core diameter D, and index of refraction n. The optical phase delay or relative retardation of the light that propagates through both fibers without modulation is

$$\phi_{sample} = \phi_{reference} = kL, \quad (1)$$

so the resulting output signal is zero.

If the fiber in the sample arm is deformed due to applied stress, the resulting total sample phase delay is

$$\phi_s = kL + k\Delta L + L\Delta k, \quad (2)$$

and the output signal is proportional to the phase difference

$$\Delta\phi = \phi_s - \phi_r$$

$$= k\Delta L + L\Delta k, \quad (3)$$

if the applied stress is small.

Equation (3) may be evaluated as

$$\Delta\phi = \frac{P}{E} kL(2\nu - 1) + L\frac{\delta k}{\delta n}\Delta n \quad (4)$$

$$+ L\frac{k}{d}\Delta D,$$

where P is the pressure, E is Young's modulus and ν is Poisson's ratio [10]. For ITT-110 fiber, the change in $\Delta\phi$ in phase per unit pressure per unit fiber length may be approximated as

$$\frac{\Delta\phi}{PL} = 4 \times 10^{-5} \frac{\text{radians}}{\text{Pa} - \text{m}} \quad (5)$$

Changes in $\Delta\phi$ cause the fringes at the output of the interferometer to shift. Several authors have measured this fringe shift by scanning the optical intensity distribution using a photomultiplier with a pinhole aperture [7,9]. If instead the interference pattern is interrogated with a straight line spatial filter as shown in Figure 1, sensitivity is increased [20]. For example, if the size of the pinhole is one-fourth the width of one fringe in a square pattern of 10 fringes, spatial filtering increases total sensitivity by approximately three orders of magnitude.

To calibrate the interferometer, the differential system shown in Figure 2 was used. The two interferometer layers were doubled back on themselves and glued to opposite sides of a 0.3 cm-thick plexiglass bar 6-cm wide and 35-cm long. Clamping one end of the bar and bending it as a cantilever produces tension in one fiber, compression in the other, and a fringe shift at the output. Figure 3 shows the dc strain sensitivity calibration for this system as a function of bar length. Strain is calculated as $\varepsilon = 3da/4L^2$, where d is the displacement of the free end of the bar, and a and L are the thickness and length of the bar, respectively. Average experimental strain data agree within 8 percent to the theoretical value in equation (5) and indicate an improvement in the minimum detectable strain to approximately 10^{-10} by spatial filtering [7,9].

Acknowledgements

When part of this research was performed, R. O. Claus was a Visiting Scientist at the NASA Langley Research Center. Part of this research has been supported by NASA Grant No. NAG-1-6R. The authors wish to thank A. Inge, T. Clark, and M. Turry for their assistance and the ITT Electro-Optics Division for donating fiber.

References

[1] W. O. Schlosser: "Delay Distortion in Weakly Guiding Optical Fibers Due to Elliptic Deformation at the Boundary," Bell Sys. Tech. J. 51, 487 (1972)

[2] D. E. N. Davies and S. Kingsley: "Method of Phase-Modulating Signals in Optical Fibres: Applications to Optical-Telemetry Systems," Elect. Lett. 10, 21, (1974).

[3] S. A. Kingsley: "Optical-Fibre Phase Modulator," Elect. Lett. 11, 453, (1975)

[4] B. Culshaw, D. E. N. Davies, and S. A. Kingsley: "Acoustic Sensitivity of Optical-Fibre-Wave-guides," Elect. Lett. 13, 760 (1977).

[5] J. H. Cole, R. L. Johnson, and P. G. Bhuta: "Fiber-Optic Detection of Sound," J. Acoust. Soc. Am. 62, 1136 (1977).

[6] J. A. Bucaro, H. D. Dardy, and E. F. Carome: "Optical Fiber Acoustic Sensor," Appl. Opt. 16, 1961 (1977)

[7] J. A. Bucaro, H. D Dardy, and E. F. Carome: "Fiber-Optic Hydrophone," J. Acoust. Soc. Am. 62, 1302 (1977).

[8] J. A. Bucaro and E. F. Carome: "Single Fiber Interferometric Acoustic Sensor," Appl. Opt. 17, 330 (1978).

[9] P. Shajenko, J. P. Flatley and M. B. Moffett: "On Fiber-Optic Hydrophone Sensitivity," J. Acoust. Soc. Am. 64, 1286 (1978).

[10] J. A. Bucaro and T. R. Hickman: "Measurement of Sensitivity of Optical Fibers for Acoustic Detection," Appl. Opt. 18, 938 (1979).

[11] P. G. Cielo: "Fiber Optic Hydrophone Improved Strain Configuration and Environmental Noise Protection," Appl. Opt. 18, 2933 (1979).

[12] G. B. Hocker: "Fiber-Optic Acoustic Sensors with Increased Sensitivity by use of Composite Structures," Opt. Lett. 4, 320 (1979).

[13] G. B. Hocker: "Fiber Optic Acoustic Sensors with Composite Structure: An Analysis," Appl. Opt. 18, 3679 (1979).

[14] B. Budiansky, D. C. Drucker, G. S. Kino, and J. R. Rice: "Pressure Sensitivity of a Clad Optical Fiber," Appl. Opt. 18, 4085 (1979).

[15] R. Hughes and J. Jarzynski: "Static Pressure Sensitivity Amplification in Interferometric Fiber-Optic Hydrophones," Appl. Opt. 19, 98 (1980).

[16] F. P. Kapron, N. F. Borelli, and D. B. Keck: Birefringence in Dielectric Optical Waveguides," IEEE J. Quant. Elect. QE-8, 222 (1972).

[17] A. M. Smith: "Birefringence Induced by Bends and Twists in Single-Mode Optical Fiber," Appl. Opt. 19, 2606 (1980).

[18] C. Roychoudhuri: "Multimode Fiber-Optic Interferometry," Appl. Opt. 19, 1903 (1980).

[19] G. B. Hocker: "Fiber-Optic Sensing of Pressure and Temperature," Appl. Opt. 18, 1445 (1979).

[20] C. H. Palmer, R. O. Claus, and S. E. Fick: "Ultrasonic Wave Measurement by Differential Interferometry," Appl. Opt. 16, 1849 (1977).

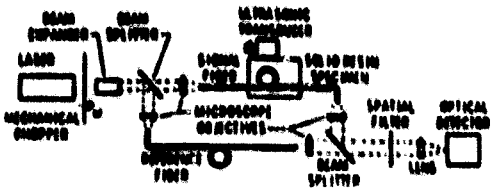

Figure 1. Basic optical interferometer system. By spatially filtering the output interference pattern prior to detection, a gain in sensitivity is achieved.

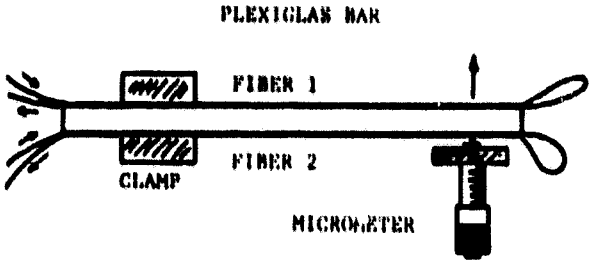

Figure 2. Experimental arrangement used for the dc calibration of the fiber interferometer.

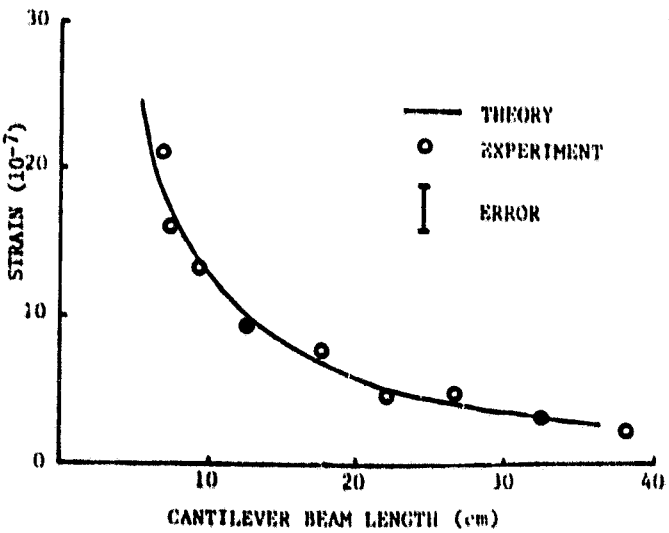

Figure 3. Cantilever beam theoretical and experimental calibration data for fiber interferometer.

J. C. Wade, P. S. Zerwekh, and R. O. Claus, "Detection of Acoustic Emission in Composites by Optical Fiber Inteferometry," Proc. 1981 IEEE Ultrasonics Symposium (Chicago, IL), Oct. 1981.

DETECTION OF ACOUSTIC EMISSION IN COMPOSITES BY OPTICAL FIBER INTERFEROMETRY

JANET C. WADE, PAUL S. ZERWEKH, and RICHARD O. CLAUS

Department of Electrical Engineering
Virginia Polytechnic Institute and State University
Blacksburg, VA 24061

Abstract

Acoustic emission in prestressed composite panels has been detected using embedded single mode optical fibers. Static loading of the composite matrix produces acoustic emission events, pulsed ultrasonic waves, which mechanically modulate the embedded fiber geometry and phase modulate the transmitted optical field. This modulation is detected by optical interferometry and Fourier optical processing techniques to produce an electronic signal proportional to acoustic field amplitude integrated along the length of the fiber in the specimen. Experimental static and dynamic calibration of the detection system is discussed and frequency domain characterization of the acoustic field interaction with the fiber is presented. Potential applications in the nondestructive analysis of structural composites are suggested.

1. Introduction

Optical fiber waveguide has been used as the light transmission path in a Mach-Zehnder interferometer to sense temperature and pressure [1] and to detect low frequency acoustic waves in liquids [2-5] as well as ultrasonic waves in liquids and solids [6]. By embedding an optical fiber within a solid material, such an optical fiber system may be used as an acoustic monitor to directly detect pulsed internal acoustic emission events and slowly varying integrated residual stresses [7-8]. The mechanical resemblence between optical fiber waveguide and the fiber members in a composite matrix suggests that replacing composite fibers with optical fiber sensors may provide a viable method for the nondestructive evaluation of composite materials. Specifically, this suggests a convenient technique for internal measurements in composites using a sensor which is built in during manufacturing.

A modified Mach-Zehnder fiber interferometer is used to measure the changes in the difference in phase delay between two optical fiber paths. As a strain gauge in composites such a fiber system has several advantages over conventional nondestructive evaluation techniques. First, the fiber may be embedded inside the composite so that direct interaction with internal stress fields occurs. Internal fields thus are not inferred from external surface particle displacement and, in addition, surface loading from external devices is eliminated. Second, the technique has a high absolute pressure sensitivity comparable to that of standard Michelson and differential acoustooptic interferometers and greater than those of standard acoustic wave methods. Third, the 10 micron two-dimensional resolution of the interferometer is restricted only by the fiber diameter. The problems of time-bandwidth and spatial resolution associated with pulsed acoustic techniques are not limiting factors. Fourth, the fiber sensing technique may be used for measurements of both high and low frequency CW acoustic fields as well as high frequency stress wave transients of the type associated with acoustic emission events. Finally, absolute calibration of the system may be accomplished [9].

This paper reports the detection of acoustic emission in prestressed graphite-epoxy composite panels using embedded single mode optical fibers and suggests the use of internal fiber probes in the nondestructive evaluation of composites in critical high strength structural applications.

2. Theory

A Mach-Zehnder interferometer has been constructed as shown in Figure 1 using lengths of optical fiber waveguide to transmit the light in the reference and sample arms [2, 10, 11]. If the optical pathlengths in the two fibers are nearly equal, fixed, and less than the coherence length of the common monochromatic input light source, optically heterodyning the output light from the two fibers produces a stationary pattern of concentric interference fringes. If the difference between the optical pathlengths changes, this fringe-pattern is displaced. By spatially filtering the light in the fringe pattern and optically detecting the light transmitted by the filter, an electrical signal related to the pathlength difference $\Delta\ell$ may be obtained [12]. In general, this relationship is a complicated nonlinear function but if the pathlength is small, $\Delta\ell$ is directly proportional to the electrical output signal [1, 9].

Several physical mechanisms may produce a pathlength change in one of the fibers; these mechanisms are responsible for the performance of the fiber interferometer as an acoustic monitor. Let the optical fibers in both the sample and reference arms have length L, core diameter D, and core index of refraction n [1]. If the laser light has a free space propagation constant k_0 and a single mode propagation constant k inside the fiber, then the optical phase delay or relative retardation of

preprint 1981 IEEE Ultrasonics Symposium, Chicago, IL

the light that propagates through both the fibers is

$$\phi_{sample} - \phi_{reference} = kL, \quad (1)$$

and the resulting output signal in Figure 1 is zero. If the fiber in the sample is deformed due to applied stress, a nonzero output signal results. The total sample phase delay is

$$\phi_s = kL + k\Delta L + L\Delta k \quad (2)$$

and the output signal is proportional to the phase difference

$$\Delta\phi = \phi_s - \phi_r = k\Delta L + L\Delta k \quad (3)$$

if the applied stress is small. The effective causes of the optical phase modulation have been investigated by several authors [1, 10-15]. The first term represents the phase modulation produced by varying the length of the sample fiber in the axial direction. The second term represents modulation caused by an effective change in the propagation constant k produced either by the strain optic effect in the fiber material or by optical waveguide mode dispersion. Equation (3) may be evaluated to determine the fiber sensitivity to each of these effects [1].

An acoustic emission event in a composite specimen will modulate the embedded fiber in two ways. First, if the event generates acoustic waves that are perpendicular to the lateral surface of the fiber, the field will compress the fiber, thus altering n and k. An acoustic wave perpendicular to the axial direction of the fiber will cause a change in the fiber length, thus modulating the fiber. In the general case, the acoustic field will occur at an angle that is neither perpendicular to the axial or lateral surfaces so the modulation will be a combination of these two effects. Additionally, the acoustic field will generate an uneven pressure distribution along the fiber that is spatially dependent upon the angle measured from the radius of the source to the fiber. Several authors have analyzed this dependence for a remote linear source and have found that it produces the same sound pressure on the surface at the azimuthal angle as an indentical source having the same velocity and being located at the surface of the cylinder at the same angle [16-18]. Because the output of the sample arm is effectively the result of the integrated strain along the entire length of the sample, we assume that Equation (3) may still be applied to the system.

The adhesion of the embedded optical fiber to the composite matrix as well as to the jacketing material around the fiber will influence the performance of the interferometer as an acoustic monitor. The elastic material jacket is deformed during applied stresses which increases the overall sensitivity; however, the coupling characteristics of the fiber-resin boundry limit the bandwidth response of the interferometer [6].

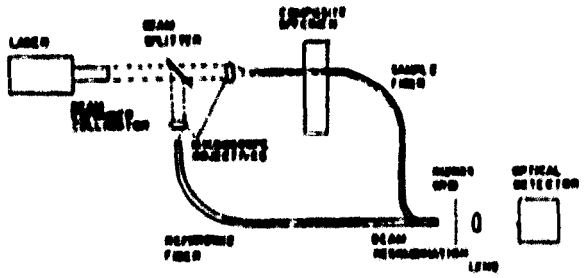

Fig. 1 Basic optical system of single mode fiber interferometer. Interference fringe pattern at output is optically demodulated using a ruled spatial filter, then optically detected and electronically synchronously detected.

3. Experiment

The basic optical system described above was constructed as shown in Figure 1. Light from an adaptively stabalized 0.5 mW helium-neon laser source is collimated, expanded, focused, and divided into two beams which are focused using standard 10X microscope objectives onto the input ends of two ITT-110 single mode fibers having nominal 4.5-micron-diameter cores. The external plastic jacketing and inner RTV sleeving were removed from the first several centimeters of both ends of both fibers, and approximately cm of exposed fiber was painted with index matching mode stripping fluid.

Both optical fibers were nominally 1 m long. The sample fiber was attached to the specimen using several different techniques which are shown in Figure 2. In Figure 2a the fiber is shown adhesively bonded to the surface of a prestressed graphite-epoxy composite specimen bar. The orientation of the fiber is perpendicular to the length of the bar to eliminate integrated dc strain due to loading; however, since acoustic emission event location is not known, this geometry does not permit optimal pulse wave detection. A piezoelectric transducer was placed beside the fiber for comparison measurements. The specimen was clamped at one end and a load force was applied at the other end, bending the bar and inducing acoustic emission due to fiber breakage and layer delamination. Figure 2b shows the fiber embedded in casting plastic resin while Figure 2c shows the optical fiber mounted in an additional protective end sleeve and molded into an SMC short chopped fiber composite panel. At the output, the sample fibers in all three geometries and reference fibers were placed together in a three-axis fiber mount so the two emerging beams combined to produce a straight line interference pattern. The intensity pattern was spatially filtered with a Ronchi ruling and optically detected. Figure 3a shows the detected optical signal corresponding to a typical event in the composite; Figure 3b shows the same event detected using the piezoelectric transducer.

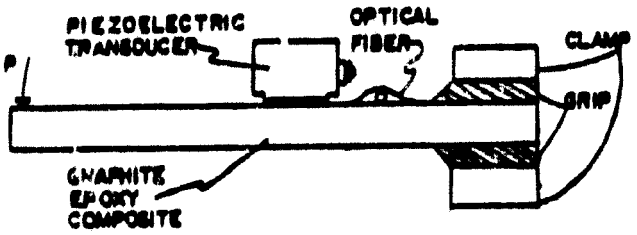

Fig. 2a Technique for comparing optical fiber measurements to piezoelectric transducer measurements in a prestressed graphite epoxy composite.

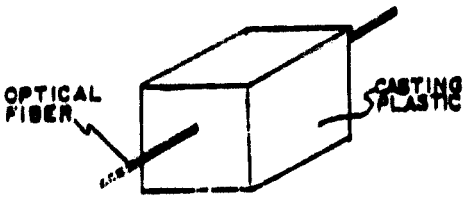

Fig. 2b Optical fiber embedded in casting plastic resin.

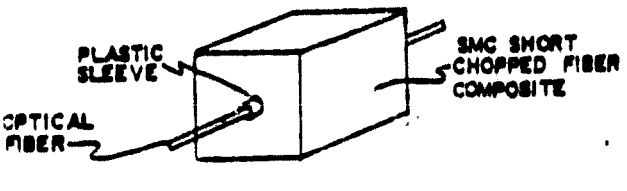

Fig. 2c Optical fiber embedded in molded SMC short chopped fiber composite block.

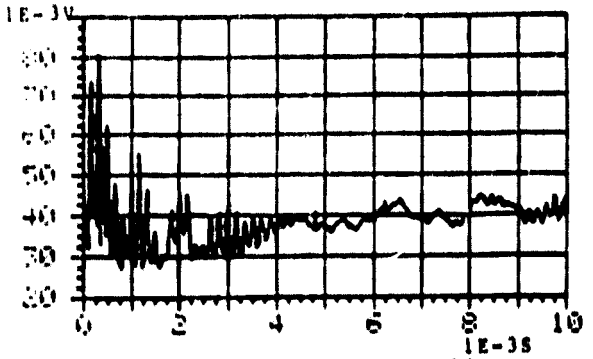

Fig. 3a Acoustic emission event in graphite-epoxy composite detected by single mode optical fiber.

The interferometer was calibrated using a plexiglass bar clamped at one end as a cantilever beam. Average experimental strain data agree within 8 percent of the theoretical value in Equation (3) and indicate an improvement in the minimum detectable strain to approximately 10^{-10} by spatial filtering [4, 6, 19].

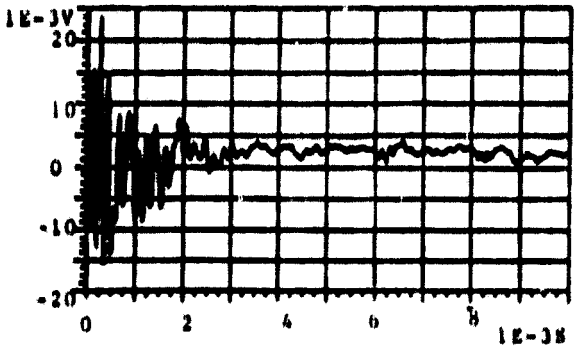

Fig. 3b Acoustic emission event in graphite-epoxy composite detected by surface contact acoustic emission transducer.

4. Discussion

Recorded calibration data agrees closely with theory and in addition pulsed acoustic wave data obtained when the fiber was adhesively bonded to the composite surface is similar to piezoelectric data taken using the same composite. The data suggests further application to a three-dimensional technique in which multiple fibers could be manufactured in a three-dimensional matrix array within the composite and used to obtain three-dimensional acoustic emission pulsed field measurement resolution.

5. Acknowledgements

Part of this research was supported by NASA Grant NAG-1-68 and National Science Foundation Grant ECS-7925340. The authors thank the ITT Electrooptics Division and the Corning Glass Works for donating optical fiber and R. A. Kline for useful discussions.

References

[1] G. B. Hocker: "Fiber-Optic Sensing of Temperature and Pressure," Appl. Opt. 18, 1445 (1979).

[2] J. H. Cole, R. L. Johnson, P. G. Bhuta: "Fiber-Optic Detection of Sound," J. Acoust. Soc. Am. 62, 1136 (1977).

[3] J. A. Bucaro, H. D. Dardy, E. F. Carome: "Optical Fiber Acoustic Sensor," Appl. Opt. 16, 1961 (1977).

[4] J. A. Bucaro, H. D. Dardy and E. F. Carome: "Fiber-Optic Hydrophone," J. Acoust. Soc. Am. 62, 1302 (1977).

[5] J. A. Bucaro and E. F. Carome: "Single Fiber Interferometric Acoustic Sensor," Appl. Opt. 17, 330 (1978).

[6] R. O. Claus and J. H. Cantrell, Jr.: "Detection of Ultrasonic Waves in Solids by an Optical Fiber Interferometer," Proc. 1980 Ultrasonics Symp., 719 (1980).

[7] C. L. Pekeris: "The Seismic Surface Pulse," Nat. Acs. Sci. Proc. 41, 469 (1955).

[8] L. Knopoff: "Surface Motions of a Thick Plate," J. Appl. Phys. 29, 661 (1958).

[9] C. H. Palmer, R. O. Claus, S. E. Fick: "Ultrasonic Wave Measurement by Differential Interferometry," Appl. Opt. 16, 1849 (1977).

[10] V. Vali and R. W. Shorthill: "Fiber Ring Interferometer," Appl. Opt. 15, 1099 (1976).

[11] C. D. Butler and G. B. Hocker: "Fiber Optic Strain Gauge," Appl. Opt. 17, 2867 (1978).

[12] D. P. Jablonowski: "Simple Interferometer for Monitoring Rayleigh Waves," Appl. Opt. 17, 2064 (1978).

[13] W. O. Schlosser: "Delay Distortion in Weakly Guided Optical Fibers Due to Elliptic Deformation of the Boundry," Bell Sy. St. Tech. Jn. 51, 487 (1972).

[14] S. A. Kingsley: "Optical-Fibre Phase Modulator," Electron. Lett. 11, 453 (1975).

[15] B. Culshaw, D.E.N. Davies, and S. A. Kingsley: "Acoustic Sensitivity of Optical Fibre Waveguides," Electron. Lett. 12, 761 (1977).

[16] P. M. Morse, K. U. Ingard: Theoretical Acoustics, McGraw-Hill (1968).

[17] S. N. Rzhevikin: A Course of Lectures on the Theory of Sound, Macmillan Co. 1963.

[18] W. P. Mason, R. N. Thurston, Physical Acoustics VOL X, Academic Press, 1973.

APPENDIX B

Application of Ultrasonic Interface Waves to Nondestructive Evaluation

R. O. Claus and R. A. Kline, "Pulsed Ultrasonic Leaky Waves on a Titanium-Aluminum Boundary," Acoust. Soc. Am. Annual Meeting (Los Angeles, CA), Nov. 1980; also in J. Acoust. Soc. Am 68, S107 (1980).

Pulsed ultrasonic leaky waves on a titanium-aluminum boundary.

Richard O. Claus (Department of Electrical Engineering, Virginia Polytechnic Institute and State University, Blacksburg, VA 24061) and Ronald A. Kline (General Motors Research Laboratory, Warren, MI 48090)

Pulsed 2.1-MHz leaky waves on an adhesively bonded titanium-aluminum interface have been generated and detected by aluminum Rayleigh wave mode conversion. Specimens were prepared by bonding 0.95-cm x 1.27-cm etched titanium alloy bars to large aluminum substrates and compressing so the thickness of the adhesive layer was much smaller than the acoustic wavelength. Total losses of less than 12 dB due to mode conversion and attenuation along the 1.27-cm interface have been observed. The adhesive bond geometry is modeled as a liquid layer of thickness H separating two isotropic solid half-spaces [A. K. Banghar, G. S. Murty, and T. V. V Raghavacharyulu, J. Acoust. Soc. Am. 60, 1071-1078 (1976)]. Measured leaky wave velocity is approximately predicted by the case where H approaches zero and the viscosity of the liquid becomes large [D. A. Lee and D. M. Corbly, IEEE Trans. Sonics Ultrason. SU-24, 206-212 (1977)]. Particle displacements near the boundary in both the titanium and the aluminum are derived for this case and changes in leaky wave attenuation due to small variations in H are predicted. [Work partially supported by NSF.]

Technical Committee: Physical Acoustics

PACS numbers : 43.35.Pt, 68.25.+j

Telephone number : (703) 961-7203 (R. O. Claus)

Acoust. Soc. Am. Nat. Meeting, Los Angeles, CA, November, 1980.

T. M. Turner and R. O. Claus, "Pulse-Echo Interface Wave Characterization of Bolted Plates," Proc. 1981 IEEE Region 3 Conf. (Huntsville, AL), April 1981.

PULSE-ECHO INTERFACE WAVE CHARACTERIZATION OF BOLTED PLATES

TYSON M. TURNER, RICHARD O. CLAUS and STEWART L. OCHELTREE

Department of Electrical Engineering
Virginia Polytechnic Institute and State University
Blacksburg, VA 24061

Abstract

Ultrasonic waves which propagate along the plane boundary separating two solid substrates have been used to characterize aluminum and titanium plates adhesively bonded and bolted together. Gated 2.25 MHz surface acoustic wave pulses were generated using a Rayleigh-angle lucite wedge on a 7079-T6 aluminum plate. These pulses were then used to produce interface waves between the aluminum and a Ti-6Al-4V titanium alloy bar by normal mode conversion. Interface wave reflections from bolt holes drilled through the interface were reconverted to surface wave pulses and detected by the same wedge by standard pulse-echo techniques. Time of flight measurements indicate that the reflected waves are a superposition of longitudinal modes and circularly symmetric waves that propagate around the bolt hole. Potential applications in the non-destructive evaluation of aerospace structures is discussed.

Introduction

Particle motion waves that travel along the boundary between solids are called interface waves. Like waves which travel over free solid surfaces, these waves have energy which is confined to the two dimensions that define the boundary. The motion of particles on either side of the boundary is attenuated rapidly with distance into each of the substrates and the motion in general is elliptical retrograde with respect to the direction of wave propagation. The two-dimensional particle motion fields are determined by the relationships between the elastic constants of the two solids and by the wavelength of the acoustic wave along the boundary [1].

Recently, several authors have reported the application of interface wave techniques to the evaluation of the material properties of the contact zone between two adjacent solids [2,3]. Of particular importance may be the use of ultrasonic interface waves to determine the integrity of completed adhesive bonds between pairs of structural materials. These types of bonds may be evaluated using standard time and frequency domain ultrasonic methods which can be used to identify gross delamination between the adhesive and adherent, or large voids either in the adhesive layer itself or in the surfaces of the two material surfaces. Standard techniques, however, are insensitive to the most important bonding problem, that of the weak bond where the solids are in intimate contact with no voids but there is little interfacial strength.

Interface waves are ideally suited to this type of bond inspection. Since the waves travel along the interface rather than through it, they sample bondline conditions over a large area. Also, the observables in the experimental measurement system, the attenuation and velocity of the waves, are functions of the material properties of the adhesive and adherent, the viscosity and surface conditions.

In this paper, recent experimental measurements of gross bond defects using pulse-echo and pitch-catch interface wave methods are discussed. The theories of interface wave propagation along an adhesive layer are first described, the experimental arrangement and results then presented, and conclusions concerning applications in non-destructive evaluation finally discussed.

Theory

There are several theories which describe the propagation of bound elastic waves along solid-solid interfaces. All have been discussed extensively in the literature and so will only be reviewed briefly here [3,4,5]. First, the boundary may be considered ideal, that is, the solids are modeled as infinite homogeneous half-spaces in contact over a perfect plane. By assuming exact continuity of particle motion and stresses across this plane, an equation of motion for waves bound to the interface may be determined. Real roots to this equation correspond to Stoneley waves, bound elastic waves that propagate without attenuation along the plane. The existence of real roots is limited to a narrow range of solid-solid material properties so Stoneley waves do not exist in general on solid-solid boundaries. Stoneley waves have been generated and detected by several authors [1,6].

The inclusion of adhesive material between the solids complicates the physical system and permits several variations in the model. If the adhesive layer is considered as a purely viscous material, observed nonlinear relationships between wave velocity and boundary layer density may be explained [1]. If the model is broadened to a viscoelastic approximation, time dependent moduli

IEEE Region 3 Conf. (Huntsville, AL), April 1981.

variations due to stress and thermal cycling may also be explained [3]. Recent work by Kline attempts to include generalized effects characteristic of each of these models [7].

Experiment

In this experiment, the effects of large defects in boundary structure on wave attenuation were measured. Surface waves were generated at 2.25 MHz on a 53.2 cm aluminum bar 15 cm wide using Harisonic ABM0204 plastic wedges as shown in Figure 1. The surface waves were incident upon a 1.0 cm wide titanium bar 0.5 cm thick which was glued to the aluminum substrate. Part of the energy in the incident wave was mode converted into a wave on the interface between the aluminum and titanium. At the opposite side of the bar, the wave was reconverted to a surface wave which was detected by a second Harisonic transducer. Metrotek ultrasonic pulsers and receivers were used to generate and receive the ultrasonic pulses which were observed on a monitor oscilloscope.

Three spearate cases were studied. Flat-bottomed holes 0.64 cm in diameter were drilled through the titanium/aluminum block. The attenuation of the transmitted interface wave was measured as a function of distance along the bar near the hole and normal to the direction of wave propagation. Pulse-echo and pitch-catch measurements of reflection and attenuation, respectively, were made for a hole through both solids. Similar data was obtained as a function of hole depth by gradually increasing the depth of the hole in increments while measuring ultrasonic pulse amplitude.

Results

The results of our measurements are shown in Figures 2, 3, and 4. Figure 2 shows the spatial cross section response obtained by pulsing one transducer and detecting the transmitted pulse by the second transducer. Significant attenuation of the pitched signal is evident at the location of the hole. Data shown in Figure 3 was obtained by pulsing one transducer and measuring the reflected signal detected by the same transducer a short time later. Here, a significant reflection is obtained at the location corresponding to the center of the hole. Data plotted in Figure 4 corresponds to the pitch-catch attenuation of interface waves incident upon a sample with a hole of increasing depth. Attenuation is seen to increase with increasing depth; more attenuation is observed for the aluminum than the titanium due to the unequal division of longitudinal and shear wave component energies in the two materials [1].

Conclusion

Transmitted and reflected ultrasonic interface waves have been used to locate bolt holes in adhesively bonded samples. Interface wave techniques are suggested as sensitive nondestructive methods in adhesive bond evaluation.

Acknowledgments

This research was partially supported by NSF Grant ECS-7925340. Samples were donated by the General Motors Research Laboratory.

References

[1] D. A. Lee and D. M. Corbly, "Use of interface waves for nondestructive inspection," IEEE Trans. Sonics Ultrason. SU-24, 206 (1977).

[2] R. O. Claus and R. A. Kline, "Adhesive bondline interrogation using Stoneley wave methods," J. Appl. Phys. 50, 8066 (1979).

[3] S. Rokhlin, M. Hefets, and M. Rosen, "An elastic interface wave guided by a thin film between two solids," J. Appl. Phys. 51, 3582 (1980).

[4] R. Stoneley, "Elastic waves at the surface of separation of two solids, "Proc. Roy. Soc. 106, 416 (1924).

[5] G. S. Murty, "Wave propagation at an unbounded interface between two elastic halfspaces," J. Acoust. Soc. Am. 58, 1094 (1975).

[6] R. O. Claus and C. H. Palmer, "Optical measurements of ultrasonic waves on interfaces between bonded solids," IEEE Trans. Sonics Ultrason. SU-27, 97 (1980).

[7] Personal correspondence, R. A. Kline, General Motors Research Laboratory.

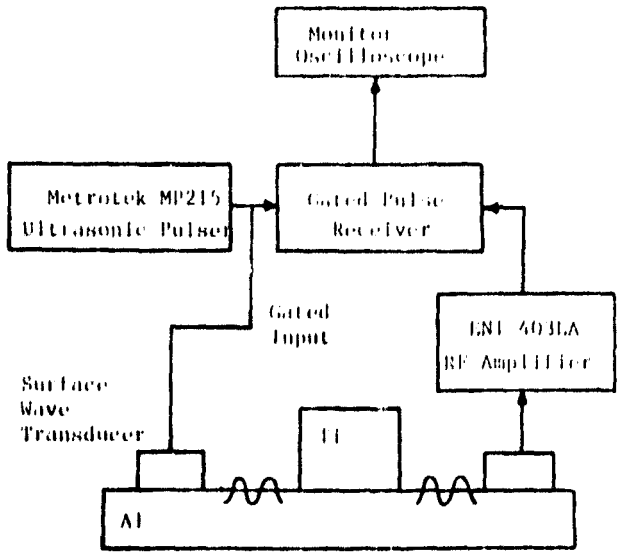

Fig. 1. Interface wave generation and detection geometry used to characterize bolted plates.

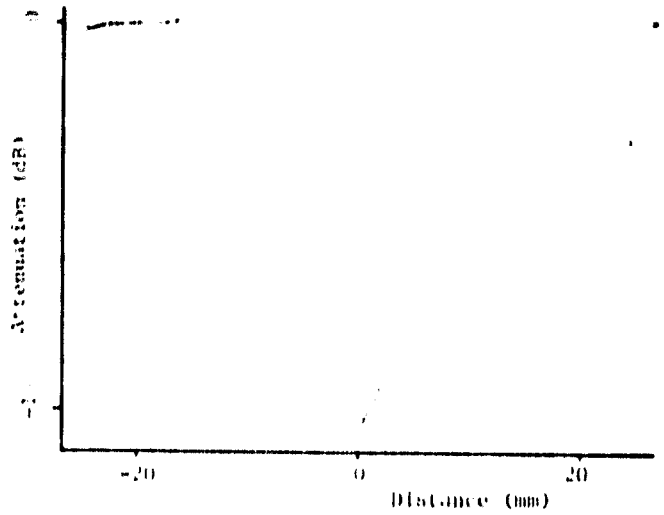

Fig. 2. Pitch-catch measurement of a 0.635 cm diameter hole in an Al-Ti bonded interface.

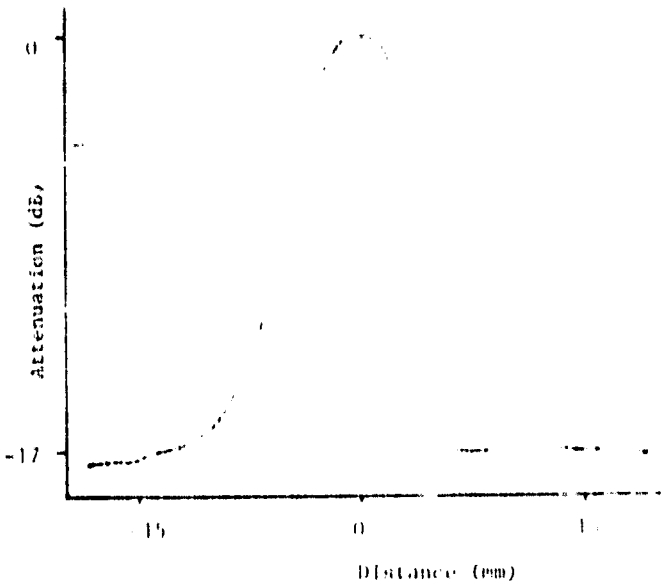

Fig. 3. Pulse-echo measurement of a 0.635 cm diameter hole in an Al-Ti bonded interface.

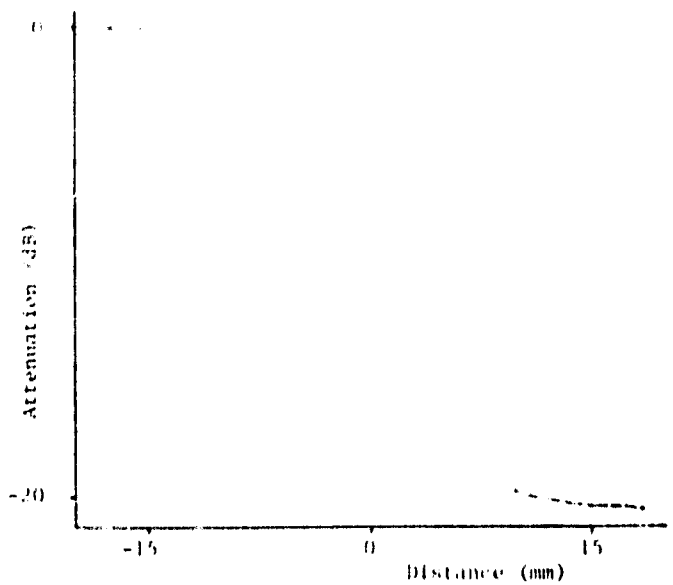

Fig. 4. Pitch-catch measurement of interface wave attenuation due to a 0.635 cm diameter hole of varying depth in an Al-Ti interface.

R. O. Claus, "Attenuation of Ultrasonic Interface Waves on Metal-Polymer-Metal Boundaries," Seventh International Conference on Internal Friction and Ultrasonic Attenuation in Solids (Lausanne, Switzerland), July 1981.

ATTENUATION OF ULTRASONIC INTERFACE WAVES ON METAL-POLYMER-METAL BOUNDARIES

Richard O. Claus
Department of Electrical Engineering
Virginia Polytechnic Institute and State University
Blacksburg, VA 24061

Seventh International Conference on Internal Friction and Ultrasonic Attenuation in Solids, 6-9 July 1981, Lausanne, Switzerland.

Abstract.- Ultrasonic Stoneley and leaky interface wave techniques have been applied to the characterization of the bondline structure and the near-surface bulk properties of flat metal alloy samples separated by a thin layer of polymer adhesive. Interface wave energy is confined to the region containing the polymer and extending approximately one ultrasonic wavelength into each of the metal substrates. The amplitude and distribution of localized particle motions both normal and parallel to the interface are sensitive to point defects at the polymer-metal boundaries as well as to grain boundaries and dislocations near the metal surfaces and to microcracks in the polymer. In this paper, the measured sensitivity of interface wave attenuation to defects near the bondline and to variations in the viscosity of the adhesive layer is compared with theoretical changes predicted by the model developed by Rokhlin. Two experimental techniques utilized to obtain these measurements are presented. First, differential interferometric optical measurements of interface wave attenuation due to defects near glass-polymer-metal boundaries are discussed. This sensitive laser probe method allows the detection of averaged periodic surface displacements as small as 4×10^{-3} Å and localized reflections and scattering from individual buried defect sites. Next, pit h-catch and pulse-echo methods which use variable-angle wedge transducers to generate and receive modified interface waves and to measure large bondline defects and adhesive viscosity are described. Potential applications to the characterization of completed polymer adhesive bonds are suggested.

1. Introduction.- Ultrasonic waves which propagate along the boundary between pairs of solids and which have wave energy confined to a thin region on either side of the boundary are known as interface waves. The spatial distributions of the particle displacement fields in both media are determined by the mechanical boundary conditions imposed at the interface and the velocity of the interface waves is bounded by the lower of the speeds of distortional waves in the bulk of each substrate and the higher of the speeds of Rayleigh waves on the free surfaces of each material independently. If the surfaces of both solids are in intimate contact such that both particle displacement and stress are continuous across the boundary, an equation of motion for classical unattenuated Stoneley waves bound to the surface may be derived[1,2]. Real roots to this equation occur only for a limited range of media pairs making Stoneley wave propagation a case of limited practical interest[3]. If either the displacement or stress continuity conditions are not satisfied, smooth

contact and slip contact approximations to the ideal welded contact case are obtained[4].

A physical model that is more appropriate for the consideration of realistic material boundaries assumes that the two solid media are separated by a thin layer of uniform thickness H as shown in Figure 1. If this layer is thought of as the combined microsurface layers of both media which have densities and elastic properties different from those of the substrates, the system may be modeled as three elastic layers and the propagation of a wave confined near the middle layer and its sensitivity to microsurface structural changes may be derived. If instead the layer is a liquid, a thin film of adhesive, for example, the relationship between the liquid viscosity η and the thickness H determines the propagation characteristics. Specifically, if the magnitudes of η and H are such that $\eta \gg H$ and the ratio η/h approaches zero, smooth bonding is defined while if η approaches zero but η/H remains finite, loose bonding occurs[5]. Finally, both the elastic and viscous damping properties of the layer may be considered by assuming the layer to be a Voigt solid and satisfying the eight acoustic potential continuity conditions at the upper and lower layer-substrate boundaries. The resulting determinantal characteristic equation may be expressed as

$$K'_a \Delta'_a + K'_r \Delta'_r + f = 0, \tag{1}$$

where Δ'_a is the characteristic function for antisymmetric Lamb waves in a viscoelastic plate with unloaded surfaces, Δ'_r is the characteristic function for Rayleigh waves on a viscoelastic half-space, and K'_a, K'_r, and f are functions of the elastic constants of both substrates and the modified viscoelastic moduli of the liquid layer[6,7].

The viscoelastic layer model predicts several interface wave attenuation mechanisms which are of specific importance in the evaluation of adhesive bond integrity. First, if there is a localized discontinuity in particle displacement at one of the layer interfaces, the effective rigidity is modified locally, causing

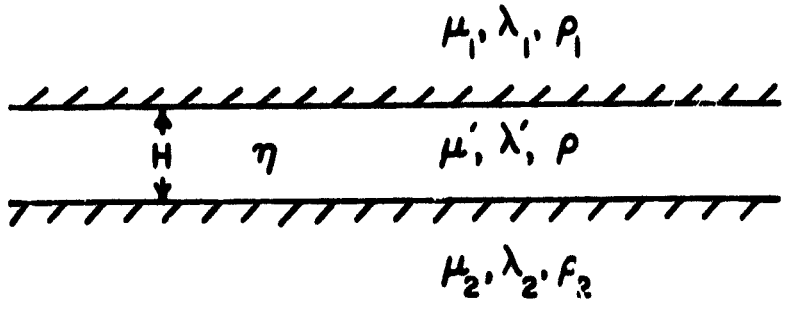

Fig. 1. Geometry of solid media denoted by subscripts 1 and 2 separated by a thin viscoelastic liquid film.

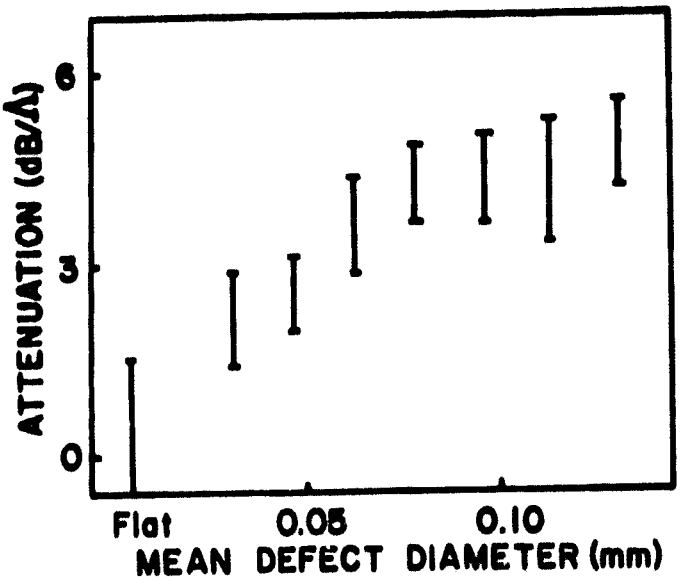

Fig. 2. 9MHz interface wave attenuation due to surface defects on 7740 pyrex-crown glass boundary.

wave reflection and damping and a decrease in interface wave velocity. Due to this effect, wave attenuation should provide a measure of the percentage of the bondline in ideal rigid adhesion. Second, changes in the physical structure of the layer vary the time-dependent viscosity and damping. Such changes have been related to the state of polymerization of the adhesive and the compressive stress applied to the layer[6].

2. Experiment.- To measure the interface wave attenuation due to slip at the layer-substrate boundaries, defects were introduced on one surface prior to bonding. Optically flat 7740 pyrex specimens were ground with increasingly coarser grades of optical abrasive polish, optically inspected to determine the surface defect size distribution, and bonded using two-part epoxy polymer adhesive to aluminized borosilicate crown glass optical flats[8]. The attenuation as a function of surface defect diameter shown in Figure 2 was determined by optically measuring interface wave amplitude along the interface using the differential interferometric system shown in Figure 3. Here, the two arms of the interferometer are focused through the transparent crown glass substrate to points at the interface separated by half an

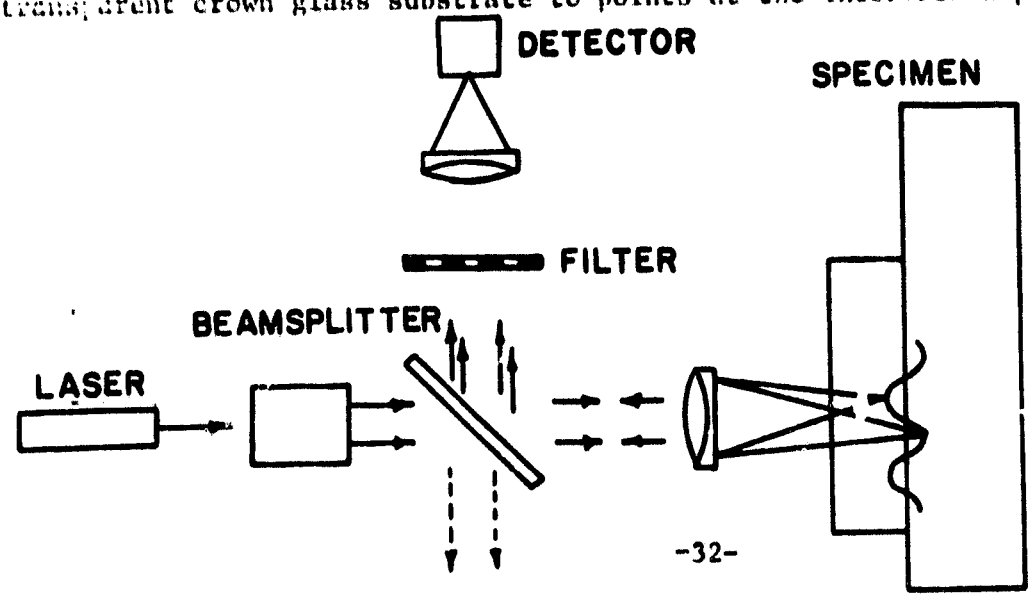

Fig. 3. Differential interferometric system for detecting interface wave particle displacement.

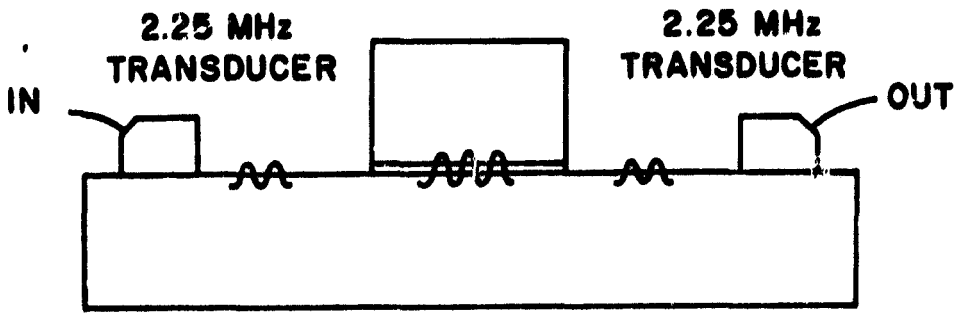

Fig. 4. Pitch-catch ultrasonic geometry used to detect 2.25 MHz interface wave attenuation and velocity variations as a function of applied compressive stress.

acoustic wavelength. Detected signal amplitude is proportional to the optical pathlength difference between the two beams and thus to the amplitude of the normal component of particle displacement at the interface. Attenuation measurements are limited by a minimum detectable wave amplitude of 4×10^{-3} Å[9].

To measure the attenuation due to variations in boundary layer structure, interface waves were generated and detected using the pitch-catch Rayleigh wave conversion geometry shown in Figure 4. Rayleigh waves generated on the surface of an optically polished nickel substrate were mode-converted into interface waves on the nickel-aluminum boundary, and changes in the amplitude of the reconverted Rayleigh waves at the output were measured. Boundary layer structure was varied for samples with and without an adhesive middle layer by applying an external compressive stress to the materials equal to seventy percent of the yield stress of the aluminum. Without the adhesive present, the microsurfaces of the substrate effectively form the layer since density near the surface is less than that in the bulk. Compressive stress increases this surface density and, in qualitative agreement with theory, nonlinearly increases both wave velocity and attenuation as shown in Figure 5[10]. With the viscoelastic adhesive present, stress increases layer

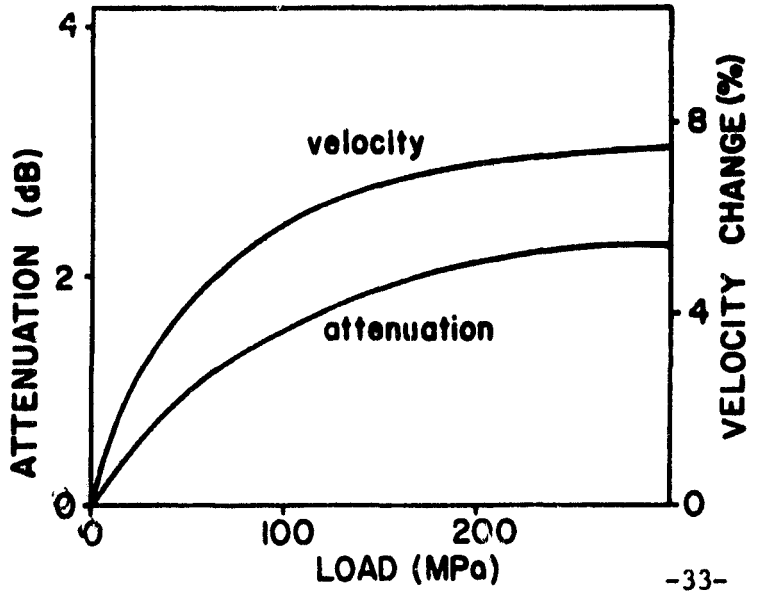

Fig. 5. Nonlinear changes in 2.25 MHz interface wave velocity and attenuation versus applied compressive stress.

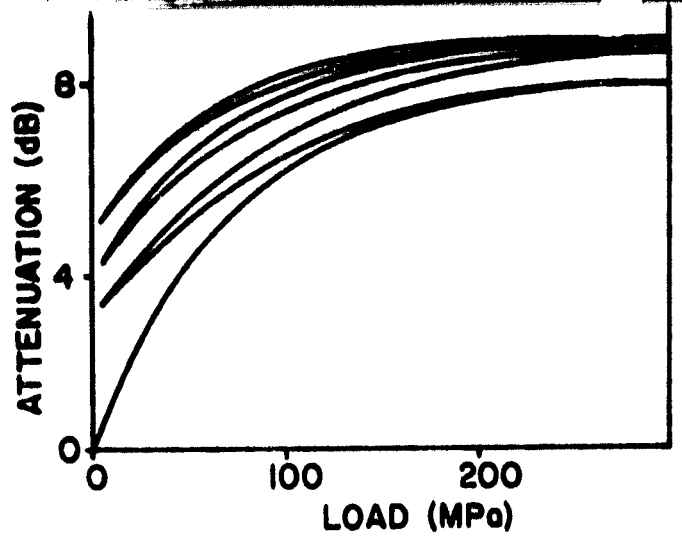

Fig. 6. Hysteresis in 2.25 MHz interface wave velocity versus sixty second compression cycling.

viscosity, also causing velocity and attenuation to increase. Figure 6 shows representative velocity hysteresis measured for sixty second compression cycling due to the time-varying behavior of μ' in the layer.

3. Results.- Modeled effects on interface wave attenuation due to both boundary defects and interface layer viscosity variations have been experimentally measured. Resulting wave attenuation may be used to indicate the percentage of interfacial area not in ideal adhesion and the state of polymerization of interface adhesive materials and thus to characterize interface bond integrity.

4. Acknowledgments.- The author thanks S. Rokhlin, V. Kumar, and R. Kline for useful discussions and J. Chern for assistance with the measurements of velocity hysteresis. This work was supported by NSF Grant ECS-7925340 and NASA Grant NAG-1-68.

Bibliography

[1] R. Stoneley, "Elastic waves at the surface of separation of two solids," Proc. Roy. Soc. 106, 416 London(1924).

[2] W. L. Pilant, "Complex roots of the Stoneley wave equation," Bull. Seismol. Soc. Am. 62, 285(1975).

[3] K. Sezawa and K. Kanai, "The range of possible existence of Stoneley waves and some related problems," Bull. Earthquake Res. Inst. 17, 1(1939).

[4] G. S. Murty, "Wave propagation at an unbounded interface between two elastic half-spaces," J. Acoust. Soc. Am. 58, 1094(1975).

[5] A. R. Banghar, G. S. Murty, and I. V. V. Raghavachargulu, "On the parametric model of loose bonding of elastic half spaces," J. Acoust. Soc. Am. 60, 1071 (1976).

[6] S. Rokhlin, M. Hefe[illegible] and M. Rosen, "An elastic interface wave guided by a thin film between two solids," J. Appl. Phys. 51, 3579(1980).

[7] R. A. Kline and R. O. Claus, in preparation.

[8] R. O. Claus and R. A. Kline, "Adhesive bondline interrogation using Stoneley wave methods," J. Appl. Phys. 50, 8066(1979).

[9] C. H. Palmer, R. O. Claus, and S. E. Fick, "Ultrasonic wave measurement by differential interferometry," Appl. Opt. 16, 1849(1977).

[10] D. A. Lee and D. M. Corbly, "Use of interface waves for nondestructive inspection," IEEE Trans. Sonics Ultrason. SU-24, 206(1977).

R. O. Claus, "Characterization of Metal-Polymer Boundaries using Stoneley and Leaky Interface Waves," International Symposium on Physicochemical Aspects of Polymer Surfaces (New York, NY), Aug. 1981.

CHARACTERIZATION OF METAL-POLYMER BOUNDARIES USING STONELEY AND LEAKY WAVES

Richard O. Claus
Department of Electrical Engineering
Virginia Polytechnic Institute and State University
Blacksburg, VA 24061

ABSTRACT

Bondlines between polymer adhesive layers and aluminum and nickel alloys adjacent to the layers have been characterized using ultrasonic interface waves which propagate along the polymer-metal boundary and sample bondline structure. Since the depth of penetration of bounded wave motion is limited to approximately one acoustic wavelength within the material on either side of this boundary, sensitivity to subsurface defects may be altered by varying wave frequency. Interface wave propagation models based on viscous, elastic, and viscoelastic mechanical properties are reviewed. Gross boundary anomalies such as large defects and localized disbond regions have been measured using conventional high-frequency pulse-echo and pitch-catch ultrasonic techniques. Bond durability has been estimated by comparing detected wave attenuation versus frequency as a function of pre-bond surface preparation with the experimental limit obtained for perfect welded contact. Sensitivity of interface acoustic field periodicity to both residual and dc applied stress at the boundary surface has been observed as well as hysteresis due to viscoelastic polymeric behavior as the applied stress is cycled. Optical and acoustooptical techniques for bonded surface inspection and interface wave detection are discussed.

International Symposium on Physicochemical Aspects of Polymer Surfaces, New York, August 1981.

INTRODUCTION

Ultrasonic waves which propagate along the boundary between pairs of solids and which have wave energy confined to a thin region on either side of the boundary are known as interface waves. The spatial distributions of the particle displacement fields in both media are determined by the mechanical boundary conditions imposed at the interface and the velocity of the interface waves is bounded by the lower of the speeds of distortional waves in the bulk of each substrate and the higher of the speeds of Rayleigh waves on the free surfaces of each material independently.

If the surfaces of both solids are in intimate contact such that both particle displacement and stress are continuous across the boundary, an equation of motion for classical unattenuated Stoneley waves bound to the surface may be derived [1]. Real roots to this equation occur only for a limited range of media pairs making Stoneley wave propagation a case of limited practical interest [2]. If either the displacement or stress continuity conditions are not satisfied, smooth contact and slip contact approximations to the ideal welded contact case are obtained [3].

A physical model that is more appropriate for the consideration of realistic material boundaries assumes that the two solid media are separated by a thin layer of uniform thickness H. If this layer is thought of as the combined microsurface layers of both media which have densities and elastic properties different from those of the substrates, the system may be modeled as three elastic layers and the propagation of a wave confined near the middle layer and its

sensitivity to microsurface structural changes may be derived. If instead the layer is a liquid, a thin film of polymer adhesive, for example, the relationship between the film viscosity η and its thickness H determines the propagation characteristics. Specifically, if the magnitudes of η and H are such that $\eta >> H$ and the ratio η/H approaches zero, smooth bonding is defined while if η approaches zero but η/H remains finite, loose bonding occurs [4]. Finally, both the elastic and viscous damping properties of the layer may be considered by assuming the layer to be a Voigt solid and satisfying the eight acoustic potential continuity conditions at the upper and lower layer-substrate boundaries [5].

Recent analytical research of the interface wave field problem has centered on the implications of solutions of this general case to practical physical systems [6, 7]. Specifically, the viscoelastic layer model predicts several interface wave attenuation mechanisms which are of direct importance in the evaluation of the integrity of completed adhesive bonds. First, if there is a localized discontinuity in particle displacement at one of the layer interfaces, the effective rigidity is modified locally, causing backward wave reflection and forward wave attenuation and a change in interface wave velocity. Due to this effect, wave speed and damping provide an indication of the percentage of the bondline that is in ideal rigid adhesion according to this model. Second, changes in the physical structure of the layer may also vary interface wave attenuation via modulation of layer viscosity. Such changes may be related to the state of polymerization of the adhesive or to either compressive stress applied externally to the layer or internal residual stress.

In this paper, analytical and experimental results obtained for metal-polymer boundaries are reviewed. Interface wave models are briefly described in terms of ultrasonic field parameters. Ultrasonic wave detection of gross boundary defects by pulsed surface acoustic wave techniques and small defects by continuous wave attenuation measurements are discussed and observed nonlinear changes and hysteresis in wave velocity due to applied stress are explained in terms of a simple nonlinear polymer density model. Finally, optical measurement systems for the detection of interface wave observables and their advantages over surface contact transducer methods are noted.

THEORY

A simple three layer model for the geometry of a polymer-metal boundary is shown in Figure 1 where λ and μ are the Lamé constants and ρ the density of the layers. Here the subscript 2 denotes the metal substrate on the bottom, subscript 0 denotes the polymer material of thickness H shown in the center, and subscript 1 refers to the top layer. By specifying λ_1, μ_1, and ρ_1 and the boundary conditions at the upper surface of the polymer layer, substrate 1 may be chosen to be vacuum for the case of a simple polymer-metal bond or a second metal substrate for the case of a metal-polymer adhesive-metal bond. Ultrasonic wave propagation along the one or two resulting interfaces is dependent upon the nine elastic constants shown and upon the layer thicknesses. Since the wave-induced particle motion is confined to a region extending approximately one acoustic wavelength into each material in the z-direction, the field expressions that may be derived assuming infinite half-space substrates must be modified if the layers are thinner than several wavelengths in order to account for the field interactions at both boundaries of the polymer. Typically, interface wavelengths at several megahertz are less than one millimeter and the generated normal components of particle displacement at the interfaces have maximum deviations from the unperturbed surface level of several tens of Angstroms.

For the simplified case of a thick polymer layer perfectly bonded to a thick metal substrate, both particle displacement and stress are continuous across the metal-polymer interface and interface wave velocity, C, satisfies the resulting characteristic equation

$$C^4((\rho_1 - \rho_2)^2 - (\rho_1 M_2 + \rho_2 M_1)(\rho_1 N_2 + \rho_2 N_1))$$

$$+ 2PC^2(\rho_1 M_2 N_2 - \rho_2 M_1 N_1 - \rho_1 + \rho_2) \qquad (1)$$

$$+ P^2(M_1 N_1 - 1)(M_2 N_2 - 1) = \Delta_s$$

$$= 0.$$

In this equation,

$$M_i = (1 - C^2/\alpha_i^2)^{\frac{1}{2}} \; ; \; i = 1, 2; \qquad (2)$$

$$N_i = (1 - C^2/\beta_i^2)^{\frac{1}{2}} \text{ , and} \qquad (3)$$

$$P = (\rho_1 \beta_1^2 - \rho_2 \beta_2^2), \qquad (4)$$

where α_1 and α_2 are the dilitational (compressional) wave speeds in the two media and β_1 and β_2 are the shear wave speeds. The range of existence of real solutions for C in (1) is determined by the relationship between substrate and layer elastic constants [8]. Because the ratio of the ratios of density and rigidity modulus of many polymers and nickel metal alloys are approximately unity, (1) has real solutions for many boundaries of polymers with these materials [9]. These real solutions correspond to the propagation of unattenuated waves along the interface and such waves are especially useful for the experimental characterization of interfacial properties.

If instead of a single polymer-metal interface the more general case of a film of polymer adhesive between two metal layers is considered, solutions to two equations similar to (1) must be obtained corresponding to waves at both film-metal boundaries. For thin films the interaction of the two wave solutions with the opposite film

boundaries causes a partial acoustic wave guiding effect within the layer and the equation for guided wave velocity becomes

$$\frac{2}{a_1}\left(\frac{M_0}{\mu}\right)^2 a_1 \Delta a \sum_{j=1}^{\infty} \frac{J_0(n_j C)}{n_j J_1(n_j a_1)}$$

$$+ \frac{\mu_0}{\mu}(\gamma S_1 - \beta Q_1) + 2\alpha^2 \frac{\mu_0}{\mu} \tag{5}$$

$$\times a_2(2S_2 + W_0 Q_2) + \Lambda_R(S_2 + \alpha^2 Q_2) = 0,$$

where $\alpha = k/k_t$, $\bar{h} = k_t h, \xi = k_1/k_t$, $\eta_0 = k_t^0/k_t$,

$\xi_0 = k_1^0/k_t, \beta = (\alpha^2 - 1)^{1/2}$, $\gamma = (\alpha^2 - \xi^2)^{1/2}$,

$\beta_0 = (\eta_0^2 - \alpha^2)^{1/2} = [\mu\rho_0/(\mu_0\rho) - \alpha^2]^{1/2}$,

$\gamma_0 = (\xi_0^2 - \alpha^2)^{1/2}$, $a_1 = \alpha^2 - \beta\gamma$, $a_2 = 2\beta\gamma - W$,

$W = \alpha^2 + \beta^2$, $W_0 = \alpha^2 - \beta_0^2$, $S_1 = \beta_0 \sin\beta_0 h$

$\times \{[\sin(\gamma_0 \bar{\bar{h}})]/\gamma_0\}$, $Q_1 = \cos(\beta_0 \bar{\bar{h}}) \cos(\beta_0 h) \cos(\gamma_0 \bar{\bar{h}})$,

$S_2 = \beta_0 \sin(\beta_0 \bar{\bar{h}}) \cos(\gamma_0 \bar{\bar{h}})$, $Q_2 = \cos(\beta_0 \bar{\bar{h}}) \{[\sin(\gamma_0 h)]/\gamma_0\}$.

$\Delta_r = W^2 - 4\alpha^2\beta\gamma$ is the characteristic function for the Rayleigh waves; $\Lambda_a = W_0^2 Q_2 + 4\alpha^2 S_2$ is the characteristic function for the antisymmetric Lamb waves in an elastic layer with free boundaries. k_t and k_1 are the wave numbers for the shear and longitudinal waves

in the half-spaces. k_t^0 and k_l^0 are the corresponding wave numbers for the layer. k is the wave number of the interface wave [10].

If (5) is simplified into the form

$$\Delta_s + F(\Delta_r + \Delta_a + M) = 0, \tag{6}$$

where Δ_s is the characteristic equation for Stoneley wave propagation in (1) and F and M are constants, variation of F from zero to one corresponds to the change in boundary conditions from the two media interface wave case in (1) to the guided wave mode case in (5). The effects of changes in field component solutions as a function of this parameter are described elsewhere [11].

POLYMER-METAL SURFACE DEFECT EFFECTS

Experimentally, boundary conditions require that no relative displacement occurs between the two media surfaces and that no voids exist at the boundary. Stress discontinuities and slip at the interface could originate at inclusions, voids, porosity, or regions of poor adhesion. All of these factors can affect the propagation of waves along the boundary and the wave observables may be used inversely to determine these factors.

The effects of defects with dimensions both large and small compared to an acoustic wavelength have been measured. Detection of large defects at the boundary using conventional pulse-echo and pitch-catch ultrasonic techniques was performed to demonstrate the capabilities of interface wave probing using these standard surface acoustic wave (SAW) methods. The interface wave generation and detection geometry is shown in Figure 2. Repetitively gated ultrasonic SAW pulses with 2.1, 8.0, and 9.0 MHz rf carrier frequencies were initially generated on the plane surface of an optically reflective 14.2cm × 6.8cm × 2.5cm aluminum substrate by an x-cut piezoelectric quartz crystal transducer mounted on a conventional Rayleigh angle wedge. SAW with 42Å peak-to-peak maximum surface particle displacement amplitudes were optically measured one millimeter from the top of the wedge. At the near edge of the 6.2cm × 6.2cm × 1.2cm titanium alloy block shown bonded with polymer adhesive to the substrate in Figure 2, more than 95% of the energy in the incident SAW was reflected and a large SAW SWR was observed on the substrate surface between the transducer wedge and the block. Incident SAW were mode converted at the

front corner of the block into waves on the interface between the substrate and the block as well as into dilitational and shear waves in both media. Interface wave attenuation from the front edge to the back edge of the block was determined by optically measuring input and output SAW amplitudes as shown.

Large defects at the boundary were produced by drilling 6.35 mm diameter holes normally through the entire Al-polymer-Ti sandwich at the center of the Ti block [12]. The location of these holes was ultrasonically determined by scanning both the positions of the input wedge transducer and similar output receiving transducers. The location of the drilled holes is well characterized by the received pulsed signal amplitudes plotted for both pitch-catch attenuation and pulse echo magnitude modes in Figure 3.

Interface wave sensitivity to near-boundary defects and substrate thickness has also been determined using a similar hole geometry. By milling 6.35 mm diameter flat-bottomed holes of increasing depth into the titanium alloy sample, the distance d between the hole bottom and the interface may be modulated. As d decreases, transmitted interface wave pulse attenuation increases as shown in Figure 4 where the theoretical decrease for a titanium sample and experimental data are compared. It should be noted that since the decay of field components into each substrate occurs at a different rate, a different attenuation versus depth curve would be obtained if the hole were drilled instead through the aluminum block.

Much smaller interface geometry defects were generated by roughening the metal substrate surfaces, which were originally polished optically

flat, with different grades of optical abrasive. The substrates were then cleaned and again bonded using polymer films. Surface pits optically measured prior to bonding were produced by abrasion and were filled with the film material causing a nonuniform film thickness between the substrates. Continuous interface wave attenuation due to the variation of the thickness of this film versus pit size is shown in Figure 5. A significant difference in attenuation between 2.1 and 9 MHz waves has been observed [12].

POLYMER LAYER AND BOUNDARY EFFECTS

Internal polymer layer and polymer-metal boundary properties may be characterized by observing interface wave velocity shifts caused by changes in polymer structure. Such changes were produced in several ways and the resulting shifts monitored. First, both external dc and cycled compressive stress loads were applied to the polymer layer between metal samples as shown in Figure 6 such that the maximum applied stress was eighty percent of the lower yield stress of the two substrates. Assuming that the polymer under dc compression behaves as a randomly arranged molecular powder, the density of the polymer layer may be modeled by the relation [13].

$$\rho_{polymer} = \rho_0 \left[\frac{P}{P_0}\right]^{-a} , \qquad (7)$$

where ρ_0 is the density in the unstressed state, P is the applied stress, P_0 is the yield stress, and a is a constant determined by the material. The change in ρ with a static load P increases wave velocity as shown in Figure 7. If the load is repetitively cycled from zero to P to zero again, hysteresis is observed. For a ramped load cycle of 0.1 Hz the velocity hysteresis also shown in Figure 7 is obtained. The rate of decay of the stored energy per cycle in this reaction may be directly related via polymer compression and chain cross-linking to the internal friction [14] and shear modulus modulation [15] in the layer. Finally, similar effects due to cross-linking have been observed by allowing a thin film of polymer adhesive between metal substrates to cure while monitoring the velocity of the transmitted wave [12].

OPTICAL METHODS FOR POLYMER-METAL INTERFACE WAVE MEASUREMENTS

Non-contacting optical probe techniques may be used to minitor interface wave characteristics with a minimum of interaction with wave observables. The probe beams indicated in Figure 2 are part of the differential interferometric system shown in Figure 8. At the right side of that figure, dual laser probe beams are focused to small spots spaced half an acoustic wavelength apart on the substrate surface. Upon reflection the beams, now slightly out of phase due to the wave-induced differential path length difference, recombine to form a shifted optical interference pattern. This pattern is spatially filtered and the filter output is optically detected. Assuming small SAW amplitudes, point focusing and correct point separation, the instantaneous detected signal power is

$$P_s = \frac{\alpha P_i}{2} - \frac{4\alpha P_i \Delta L}{\lambda} , \tag{8}$$

where P_i is the total incident laser power, α is the sensitivity (ampere/watt optical power) of the optical detector, λ is the optical wavelength, and ΔL is half the instantaneous path length difference. For a CW wave, $\Delta L = \Delta L_0 \cos \omega_a t$, where ΔL_0 is the peak wave amplitude and ω_a is the acoustic radian frequency. The resulting ac term in (8) then is proportional to ΔL_0 and the normal component of particle motion at the location of the focused beams [16]. Interface wave attenuation and velocity are determined by comparing optical measurements of input and output waves. Optical system sensitivity allows the narrowband detection of 0.01 Angstrom interface wave amplitudes [16].

CONCLUSIONS

This research demonstrates the potential of using interface wave techniques for the evaluation of polymer-metal boundaries, especially those in adhesively bonded structures. It is recognized that surface conditions and the viscoelastic properties of the interface region are the most critical factors in ultrasonically determining the mechanical boundary behavior. Measurements of interface wave attenuation as a function of boundary surface roughness and velocity as a function of polymer compression indicate that the technique is sensitive to changes in both interfacial conditions and internal polymer layer properties. Remote nondestructive measurements of the curing of polymer adhesives using this experimental method suggest its application in bond strength determination in high-strength adhesive systems. Further attention now should be directed toward assessing the effects of chemical surface contamination on interface wave propagation observables.

ACKNOWLEDGMENTS

This research has been partially supported by NSF Grant ECS-7925340 and NASA Grant NAG-1-68. The author would like to thank C. H. Palmer, R. A. Kline, and S. Rokhlin for useful discussions and Summers Laboratories, Inc., Fort Washington, PA, for supplying MILBOND polymer adhesives.

BIBLIOGRAPHY

[1] R. Stoneley, "Elastic waves at the surface of separation of two solids," Proc. Roy. Soc. 106, 416 London (1924).

[2] W. L. Pilant, "Complex roots of the Stoneley wave equation," Bull. Seismol. Soc. Am. 62, 285(1975).

[3] G. S. Murty, "Wave propagation at an unbounded interface between two elastic half-spaces," J. Acoust. Soc. Am. 58, 1094(1975).

[4] A. R. Banghar, G. S. Murty, and I. V. V. Raghavachargulu, "On the parametric model of loose bonding of elastic half spaces," J. Acoust. Soc. Am. 60, 1071(1976).

[5] S. I. Rokhlin and M. Rosen, "New ultrasonic method for measuring the shear modulus of thin interface films," Proc. IEEE Ultrasonics Symposium (Boston, MA), Oct. 1980.

[6] D. A. Lee and D. M. Corbly, "Use of interface waves for nondestructive inspection," IEEE Trans. Sonics Ultrason. SU-24, 206(1977).

[7] R. O. Claus and C. H. Palmer, "Optical measurements of ultrasonic waves on interfaces between bonded solids," IEEE Trans. Sonics Ultrason. SU-27, 97(1980).

[8] K. Sezawa and K. Kanai, "The range of possible existence of Stoneley waves and some related problems," Bull. Earthquake Res. Inst. 17, 1(1939).

[9] J. G. Scholte, "The range of existence of Rayleigh and Stoneley waves," R. Astron. Soc. London Monthly Notices Geophys. Suppl. 5, 120(1947).

[10] S. I. Rokhlin, J. Acoust. Soc. Am. 67, 1157(1980).

[11] R. O. Claus and R. T. Rogers, "Waves guided by a thin visoelastic layer between elastic solids," Proc. IEEE Ultrasonics Symp. (Chicago, IL), October 1981.

[12] T. M. Turner and R. O. Claus, "Pulse-echo interface wave characterization of bolted plates," Proc. IEEE Region 3 Conf. (Huntsville, AL), April 1981.

[13] H. A. Kuhn and C. L. Downey, "Deformation characteristics and plasticity theory of sintered powder materials," Intl. J. of Powder Metallurgy 7, 15(1971).

[14] R. O. Claus, "Attenuation of ultrasonic interface waves on metal-polymer-metal boundaries," Seventh Intl. Conf. on Internal Friction and Ultrasonic Attenuation in Solids (Lausanne, Switzerland), July 1981.

[15] S. I. Rokhlin, M. Hefets, and M. Rosen, "Elastic interface wave guided by a thin film between two solids," J. Appl. Phys. 51, 3579(1980).

[16] R. O. Claus and C. H. Palmer, "Direct measurement of ultrasonic Stoneley waves," Appl. Phys. Lett. 31, 547(1977).

FIGURE TITLES

Figure 1. Multilayer boundary geometry.

Figure 2. Generation and detection of 2.1 MHz ultrasonic interface waves along the polymer layer between aluminum and titanium substrates.

Figure 3. Pitch-catch (a) and pulse-echo (b) interface wave scans of a 6.35 mm diameter hole in a metal-polymer-metal boundary.

Figure 4. Pitch-catch attenuation caused by a 6.35 mm diameter flat bottomed hole.

Figure 5. Attenuation of CW interface waves versus average diameter of abrasive particle size.

Figure 6. Geometry for compressive stress loading of polymer adhesive film.

Figure 7. Ultrasonic interface wave velocity modulation due to dc stress applied to polymer layer between metal substrates (a) and hysteresis caused by stress cycling (b).

Figure 8. Differential interferometric optical system for the detection of ultrasonic interface waves.

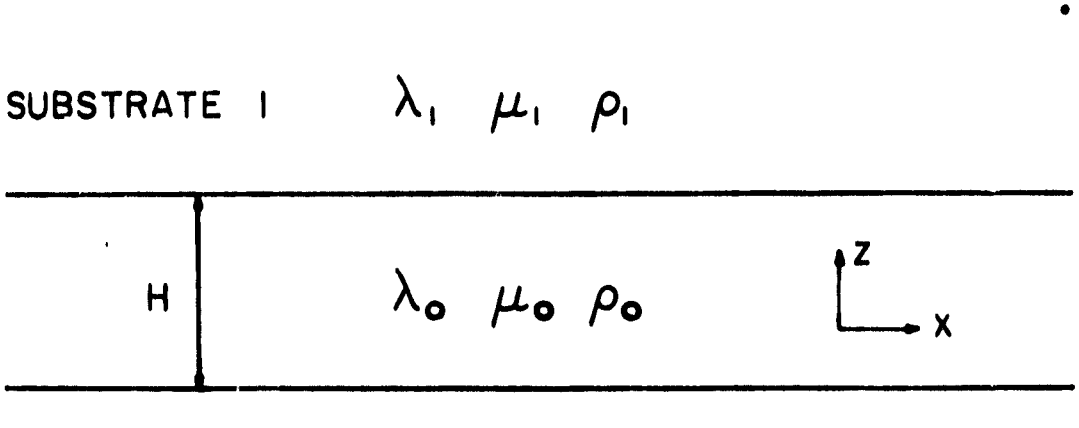
SUBSTRATE 1
λ_1 μ_1 ρ_1
H
λ_0 μ_0 ρ_0
Z
X
SUBSTRATE 2
λ_2 μ_2 $\rho_2 > \rho_1$

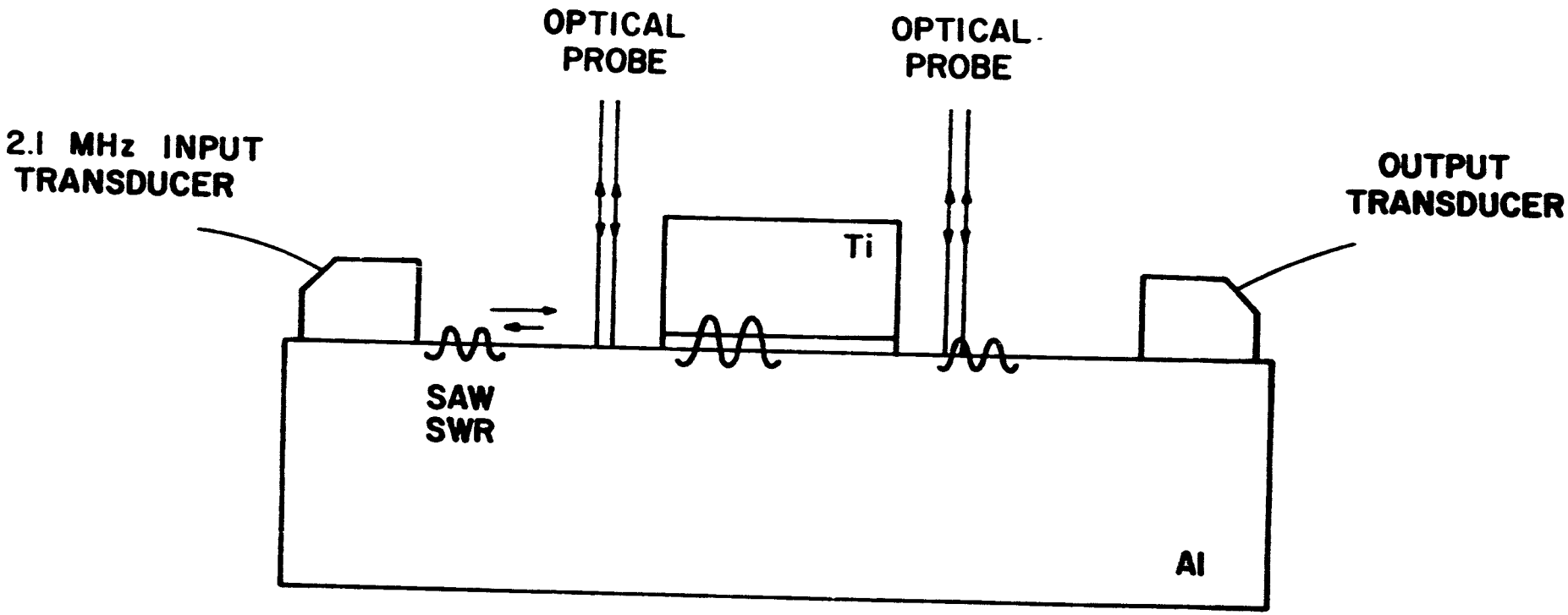
OPTICAL
PROBE
OPTICAL
PROBE
2.1 MHz INPUT
TRANSDUCER
OUTPUT
TRANSDUCER
Ti
SAW
SWR
Al

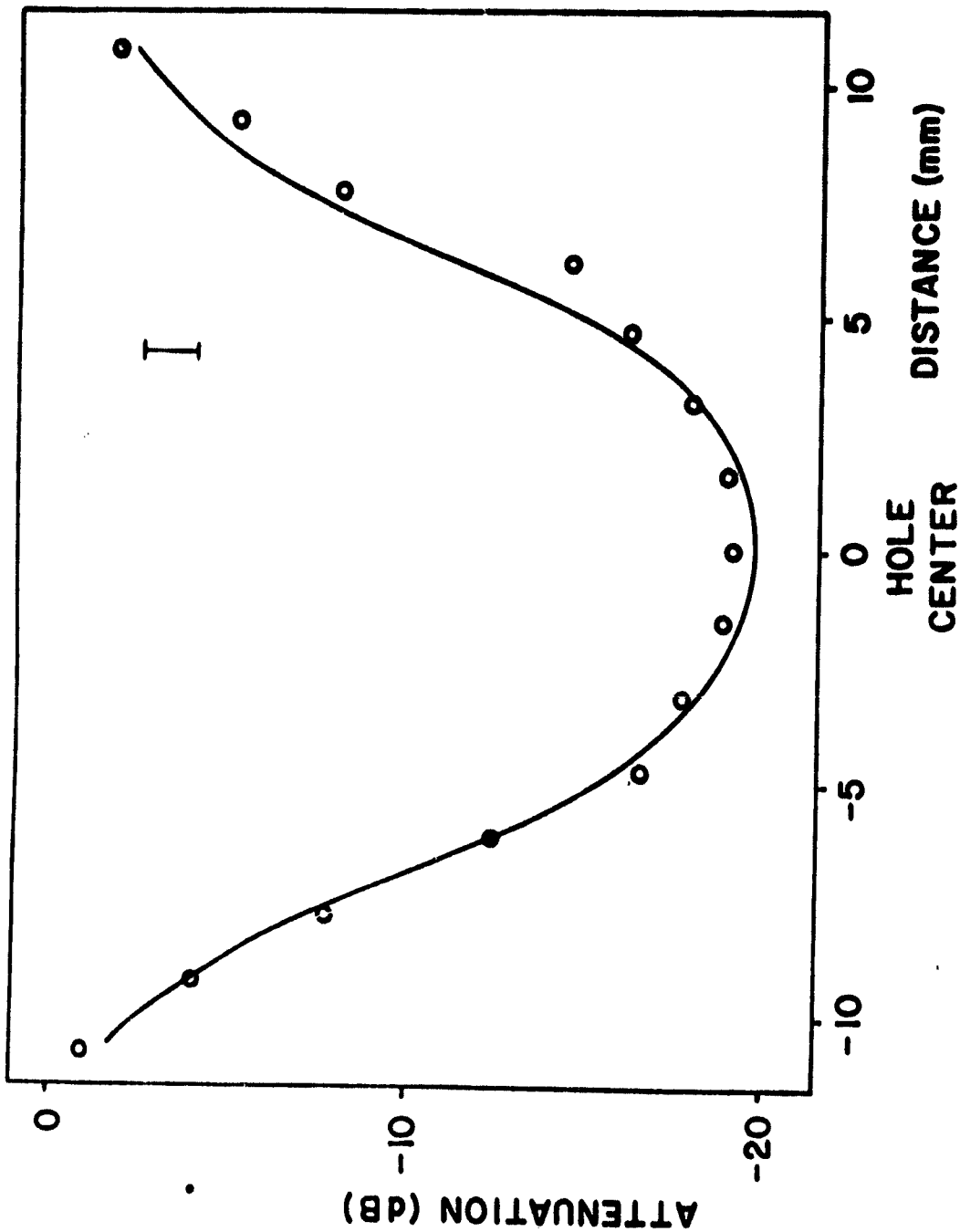
ATTENUATION (dB)
0
-10
-20
-10
-5
0
5
10
HOLE CENTER
DISTANCE (mm)

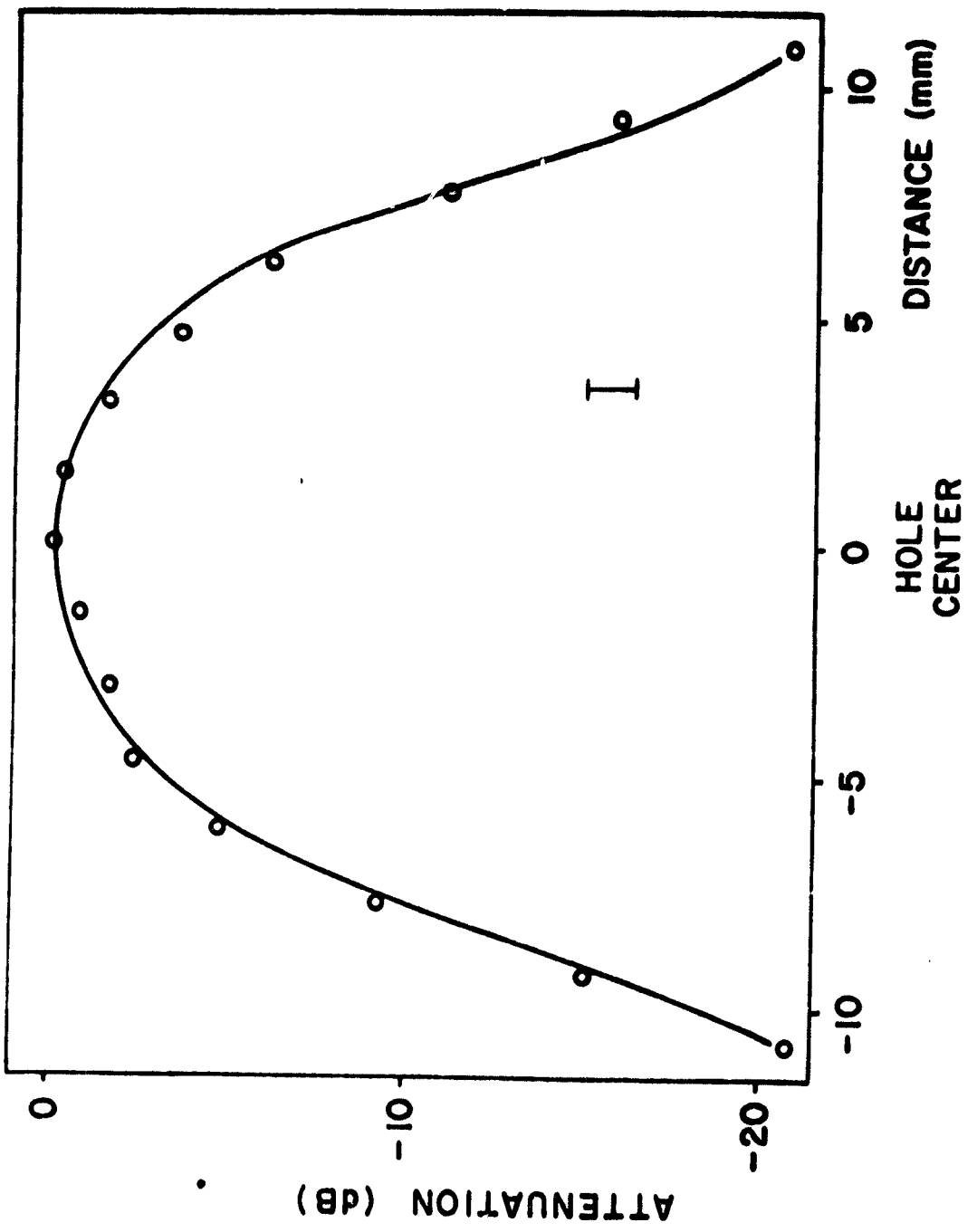
ATTENUATION (dB)
0
-10
-20
-10
-5
0
5
10
HOLE CENTER
DISTANCE (mm)

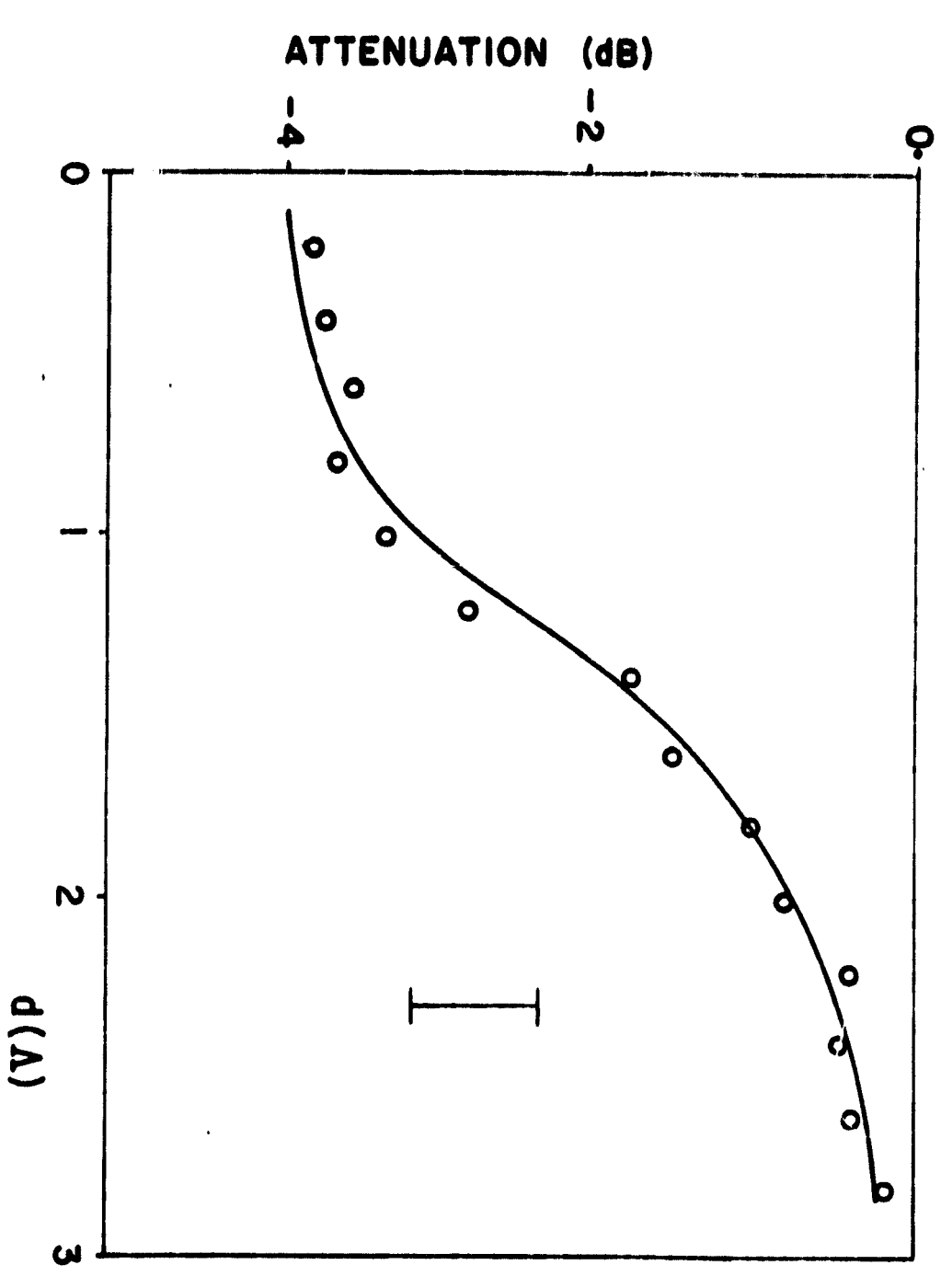
ATTENUATION (dB)
-4
-2
0
0
1
2
3
d(V)

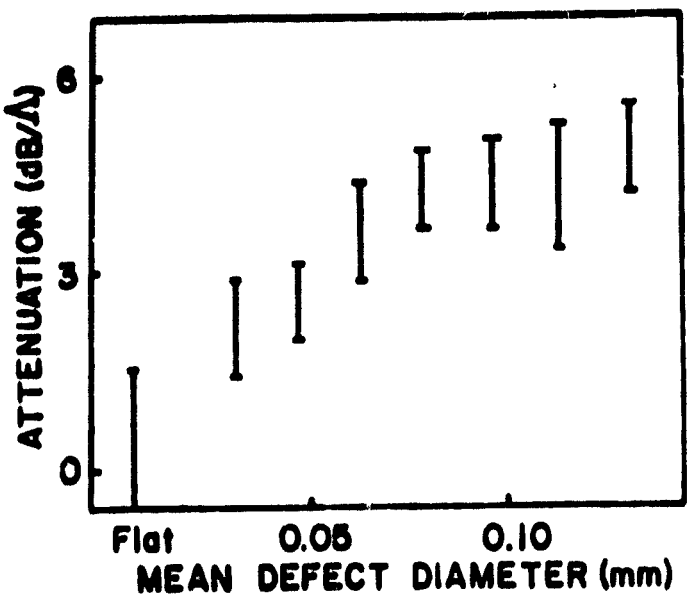
ATTENUATION (dB/A)
6
3
0
Flat
0.05
0.10
MEAN DEFECT DIAMETER (mm)

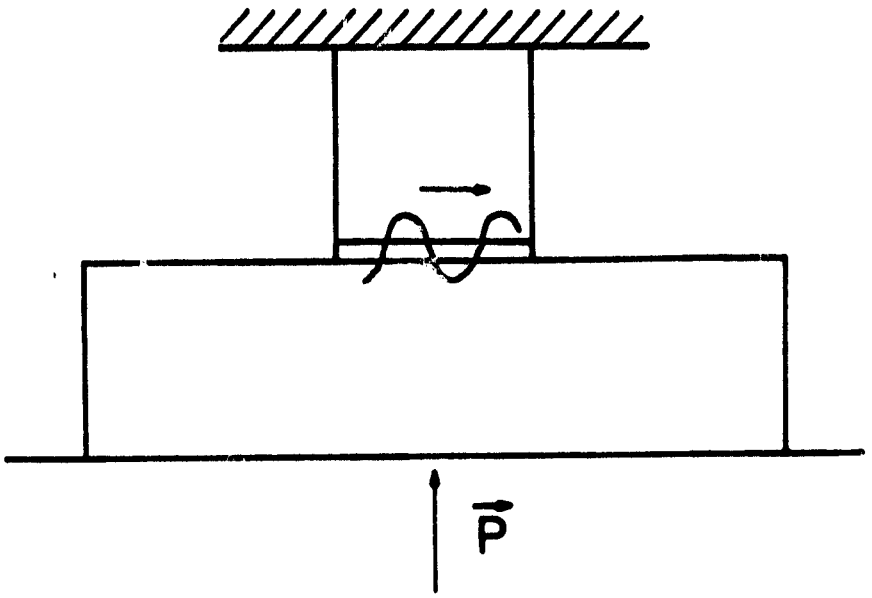
P

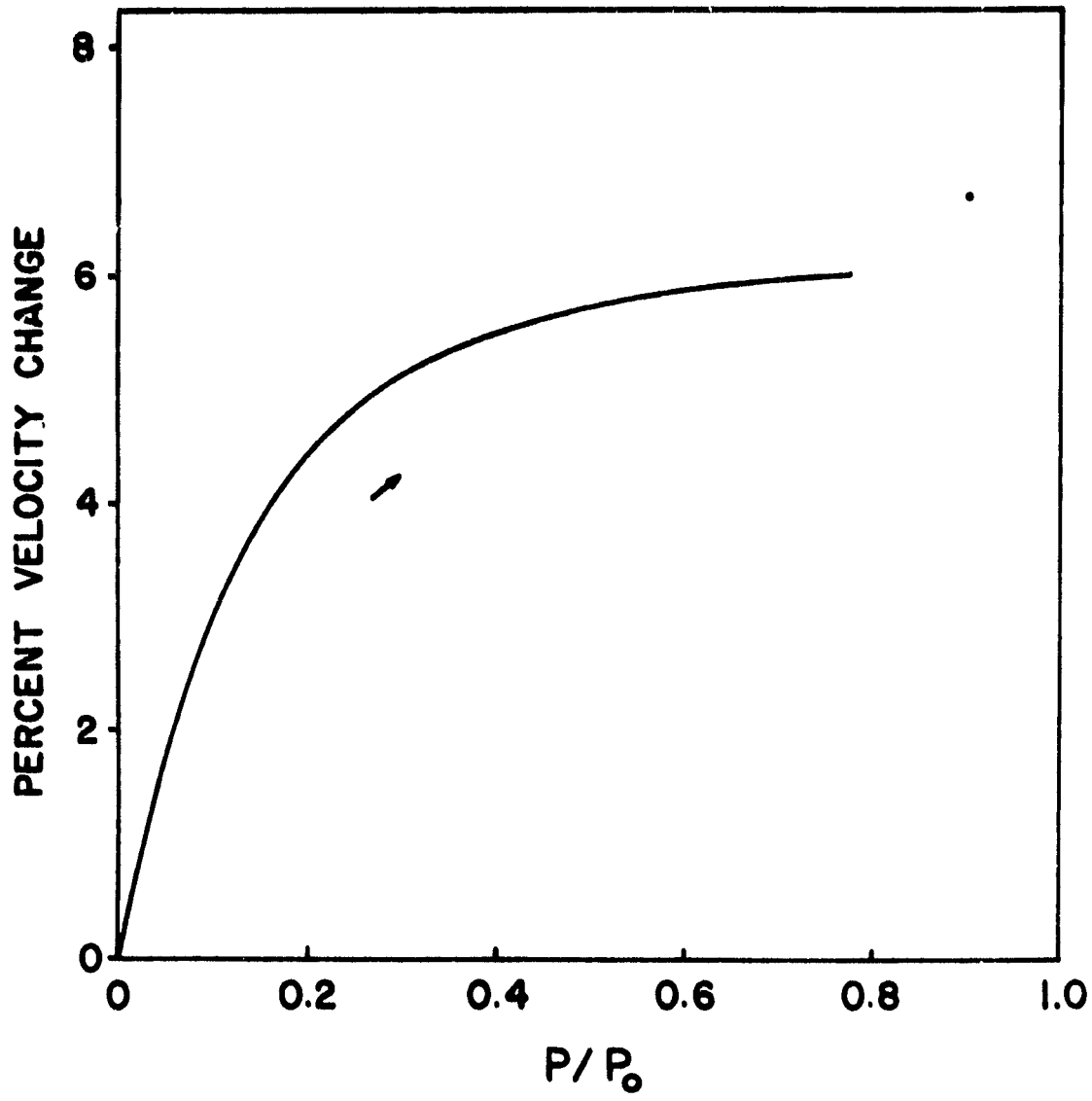
PERCENT VELOCITY CHANGE
8
6
4
2
0
0
0.2
0.4
0.6
0.8
1.0
P/ P₀

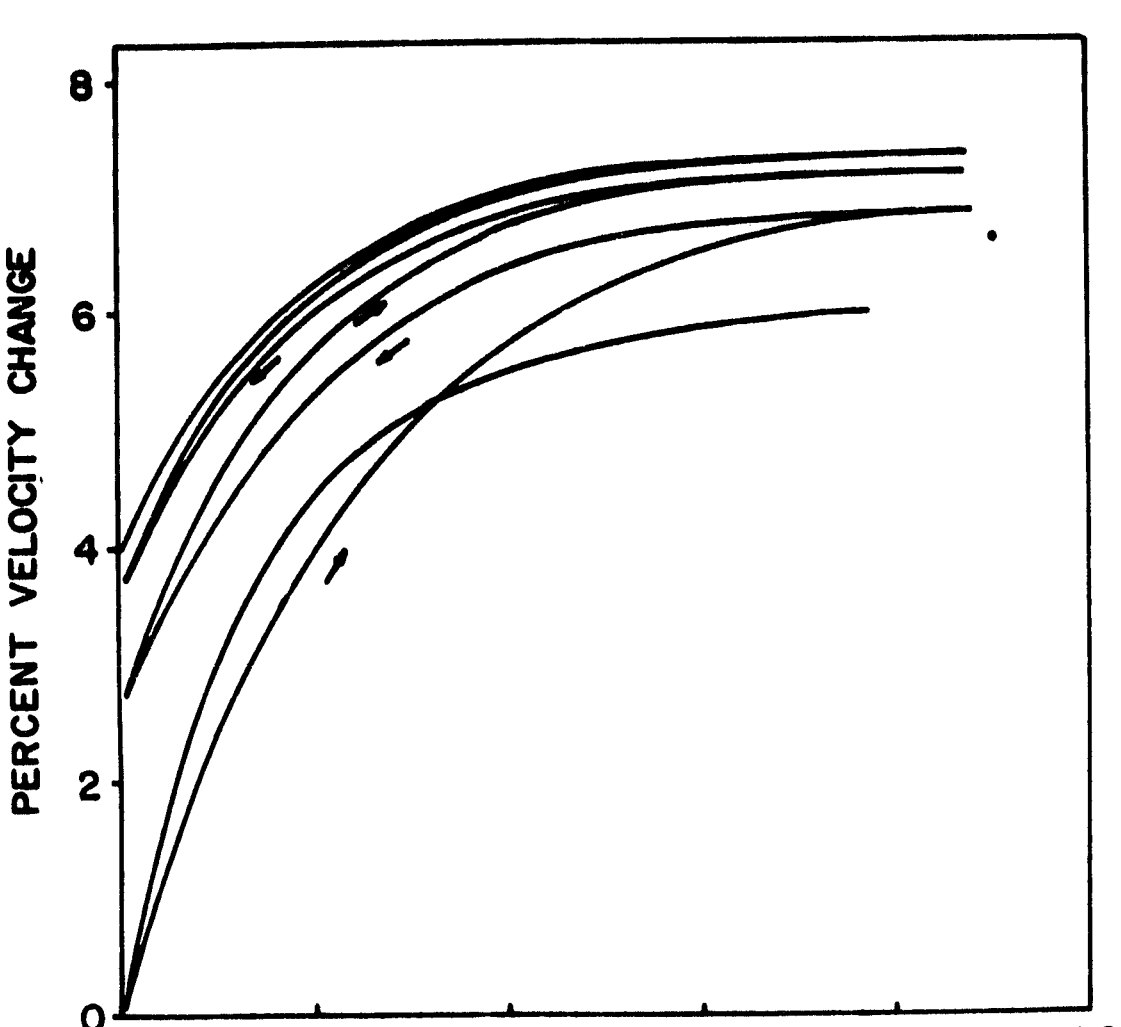
PERCENT VELOCITY CHANGE
8
6
4
2
0
0
0.2
0.4
0.6
0.8
1.0
P/P$_o$

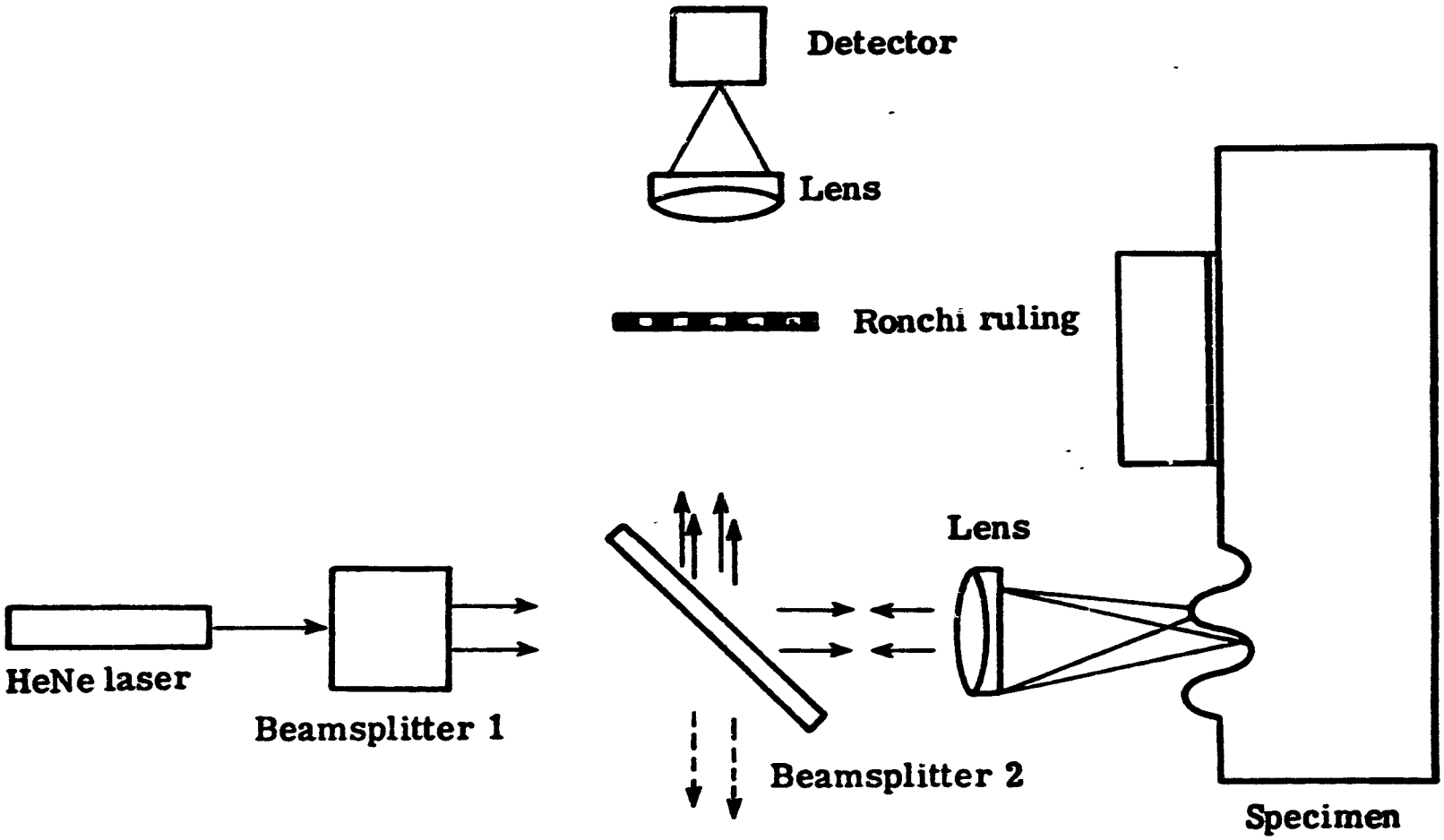
Detector
Lens
Ronchi ruling
Lens
HeNe laser
Beamsplitter 1
Beamsplitter 2
Specimen

R. O. Claus and R. T. Rogers, "Waves Guided by a Thim Viscoelastic Layer Between Elastic Solids," Proc. 1981 IEEE Ultrasonics Symposium (Chicago, IL), Oct. 1981.

WAVES GUIDED BY A THIN VISCOELASTIC LAYER BETWEEN ELASTIC SOLIDS

Richard O. Claus and Robert T. Rogers

Department of Electrical Engineering
Virginia Polytechnic Institute and State University
Blacksburg, VA 24061

Abstract

The propagation of ultrasonic waves guided along a viscoelastic layer which separates two dissimilar elastic solid half-spaces is described. Layer and half-space wave potential solutions to the general eight-by-eight determinant equation obtained by satisfying stress and displacement boundary conditions at both layer-substrate interfaces are determined as functions of layer thickness and elastic constants. For the limiting cases of rigid and soft bonding by a layer thin compared to acoustic wavelength, Stoneley and independent Rayleigh wave characteristic equations, respectively, result. For combinations of layer rigidity and wave-length that correspond to guided wave propagation, external cyclic loading of the layer produces mechanical hysteresis and a resulting dynamic change in bond properties. Experimental measurements of the observed velocity hysteresis in an aluminum-polymer adhesive-aluminum system are described and potential applications in nondestructive bond characterization are indicated.

1. Introduction

Ultrasonic waves which propagate along the interface between two materials have been suggested as a potential tool in the nondestructive evaluation of adhesively bonded solids and layered structural media. Unlike ultrasonic bulk waves used in localized transmission or reflection bond inspection techniques, interface waves can propagate along the boundary and integrate the effects of bond structure over a long pathlength prior to detection. As a function of propagation distance, several interface wave observables may vary depending upon the thickness of the adhesive bond, the structural integrity of the bond, and local elastic constants of the bond and substrate materials. Specifically, interface wave amplitude may be attenuated and a redistribution of wave energy into components of particle motion normal and parallel to the boundary may occur. In this paper, interface wave velocities are derived for several pairs of media substrates, particle displacements versus depth into each substrate are shown for several media combinations and bond thicknesses, and qualitative experimental results which indicate a change in interface wave velocity due to a change in bond ness and density are presented.

2. Theory

Elastic particle waves which have energy confined to the thin region on either side of a material boundary may exist for a wide range of substrate pairs. Stoneley first considered unattenuated waves of this type [1] and the literature which describes these classical Stoneley waves and similar generalized attenuating waves with complex speeds is extensive [2]. Recently, several authors have detected interface wave modes using ultrasonic and optical imaging techniques [3,4,5].

Consider the ideal material bond geometry between the substrates shown in Figure 1. The dilatational and shear wave displacement potentials may be expressed here as

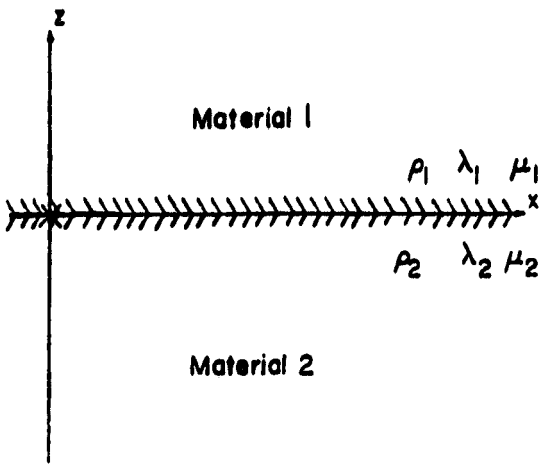

Figure 1. Material boundary coordinate geometry.

$$\begin{aligned} \phi_1 &= \exp(-kA_1 x + ikz - i\omega t), \\ \psi_1 &= \exp(-kB_1 x + ikz - i\omega t), \\ \phi_2 &= \exp(kA_2 x + ikz - i\omega t), \\ \psi_2 &= \exp(kB_2 x + ikz - i\omega t), \end{aligned} \tag{1}$$

Reprint 1981 IEEE Ultrasonics Symposium (Chicago, IL).

where

$$A_{1,2} = \pm (1 - c^2/a_{1,2}^2)^{\frac{1}{2}},$$

$$B_{1,2} = \pm (1 - c^2/b_{1,2}^2)^{\frac{1}{2}}, \qquad (2)$$

$$c = \omega/k,$$

and $a_{1,2}$ and $b_{1,2}$ are the dilatational and shear wave speeds in media 1 and 2, respectively. From (1), the displacements in both materials may be expressed as

$$u_{1,2} = \frac{\partial \phi_{1,2}}{\partial x} + \frac{\partial \psi_{1,2}}{\partial z},$$

$$w_{1,2} = \frac{\partial \phi_{1,2}}{\partial z} + \frac{\partial \psi_{1,2}}{\partial x}, \qquad (3)$$

and the displacement and stress continuity equations at the boundary become

$$u_1 = u_2$$

$$w_1 = w_2$$

$$\mu_1 \left(\frac{\partial w_1}{\partial x} + \frac{\partial u_1}{\partial z} \right) = \mu_2 \left(\frac{\partial w_2}{\partial x} + \frac{\partial u_2}{\partial z} \right) \qquad (4)$$

$$\lambda_1 \left(\frac{\partial u_1}{\partial x} + \frac{\partial w_1}{\partial z} \right) + 2\mu_1 \frac{\partial w_1}{\partial z} = \lambda_2 \left(\frac{\partial u_2}{\partial x} + \frac{\partial w_2}{\partial z} \right) + 2\mu_2 \frac{\partial w_2}{\partial z}.$$

By substituting (1) and (3) into (4) we obtain

$$c^4(\rho_1 - \rho_2)^2 - (\rho_1 M_2 + \rho_2 M_1)(\rho_1 N_2 + \rho_2 N_1))$$
$$+ 2Pc^2(\rho_1 M_2 N_2 - \rho_2 M_1 N_1 - \rho_1 + \rho_2) \qquad (5)$$
$$+ P^2(M_1 N_1 - 1)(M_2 N_2 - 1) = 0,$$

where

$$M_{1,2} = (1 - c^2/a_{1,2}^2)^{\frac{1}{2}},$$

$$N_{1,2} = (1 - c^2/b_{1,2}^2)^{\frac{1}{2}}, \text{ and}$$

$$P = (\rho_1 b_1^2 - \rho_2 b_2^2).$$

Solutions to (5) have been investigated by several authors [2]. Speed solutions for the media pairs we have used for experimental measurements are given in Table 1 where, following Lee and Corbly, speeds rather than propagation constants are expressed in complex notation for attenuating interface wave modes [3]. From these speeds and (3) the particle displacement profiles on either side of the x-y plane in Figure 1 may be derived and they differ for materials which support unattenuated Stoneley waves and leaky waves. Such a difference in displacements normal to the boundary is shown for steel/titanium and steel/aluminum specimens in Figure 2.

TABLE 1

Materials	Interface Wave Speed (m/sec)
Steel/Aluminum	$3.148 \times 10^5 - j724$
Steel/Titanium	3.209×10^5
Aluminum/Titanium	$3.254 \times 10^5 - j2.491 \times 10^3$
7740 Pyrex/Nickel	2.974×10^5
Fused Quartz/Nickel	3.240×10^5

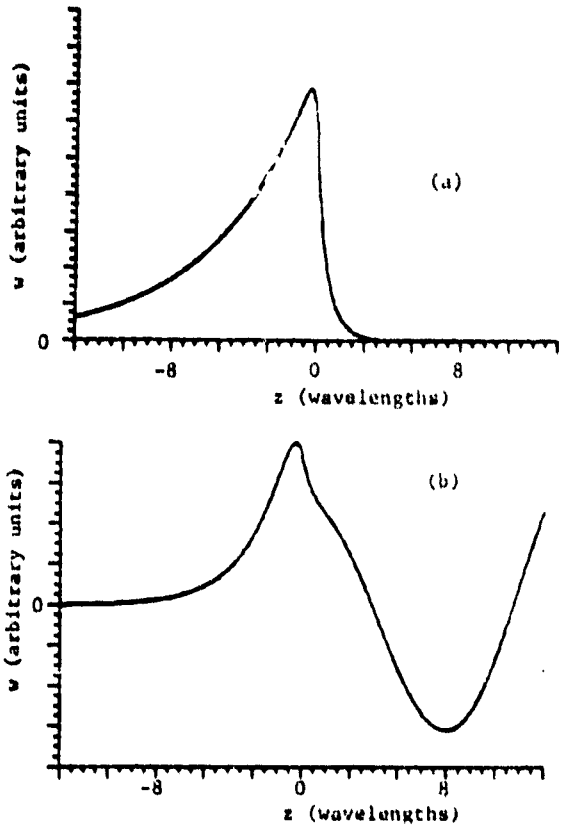

Figure 2. Components of particle motion normal to (a) steel/titanium and (b) steel/aluminum boundaries. Arbitraty units on vertical axis may be normalized to any value of initial interface wave amplitude.

For the three media geometry shown in Figure 3 displacement profiles vary with intermediate layer thickness H and the elastic constants of all three materials. Assuming that an interface wave mode is excited at one layer/substrate boundary and that reflection/transmission continuity of wave components at the other boundary is satisfied, particle displacements and the beat length of guided wave mode energy transfer from one surface to the other may be determined. The component of particle motion in the z-direction at one value of x for the real wave speeds on a steel/titanium/steel specimen and complex speeds on steel/titanium/aluminum are shown in Figure 4.

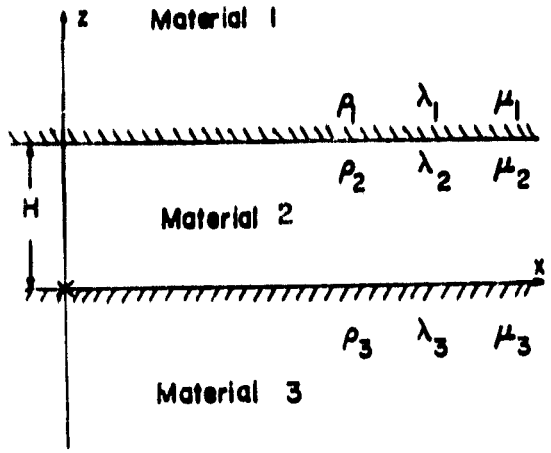

Figure 3. Bonded Three Material Geometry.

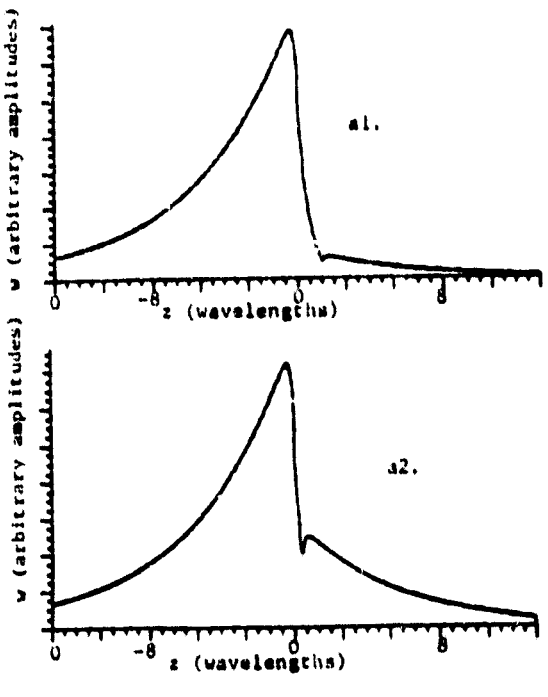

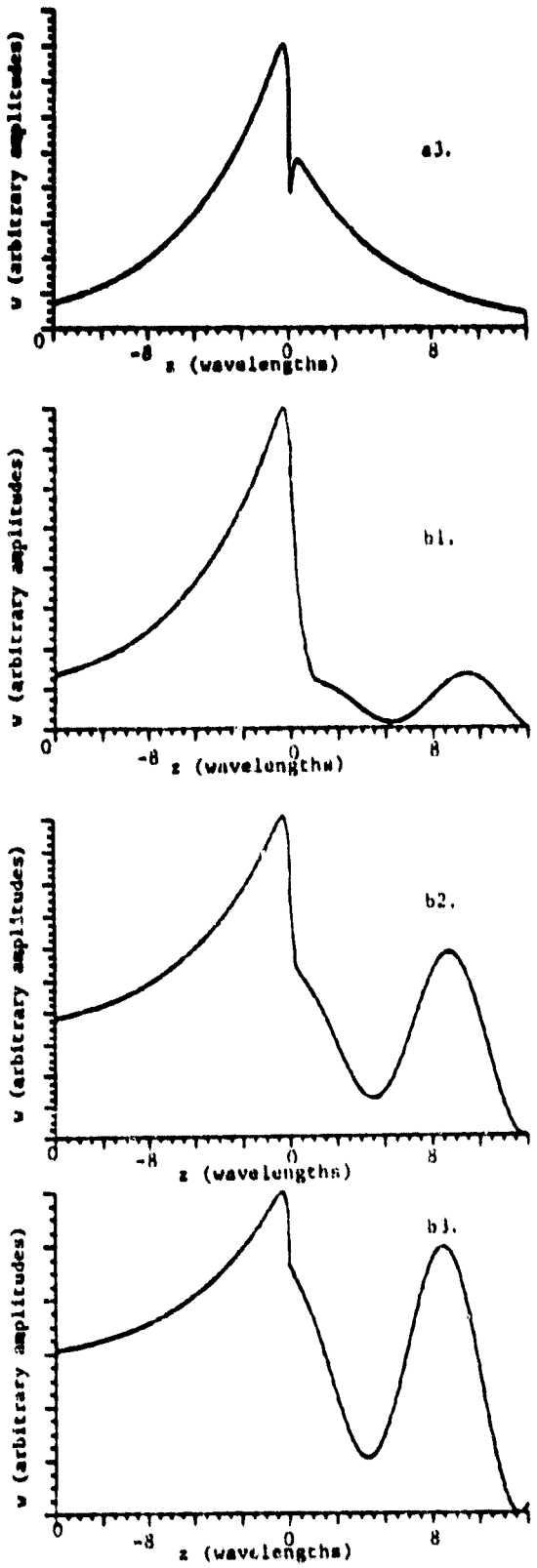

Figure 4. Components of particle motion normal boundry for (a) steel/titanium/steel and (b) steel/titanium/aluminum for H = (1) 6.8, (2) 1.9, and (3) 0.3 wavelenths.

3. Measurements

For practical measurements of interface waves on bonded solids, the above theory may be applied to solid/adhesive/solid systems where the adhesive is considered to be a viscoelastic material [6]. From (5), internal layer and boundary properties may be characterized by observing interface wave velocity shifts caused by changes in layer structure. Such changes have been produced in several ways and the resulting shifts monitored. First, both external dc and cycled compressive stress loads were applied to the polymer adhesive layer between metal samples such that the maximum applied load was eighty percent of the lower yield stress of the two substrates. Assuming that the surfaces under compression behave as randomly arranged molecular powders, the layer densities may be modeled by

$$\rho_{polymer} = \rho_0[P/P_0]^{-a}, \qquad (6)$$

where ρ_0 is the density in the unstressed state, P is the applied stress, P_0 is the yield stress, and a is a constant determined by the material. The change in ρ with a static load P increases wave velocity through (5) as shown in Figure 5 [3]. If the load is repetitively cycled from zero to P to zero again, hysteresis is observed. For a ramped load cycle of 0.1 Hz the velocity hysteresis also shown in Figure 5 is obtained. The rate of decay of the stored energy per cycle in this reaction may be directly related to material compression [8] and shear modulus modulation [5] in the layer. Finally, similar effects due to crosslinking have been observed by allowing a thin film of polymer adhesive between metal substrates to cure while monitoring the velocity of the transmitted wave[7].

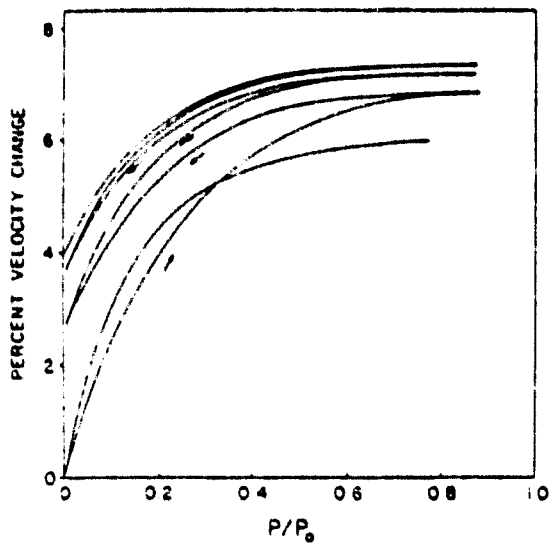

Figure 5. Change in interface wave speed produced by cyclic loading of polymer adhesive between aluminum and titanium plates.

4. Results

Interface wave speeds and particle displacement profiles have been derived for several bonded media geometries. A simple nonlinear model of polymer bond density qualitatively agrees with observed hysteresis and changes in guided wave speed as applied compressive stress is cycled.

5. Acknowledgements

Part of this research has been supported by the National Science Foundation Grant ECS-79-25340 and NASA Grant NAG-1-68.

References

[1] R. Stoneley, "Elastic waves at the surface of separation of two solids," Proc. Roy. Soc. 106, 416 (London, 1924).

[2] R. N. Thurston, "Elastic waves in rods and clad rods," J. Acoust. Soc. Am. 64, 1 (1978).

[3] D. A. Lee and D. M. Corbly, "Use of interface waves for nondestructive inspection," IEEE Trans. Sonics Ultrason. SU-23, 206 (1977).

[4] R. O. Claus and C. H. Palmer, "Optical measurements of ultrasonic waves on interfaces between bonded solids," IEEE Trans Sonics Ultrason. SU-27, 97 (1980).

[5] S. I. Rokhlin and M. Rosen, "New ultrasonic method for measureing the shear modulus of thin interface films," Proc. 1980 IEEE Ultrason. Symp. (Boston, MA).

[6] R. O. Claus and R. T. Rogers, in press.

[7] R. O. Claus, "Characterization of metal-polymer boundaries using Stoneley and leaky waves," Am. Chem. Soc. Mtg. (New York, NY), August 1981.

[8] R. O. Claus, "Attenuation of ultrasonic interface waves on metal-polymer-metal boundaries," Seventh Intl. Conf. on Internal Friction and Ultrason. Attenuation in Solids (Lausanne, Switzerland), July 1981.

APPENDIX C

Gaussian Profile Ultrasonic Transducer

P. S. Zerwekh and R. O. Claus, "Ultrasonic Transducer with Gaussian Radial Velocity Distribution," Proc. 1981 IEEE Ultrasonics Symposium (Chicago, IL), Oct. 1981.

AN ULTRASONIC TRANSDUCER WITH GAUSSIAN RADIAL VELOCITY DISTRIBUTION

P. S. Zarookh and R. O. Claus

Department of Electrical Engineering
Virginia Polytechnic Institute and State University
Blacksburg, Virginia 24061

Abstract

In materials evaluation applications requiring the interrogation of modified far field patterns of an ultrasonic transducer, it is desirable to use a transducer which produces a beam with a Gaussian profile. A transducer with a velocity profile which is Gaussian as a function of radius and independent of angle is described. The transducer has been constructed by depositing a circularly symmetric metallic multi-electrode array on a 19.1 mm diameter x-cut quartz disk. Each electrode is independently connected to an impedance network optimized to produce the Gaussian distribution with less than two percent maximum error. A computer aided electrode design and calibrated three dimensional interferometric optical and ultrasonic measurements of the far field distribution are presented.

1. Introduction

The simplified theoretical analysis of several bulk ultrasonic phenomena require the consideration of bounded ultrasonic beams having velocity distributions which are Gaussian as a function of radius [1]. Additionally, since the beam profiles in the near and far field regions are related by a Fourier transform operation, Gaussian profile beams are particularly useful in experimental situations in which a similarity between near and far field patterns is desired. A standard surface contact transducer, however, typically generates a field which is nearly uniform in the region of contact and negligible elsewhere. The resulting far field pattern thus contains significant sidelobe maxima which may be difficult to distinguish from the central beam in experiments involving beam translation and attenuation, or multiple beams produced by beam scattering.

Several transducer designs employing single electrodes of various shapes have been designed to provide a field which, when averaged around the radii is a Gaussian function of radius [2-4]. These electrode patterns, however, introduce a distribution that is a function of angular displacement on the face of the transducer and not purely a function of radius. Breazeale has described a method for generating a velocity distribution which is Gaussian in one dimension utilizing multiple linear electrodes [5].

This report describes the design and construction of a circular x-cut quartz transducer with multiple, optimally placed, concentric ring electrodes which produce a Gaussian radial electric field and thereby induce a similar velocity distribution.

2. Electrode Design

An electric field distribution which is exclusively a function of radius may be produced by a set of concentric annular electrodes. If the circumference of the rings is large with respect to the spacing between sucessive electrodes, the electric field in the gaps may be considered to be a linear function of radius. From this model, a piecewise linear function which approximates a Gaussian may then be generated on the face of the piezoelectric crystal by placing the proper voltages on the electrodes. The degree to which this function fits the desired Gaussian is determined by the width of each electrode ring, the number of electrodes, and the distribution of the electrode radii on the radius of the transducer crystal. Since the desired Gaussian voltage function attains a particular value at only one mathematical point, the electrode width should tend to zero. The photo-etching techniques used in our transducer construction, however, require a minimum electrode width of approximately 0.5 mm. The degree of fit to the desired Gaussian shape may also be improved by using a large number of electrodes, but this requires that the interelectrode spacing be small, thereby increasing the possibility of electrical breakdown between adjacent rings when high voltages are applied. It was found, however, that with as few as 5 electrodes the mean absolute fit error may be reduced to less than 1.5 percent of the peak. Since the radii of the rings are the variables over which the greatest control may be exercised during design, an iterative computer routine to minimize absolute error by optimizing electrode placement was used. Optimization program output is shown in Figure 1.

Preprint, 1981 IEEE Ultrasonics Symposium (Chicago, IL.)

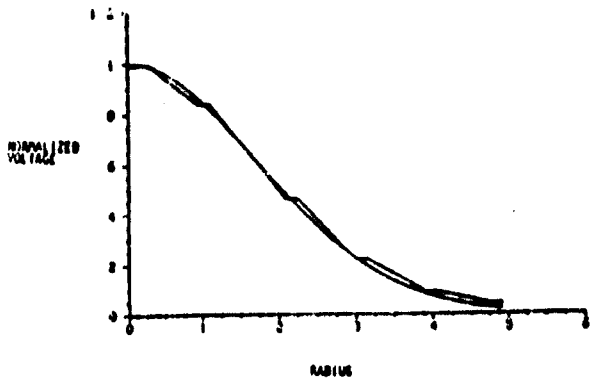

Figure 1 - Computer Fit Optimization

3. Transducer Construction

The designed electrode pattern was photoetched into a layer of chromium/gold on a 2.25 MHz circular x-cut quartz transducer. The capacitance between the electrodes and the wear plate ground plane was calculated and later empirically verified to be less than 2 picofarads, giving rise to negligable reactive impedance at the 2.25 MHz operating frequency. Since this is low, a simple resistive network may be used to fix the desired set of electrode voltages.

Figure 2a shows the construction details of the actual transducer. Leads were attached to the electrodes using a conductive adhesive and a dome of epoxy was applied to the electrode side of the crystal to provide mechanical support for the leads and to attenuate and disperse resonant surface wave modes. Further damping is accomplished by a thin semi-viscous layer of electrically conductive adhesive placed on the opposite uncoated side of the transducer disk and under a thin aluminum foil electrode/wear plate as shown in Figure 2b. The electrode leads were connected to the resistive network and coaxial cable and the entire transducer assembly was placed in a 1.3 cm inner diameter cylindrical PVC case and potted in filler-loaded epoxy.

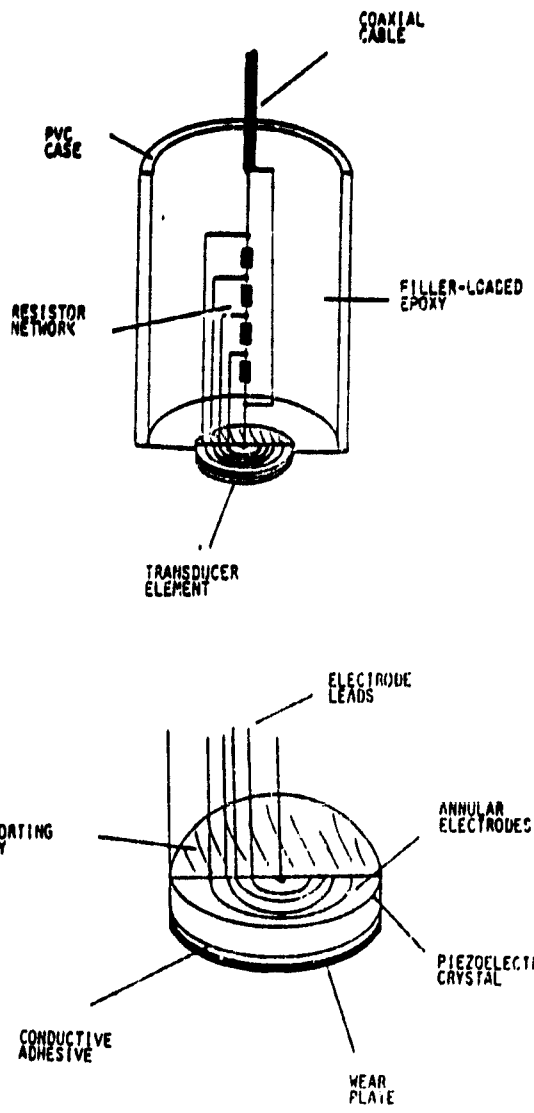

Figure 2 - Transducer Construction Details

4. Transducer Performance

The beam profile of the prototype transducer was measured using both ultrasonic and acousto-optical techniques. First, quantitative measurements were made by scanning the field distribution generated in a water tank using an aperture-stopped Harisonics G 0204 piezoelectric detecting transducer. The 6.35 mm diameter of the transducer was effectively reduced by placing an aperture mask in front of it. The mask was constructed with a diameter of 2 millimeters using metal foil coated with 2-3 mm of soft wax. Measurements were made in the tank with the receiver 4, 20, and 40 cm from the prototype. The data from these measurements is shown in Figure 3.

Second, the beam profile was scanned by translating the sample arm of a Michelson interferometer with respect to the transducer face and measuring the integrated index of refraction modulation produced by the beam. Since, for small modulation indices, index, density, and pressure are proportional, the data shown in Figure 4 indicates the pressure profile of the transducer [6,7].

5. Conclusion

An ultrasonic transducer which generates a Gaussian radial velocity distribution has been designed, constructed, and tested. Although beam divergence occurs, the far field distribution retains its Gaussian shape and sidelobe maxima are not detectable.

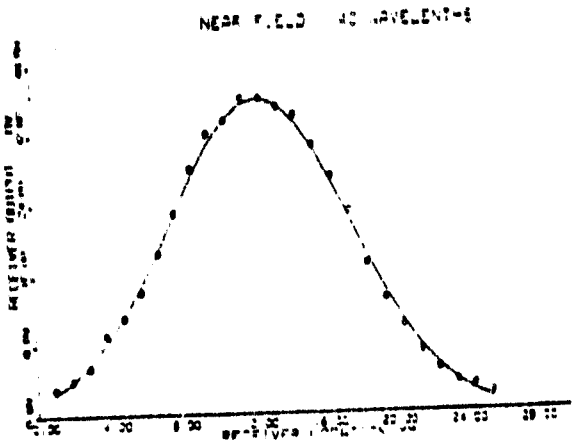

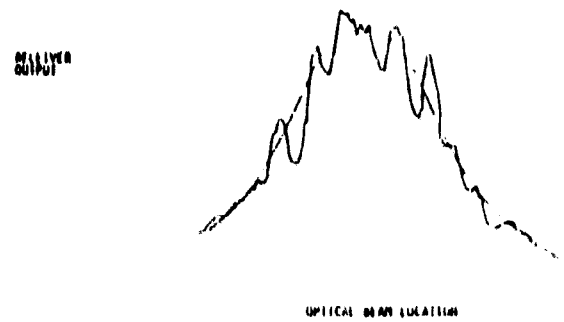

Figure 4 - Acoustooptical Scan Data

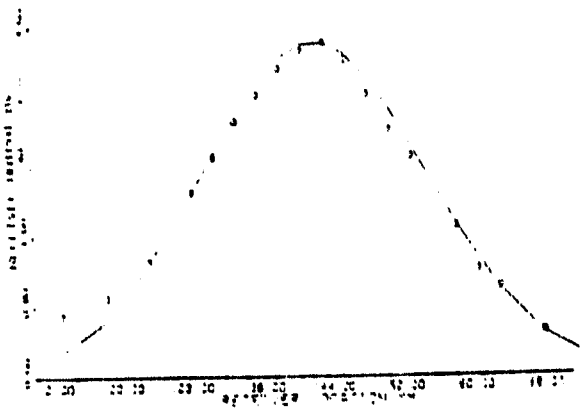

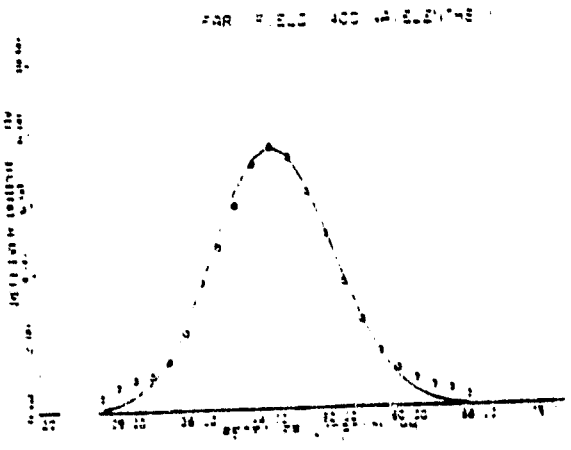

Figure 5. Ultrasonic Data

6. Acknowledgements

This work has been supported by NASA Grant NAG-1-68 and NSF Grant ECS-7925340. The authors wish to thank John H. Cantrell, Jr., for valuable discussions.

7. References

[1] W. Sachse and N.N. Hsu, "Ultrasonic transducers for materials testing and their characterization," in Physical Acoustics, Vol. 14, W.P. Mason and R.N. Thurston, eds., Academic Press (New York), 1979.

[2] K. von Haselberg and J. Krautkramer, "Ein Ultraschall-Strahler fur die werkstoffprufung mit verbesserten nahfeld," Acustica 9,359(1959).

[3] J. L. Rose, "Ultrasonic Field analysis and approximation parameters," Br. Journal of Nondestructive Testing 17,109 (1975).

[4] L. Filipczynski and J. Etienne, "Theoretical study and experiments on spetical focusing transducers with Gaussian surface velocity distribution," Acustica 28, 121(1973).

[5] F. D. Martin and M. A. Breazeale, "A simple way to eliminate diffraction lobes emmitted by ultrasonic transducers," J. Acoust. Soc. Am. 49, 1668 (1971).

[6] D. W. Sweeney and C. M. Vest, "Reconstruction of three-dimensional refractive index fields from multidirectional interferometric data," Applied Optics 12, 2649 (1973).

[7] C. H. Palmer, R. O. Claus, and S. E. Fick, "Ultrasonic wave measurements differential interferometry," Applied Optics 16, 1369(1977).

APPENDIX D

Interferometric Optical Methods for the Characterization of Wideband Surface Particle Displacements

R. O. Claus and J. H. Cantrell, "Rayleigh Wave Detection by Wideband Differential Interferometry," Acoust. Soc. Am. Annual Meeting (Los Angeles, CA), Nov. 1980; J. Acoust. Soc. Am., 68, S108 (1980).

omit

Broadband optical interferometer for monitoring Rayleigh waves.

Richard O. Claus (Department of Electrical Engineering, Virginia Polytechnic Institute and State University, Blacksburg, VA 24061) and John H. Cantrell, Jr. (NASA Langley Research Center, Hampton, VA 23665)

A wideband differential interferometer has been developed to detect ultrasonic surface wave pulses. The interferometer combines the advantages of wideband Michelson techniques with those of similar narrowband differential methods used to measure CW ultrasonic waves [C. H. Palmer, J. Acoust. Soc. Am. 53, 948 (1973); D. P. Jablonowski, Appl. Opt. 17, 2064 (1978)]. In our system, two coherent light beams are focused on the surface supporting the pulsed waves. The reflected beams are combined interferometrically, filtered, and detected using a broadband optical receiver. Receiver output is proportional to the difference between the normal components of surface particle displacement at the location of the two beams. If an acoustic pulse arrives at one beam focus at time t_1 and at the other at $t_2 = t_1 + \Delta t$, output signal bandwidth during Δt is limited only by detector response. For $t > t_2$, bandwidth is determined by the differential acoustic sensitivity which may be adjusted by altering beam separation. Sensitivity calibration for a nominal 1 MHz bandwidth and measurements of pulses on a 0.3 cm thick 7070 pyrex plate are presented.

Technical Committee: Physical Acoustics

PACS number: 43.35.Pt

Telephone number: (804) 827-3418 (R. O. Claus)

Acoust. Soc. Am. National Meeting, Los Angeles, CA, November 1980.

P. S. Zerwekh and R. O. Claus, "Optical Detection of Pulsed Surface Particle Displacements," Proc. 1981 IEEE Region 3 Conf. (Huntsville, AL), April 1981.

OPTICAL DETECTION OF PULSED SURFACE PARTICLE DISPLACEMENTS

PAUL S. ZERWEKH and RICHARD O. CLAUS

Department of Electrical Engineering
Virginia Polytechnic Institute and State University
Blacksburg, VA 24061

Abstract

The detection of acoustic surface wave pulses by a wideband differential interferometric laser technique which is insensitive to low frequency noise is described. System bandwidth is determined by the relationship between acoustic wavelength and the variable spacing between two laser probe beams focused on the solid surface which supports the waves. Theoretical sensitivity to surface displacement amplitude is equal to, or better than, that of other elect optical techniques. Response to an ideal step function displacement is analyzed and experimental measurements of gated 2.5 MHz pulses generated on an aluminized pyrex plate are discussed. Potential application in the characterization of acoustic emission in composites is described.

Introduction

Interferometric optical techniques offer excellent sensitivity for the measurement of ultrasonic surface waves. Several modifications of the Michelson interferometer with independent sample and reference arms have been used for acoustic wave detection although the inherent pathlength sensitivity to ambient low frequency acoustical noise makes the Michelson design unsuitable in many applications [1,2]. Such low frequency acoustical vibrations may produce large changes in the optical pathlength of one arm resulting in large shifts in the output fringe pattern. The large shifts mask small amplitude high frequency signals while slowly changing the operating point and gain of the interferometer. For those applications in which the acoustical signals and acoustical noise exist in separate frequency bands, vibration effects may be minimized by controlling the length of the reference arm with a feedback signal derived from the detector output [3,4]. However, nonlinear stability criteria limit the effectiveness of such feedback systems.

By folding the arms of the Michelson interferometer so both sample and reference beams are parallel and reflect off the same surface, insensitivity to vibrations is greatly improved because induced low frequency changes in the optical path lengths of both beams are made nearly the same. Narrowband CW ultrasonic waves have been detected using such differential interferometric systems [5,6]. In this paper, the application of a similar technique to the detection of wideband acoustic surface wave pulses is reported.

Experiment

The basic optical system is shown in Fig. 1. Light from a 2 mW HeNe laser is divided into two parallel and slightly separated collimated beams of equal intensity by a fixed beamsplitter. The beams are partially transmitted by a second beamsplitter and focused to points separated by a distance d on the surface of the specimen. Upon reflection the beams are partially reflected by the second beamsplitter and superimposed to form a straight line interference pattern. This pattern is filtered using a stationary Ronchi ruling having the same spatial periodicity as the interference pattern. The transmitted light is focused on a wideband optical detector. Although half of the available light is lost by the second beamsplitter, this arrangement minimizes errors due to skewed reflections at the surface.

The interferometer is sensitive to differential changes in the optical pathlengths of the two beams which cause relative motions of the output fringe pattern with respect to the fixed spatial filter. To maximize sensitivity it is necessary to move the filter $\pm\frac{1}{4}$ periods from perfect alignment [6]. Sensitivity to initial filter position may be eliminated using a rotating filter-beamsplitter.

Results

Assume now that the differential pathlength changes are caused by an ultrasonic wave propagating in the $\hat{z}$ direction on the specimen surface. Assuming no variation in $\hat{x}$, we may express the normal component of particle displacement at the surface as

$$W(t) = 2A \sin(\omega_a t - Kz), \qquad (1)$$

where A is the peak displacement from equilibrium, ω_a the acoustic radian frequency, and K the acoustic propagation constant. System response to this wave is maximized if (1) one focus point coincides with a local surface displacement minimum when the other coincides with a maximum, and (2) $\vec{d} \parallel \hat{z}$. Thus, the required separation between the focus points, $d(=|\vec{d}|)$, is

$$d = (2n + 1)\lambda/2, \qquad (2)$$

IEEE Region 3 Conf. (Huntsville, AL), April, 1981.

where $n = (0, 1, 2, \ldots)$ and $\Lambda = 2\pi/K$ is the acoustic wavelength. For $\vec{d}$ and Λ constant, the system response decreases from this maximum if either Λ or the direction of K change. Response as a function of Λ may be calculated for different values of n in Eq. (2) and is shown in Fig. 2 for $n = 0$.[6] Plotted experimental data was measured for a probe beam spacing of 0.5 mm, approximately one half the wavelength of gated 2.5 MHz pulses generated on an aluminized pyrex plate. Variations in sensitivity as a function of K allow the direction of propagation of CW waves or repetitive pulsed signals of known frequency to be determined by rotating $\vec{d}$ for maximum output signal. Theoretical and measured sensitivity versus the angle θ between $\vec{K}$ and $\vec{d}$ is plotted for $n = 0$ in Fig. 3. Theoretical response data in both Fig. 2 and Fig. 3 were calculated assuming that the focused optical beam waist is small compared to the acoustic wavelength. A detected 2.5 MHz gated pulse signal is shown in Fig. 4.

Acknowledgements

The authors wish to acknowledge useful conversations with C. H. Palmer and J. H. Cantrell. This work was partially supported by NASA Grant No. NAG-1-68 and NSF Grant ECS-7925340.

References

[1] G. I. Stegeman, IEEE Trans. Sonics Ultrason. SU-23, 33 (1976).

[2] R. L. Whitman and A. Korpel, Appl. Opt. 8, 1567 (1969).

[3] H. A. Deferrari, R. A. Darby, and F. A. Andrews, J. Acoust. Soc. Am. 42, 982 (1967).

[4] C. H. Palmer and R. E. Green, Materials Evaluation 35, 197 (1977).

[5] C. H. Palmer, H. M. South, and T. H. Mak, Ultrasonics 11, 106 (1974).

[6] D. P. Jablonowski, Appl. Opt. 13, 2064 (1978).

Fig. 4. Optically detected 2.5 MHz gated pulse signal.

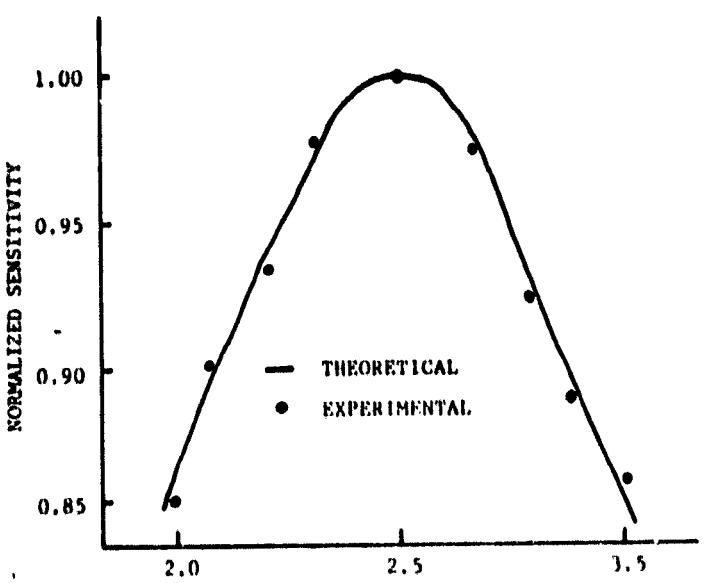

Fig. 2. Theoretical and experimental system sensitivity to acoustic wavelength.

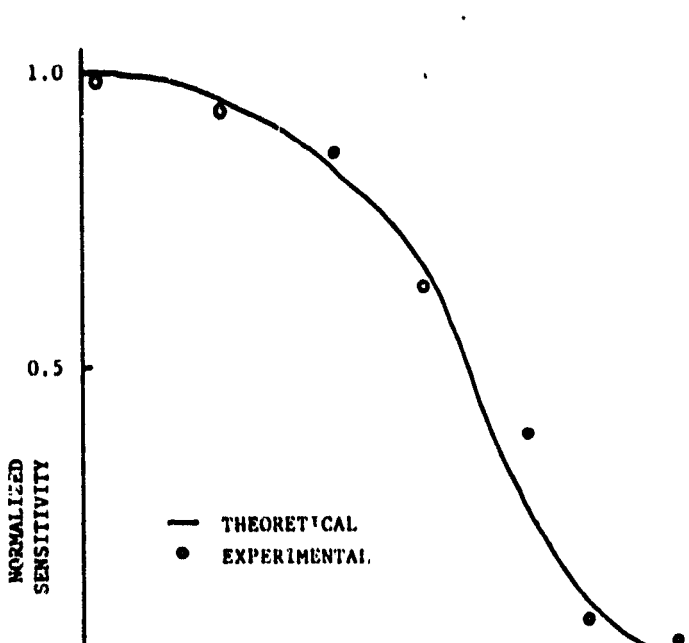

Fig. 3. Theoretical and experimental system sensitivity to the angle between the acoustic propagation vector and the vector distance between the two interferometric probe points.

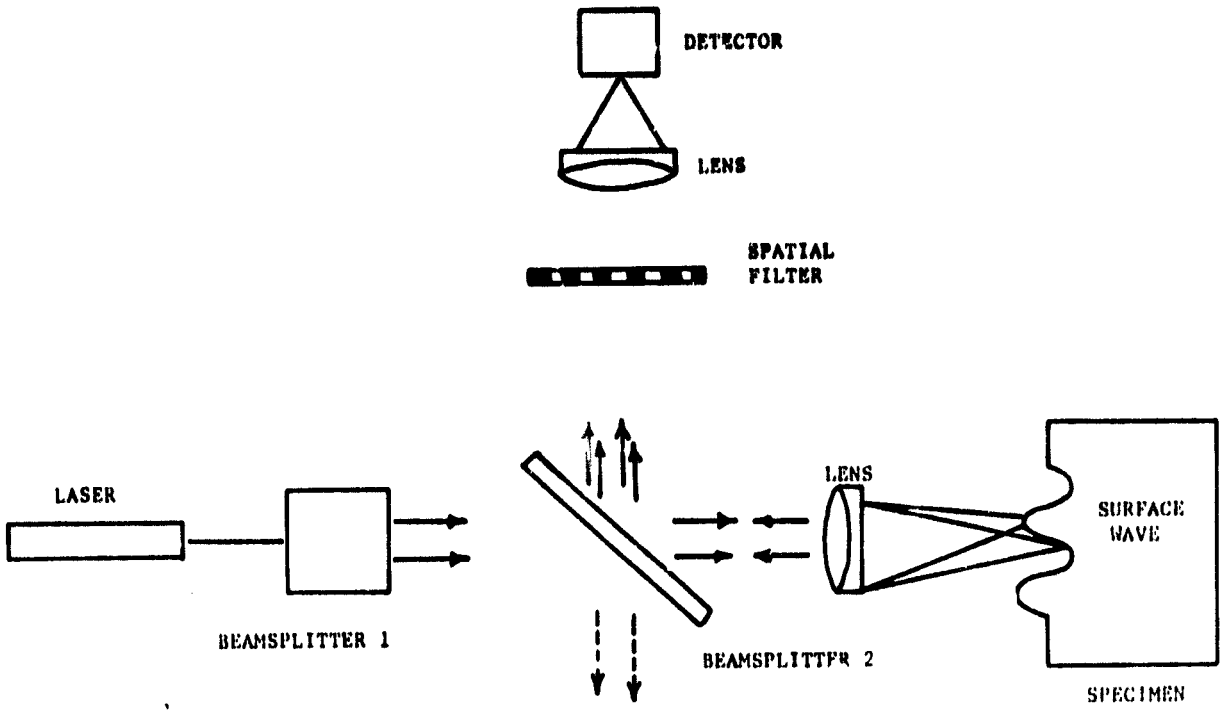

Fig. 1. Basic optical system for dual beam wideband optical interferometer. Separation distance between the probe points on the sample surface determines the acoustic bandwidth of the detection system. Additional bandwidth correction may be introduced electronically after the optical signal is demodulated. This system offers sensitivity similar to other interferometric acoustic detection techniques while providing the low frequency pathlength insensitivity not present in conventional Michelson system designs.

R. O. Claus and J. H. Cantrell, "Wideband Optical Measurements of Ultrasonic Pulses," Ultrasonics International 81 (Brighton, UK), June 1981.

WIDEBAND OPTICAL MEASUREMENTS OF ULTRASONIC PULSES

R. O. Claus
Department of Electrical Engineering, Virginia Polytechnic Institute and State University, Blacksburg, VA 24061 USA

J. H. Cantrell, Jr.
NASA Langley Research Center, Hampton, VA 23665 USA

Calibrated measurements of acoustic surface wave pulses by a wide bandwidth differential interferometric optical technique are described. By interrogating the interference pattern formed by superimposing two optical beams reflected from the surface at slightly separated points, an output signal proportional to instantaneous surface particle displacement is obtained. System bandwidth is determined by the relationship between the acoustic wavelength and the separation and size of the laser probe spots on the surface. In this paper, response to ideal propagating step function displacements is analyzed and measurements of gated pulses are described. Potential applications in the detection of acoustic emission are suggested.

INTRODUCTION

Acoustooptical techniques offer excellent sensitivity for the detection of ultrasonic waves. Interferometric systems in particular allow the simple localized measurement of the normal component of motion of a surface wave by using the surface that supports the wave as the reflecting surface in the sample arm of an optical interferometer. Such systems, however, are inherently wideband, for although the electronic bandwidth of the detection electronics may be limited to the ultrasonic range, low frequency specimen translations modulate the position of the operating point and thus the gain of the interferometer. In many practical systems the amplitudes of low frequency specimen motions produced by mechanical vibrational noise are larger than the peak surface wave amplitudes to be detected and changes in the operating point position do not permit continuous system calibration.

Several methods may be used to obtain proper calibration. First, the low frequency surface motion component may be detected separately and electronically fedback in a simple control loop to a fast transducer which changes the optical phase in the reference arm of the interferometer [1]. This effectively cancels the low frequency effect at the output but may generate harmonics in the output signal and does not allow unconditional stability [2]. Wideband differential interferometry is an alternative calibration technique and will be described below.

WIDEBAND DIFFERENTIAL INTERFEROMETRY

By aligning the two arms of a Michelson interferometer parallel so both sample and reference beams reflect off the same surface, sensitivity to low frequency waves is low because the low frequency changes in the difference in optical path length between the two beams are small. Measurements of CW surface, interface, and bulk waves obtained using this differential interferometric principle have been reported by several authors [3-5].

(a) Wideband differential interferometric system

The basic optical system is shown in Figure 1. Collimated coherent light from the laser at left is divided into two beams of approximately the same intensity and angled slightly with respect to each other. The two beams are focused to two points separated by a distance ΔX on the surface as shown in Figure 2. Light reflected from the surface at these points is deviated by a beamsplitter and superimposed to form straight line interference fringes. The fringes are spatially filtered using a binary transmission grating (Ronchi ruling) having a periodicity equal to that of the fringe spacing. Light transmitted by the grating is optically detected to produce an electronic signal with an instantaneous amplitude proportional to that of the surface wave on the specimen.

(b) Theory

Assume that the surface displacement caused by an acoustic wave may be expressed as

$$A(x, t) = 2A_0 \sin (\omega_a t - Kx), \tag{1}$$

where A_0 is the peak displacement amplitude, ω_a is the acoustic radian frequency, and K the acoustic propagation constant. System response to this signal is maximized if

$$\Delta\vec{x} \| \hat{x}, \tag{2}$$

and

$$\Delta x = (2n + 1)\, \Lambda/2, \tag{3}$$

where n is a non-negative integer and $\Lambda = 2\pi/K$ is the acoustic wavelength. For Δx and Λ constant, the system sensitivity changes if either Λ or the direction of $\vec{K}$ vary; these effects have been calculated and measured [6]. Although maximum sensitivity is obtained if (2) and (3) are satisfied, acoustic waves may still be detected with lower sensitivity if they are not. From (3), a 3dB acoustic bandwidth response to Δx is obtained for a two decade variation in Λ[2,7].

(c) Pulsed acoustic wave response

Response to an acoustic wave pulse differs from that obtained for a CW signal. If (2) is satisfied, a propagating step displacement arrives at one optical focus point before the other. During the time $t = \Delta x/v$, where v is the wave velocity, interferometric system sensitivity is unlimited in frequency because the position of only one beam is acoustically modulated. In this case, low frequency vibrations may still be neglected, however, due to the differential property of the system. Typical pulsed wave response is shown in Figure 3.

(d) Dual differential interferometry

If two pairs of optical beams such as those shown in Figure 1 are focused on the surface and oriented so one pair is parallel to $\hat{x}$ as in Figure 2 and one pair is parallel to $\hat{y}$, both $\hat{x}$ and $\hat{y}$ components of the wave may be determined [8]. Frequency response in this case is again wideband with low frequency isolation. By recording both x and y channels of directional wave information and combining them algebraically, wave amplitude and direction of propagation may be determined and the complete time evolution of ultrasonic frequency displacements in the $\Lambda/2\sqrt{2} \times \Lambda/2\sqrt{2}$ area containing the four focus points may be calculated [9]. A complete analysis of generalized dual differential system response and the measurement of broadband ultrasonic waves generated by pulsed transducers and acoustic emission events is in preparation.

CONCLUSION

Wideband differential interferometry may be used to make calibrated measurements of wideband CW and pulsed surface acoustic wave amplitudes while avoiding low frequency specimen translations. Uncompensated acoustic bandwidths of two frequency decades have been obtained. By superimposing two differential optical beam patterns oriented in orthogonal directions on the specimen surface, the localized time evolution of ultrasonic wave amplitude and direction may be determined.

ACKNOWLEDGEMENTS

This work has been partially supported by National Science Foundation Grant ECS-79-25340 and NASA Grant NAG-1-68. The authors wish to thank T. M. Turner, C. H. Palmer, and R. A. Kline for their helpful discussions.

REFERENCES

1. Kline, R. A., Green, R. E. and Palmer, C. H. "A comparison of optically and piezoelectrically sensed acoustic emission signals". J. Acoust. Soc. Am., Vol. 64 (1978), pp. 1633-1639.

2. Claus, R. O. and Cantrell, J. H. "Rayleigh wave detection by wideband differential interferometry". J. Acoust. Soc. Am., Vol. 68 (1980), p. S108.

3. Jablonowski, D. P. "Simple interferometer for monitoring Rayleigh waves." Appl. Opt., Vol. 17 (1978), pp. 2064-2070.

4. Stegeman, G. I. "Optical probing of surface waves and surface wave devices." IEEE Trans. Sonics Ultrason., Vol. SU-23 (1976), pp. 33-63.

5. Palmer, C. H., Claus, R. O. and Fick, S. E. "Ultrasonic wave measurement by differential interferometry." Appl. Opt., Vol. 16 (1977), pp. 1849-1856.

6. Claus, R. O. and Cantrell, J. H. "Optical probing of pulsed acoustic surface waves using wideband differential interferometry," in press.

7. Zerwekh, P. S. and Claus, R. O. "Optical detection of pulsed surface particle displacements." Proc. 1981 IEEE Region 3 Conf. (Huntsville, AL).

8. Turner, T. M. and Claus, R. O., "Dual differential interferometer for measurements of broadband surface acoustic waves," submitted to 1981 IEEE Ultrason. Symp. (Chicago, IL).

9. Turner, T. M. M.S. thesis, Virginia Polytechnic Institute and State University, 1981.

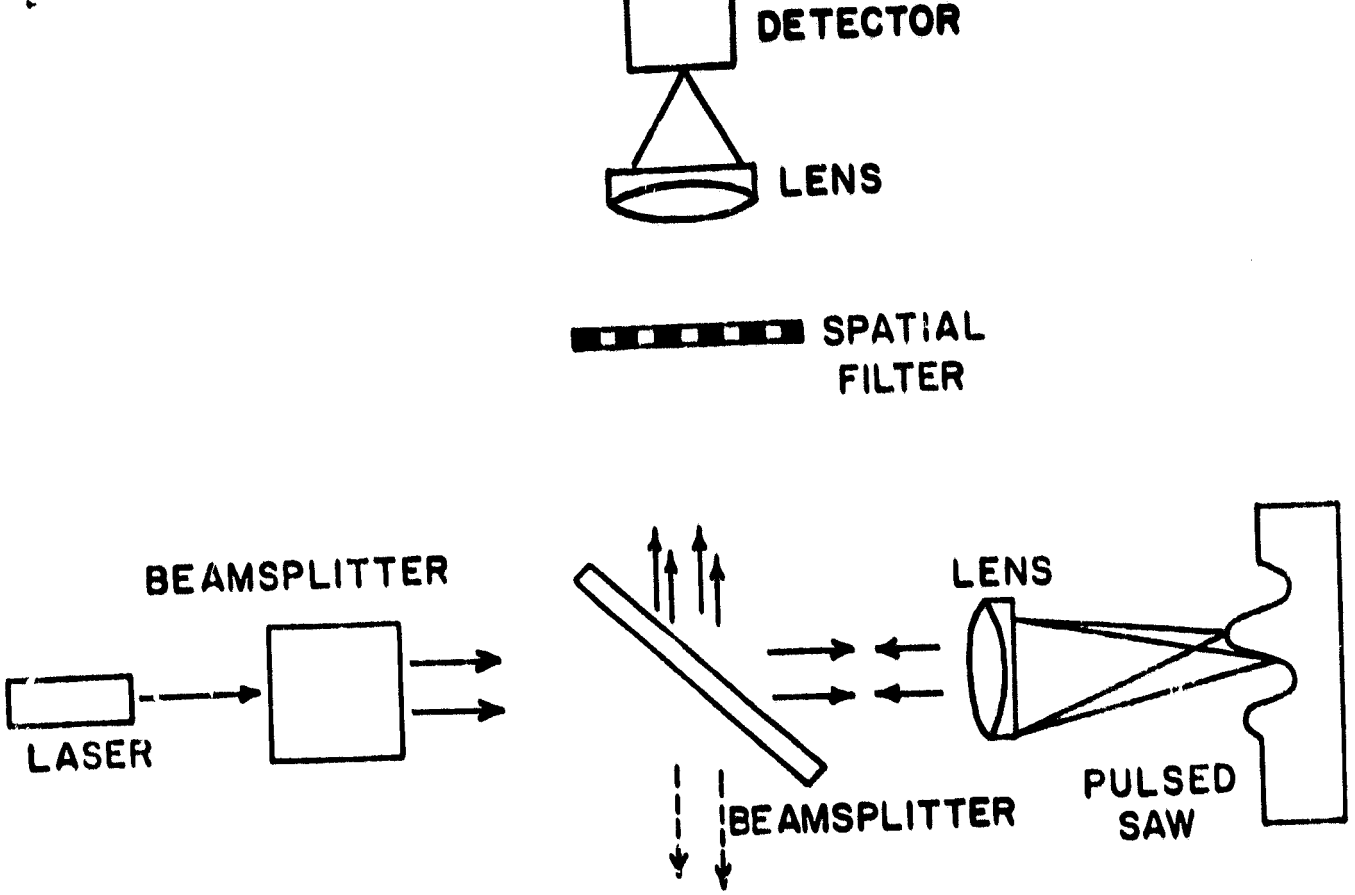

Fig. 1. Basic wideband differential interferometer optical system. Spatial filter is binary transmission grating with equal transparent and opaque regions.

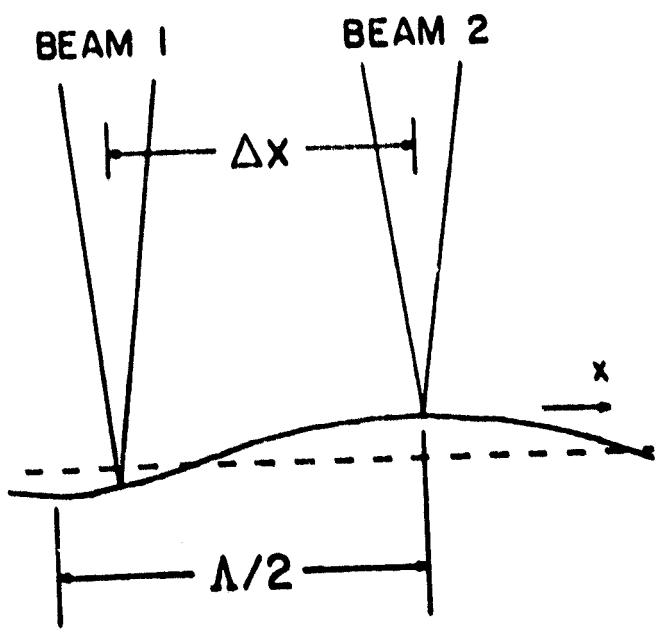

Fig. 2. Relationship between focus spot separation and surface acoustic wavelength.

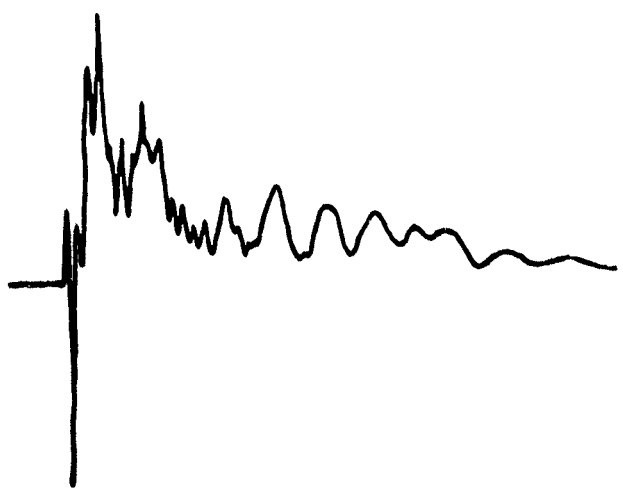

Fig. 3. Wideband differential optical recording of acoustic emission pulse.

T. M. Turner and R. O. Claus, "Dual Differential Interferometer for Measurements of Broadband Surface Acoustic Waves," Proc. 1981 IEEE Ultrasonics Symposium (Chicago, IL), Oct. 1981.

D/2

N82-11133

DUAL DIFFERENTIAL INTERFEROMETER FOR MEASUREMENTS OF BROADBAND SURFACE ACOUSTIC WAVES

TYSON M. TURNER and RICHARD O. CLAUS

Department of Electrical Engineering
Virginia Polytechnic Institute & State University
Blacksburg, VA 24061

Abstract

A simple dual interferometer which uses two pairs of orthogonally polarized optical beams to measure both the amplitude and direction of propagation of broadband ultrasonic surface waves is described. Each pair of focused laser probe beams is used in a separate wideband differential interferometer to independently detect the component of surface wave motion along one direction on the surface. By combining the two output signals corresponding to both components, the two-dimensional surface profile and its variation as a function of time may be determined. Although the system has an optically adjustable -3dB acoustic bandwidth of more than two decades (eg. 30kHz to 3MHz for acoustic emission measurements) and can detect peak displacements in the sub-Angstrom range, it is insensitive to low frequency specimen translations. Potential applications in nondestructive evaluation are described.

1. Introduction

The development of robust methods for the detection and analysis of surface acoustic waves (SAW) is of continuing importance due to increased interest in SAW applications in nondestructive evaluation, materials evaluation, and signal processing devices. A wide variety of practical SAW sensing and analysis techniques exist including a number of optical methods which employ different types of optical surface imaging. One such method is the differential interferometric system introduced by Palmer for measurements of SAW on solids [1] and later adapted to the detection of dilatational and shear waves in solids [2] and interface waves at the boundaries between transparent media [3]. This paper describes the extension of this type of acoustooptic sensing system to allow the simultaneous detection of multidirectional SAW amplitude components as well as the orientation of propagation.

The differential interferometer exhibits several characteristics which are useful for SAW measurements. First, the output signal is proportional to the SAW amplitude, phase information may be determined and the system can be easily calibrated [2]. Second, absolute system sensitivity is greater than or equal to other optical or mechanical techniques. The acoustic bandwidth may be varied to allow selectivity in SAW detection [4]. Finally, the interferometer is tolerant of optical misalignment, surface irregularities, and low frequency specimen translations of the type associated with room vibrations or mechanical specimen loading. The unique combination of these properties insures reliable, reproducible SAW measurements even in adverse testing environments.

2. Specimen Surface Profile

The two beam system does have limitations. The modulation of the two focused spots is dependent not only on SAW amplitude but also on the angular orientation of SAW propagation with respect to a chord passing through the spots. The detected SAW amplitude is thus the amplitude component of surface wave motion along the direction parallel to this chord as shown in Figure 1. This component is given by $A_m = A_s \cos\theta$ where A_m is the modulating amplitude and A_s is the SAW amplitude. Accordingly, detected signals corresponding to SAWs of unequal amplitude and different angular orientations appear identical at the output of the two-beam interferometer. In fact, a SAW propagating at a 90° incidence to the reference chord would ideally generate no output signal.

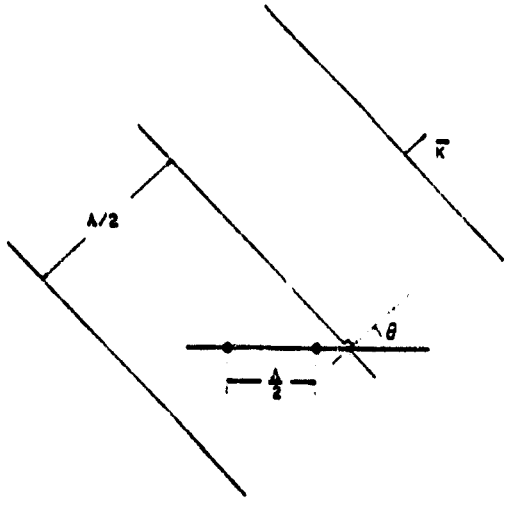

Figure 1. Angular Sensitivity of a Differential Interferometer

preprint 1981 IEEE Ultrasonics Symposium, (Chicago, IL).

To overcome these limitations, two approaches can be attempted. One is to rotate the specimen for maximum signal modulation. For randomly generated pulsed SAWs, however, rotation is an impractical solution. The other approach is to incorporate a second differential interferometer to detect the orthogonal motion component of a SAW propagating at an arbitrary angle with respect to the direction of maximum sensitivity of the first interferometer. The resulting two simultaneous outputs may then be correlated to determine the SAW amplitude and angle of propagation with respect to a surface reference. By positioning the interferometers in the crosshair configuration shown in Figure 2, the relationship between the true amplitude and that component referenced to the zero angle is a cosine function. This is $A_B = A_0\cos\theta$ where A_B is the modulation amplitude of the B interferometer focus points. The amplitude of the orthogonal component is related by $A_A = |A_0\sin\theta|$ where A_A is the amplitude component parallel to the A interferometer. SAW amplitude as well as angular orientation of propagation can thus be uniquely determined. Unequal placement from the center point distinguishes one 45° plane from the other. Surface profile information as conceptualized, however, does not indicate the direction of propagation of a measured SAW. The determination of this propagation direction can be made by either adding a third interferometer displaced slightly from the previous two or by skewing the two pairs of beam spots to obtain a third variable. This latter method, however, is not useful if SAW are normally incident to the orientation of either focus pair.

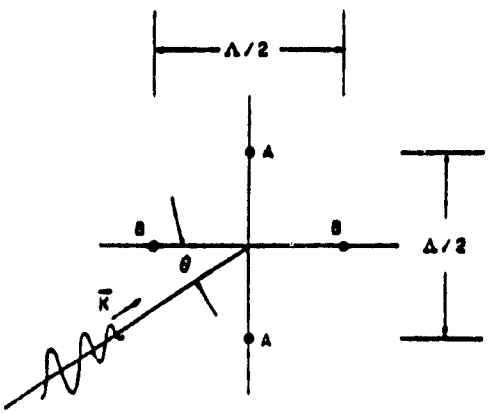

Figure 2. Dual Interferometer Focus Point Geometry

3. Dual Interferometer Discription

The separation of four beams into two non-interacting pairs is accomplished by orthogonally polarizing the pairs as shown in Figure 3. Since orthogonal polarizations can be separated by optical filtering, both pairs are transmitted through common optics and later separated for non-interactive measurement. A polarizing beamsplitter located before the detectors is used here to separate the polarizations.

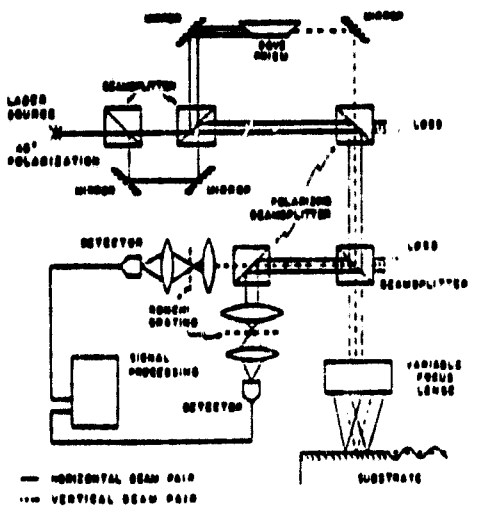

Figure 3. Optical system for Dual Dual-Differential Interferometer

The dual two-beam interferometer system first generates two pairs of parallel beams each having a forty-five degree polarization angle with respect to the horizontal as shown in Figure 4. The polarization angle of the incident light is obtained by rotating a linearly polarized HeNe laser appropriately. As shown, the two pairs of beams are split at right angles to each other and a dove prism mounted at a forty-five degree angle to the horizontal is inserted in one beam to rotate one pair so that its axis is oriented normally with respect to that of the other. Both pairs are then aligned and positioned by a polarizing beamsplitter. This alignment also results in the beams being polarized by pairs and of equal intensity. The beams propagate to the specimen surface through another beamsplitter orientated so the reflected, modulated beams are reflected toward the detectors. A second polarizing beamsplitter separates the reflected pairs and each pair is individually spatially filtered and detected.

Both interferometer beam pairs may be expanded and refocused onto the surface by a variable focus lens system. With this system, the separation of the focused spots can be varied. Beam spot separation is more easily manipulated, however, by separating pairs appropriately at the point of generation at the front of the system and is accomplished by a translation of the mirror pair adjacent to the pair of beamsplitters.

4. System Limitations

Although the dual two-beam differential interferometer does not have any disadvantages in comparison to the single interferometer, some of the single interferometer limitations remain.

Two such limitations are the errors associated with the detection of signals from SAW edge effect regions and high frequency attenuation. As shown in Figure 4, SAW edge effects can create an amplitude differential over a distance parallel to the wavefront causing erroneous signal generation. This would be particularly evident when the SAW wavefront is parallel incident to a spot pair as shown. High frequency SAW attenuation is similar in its effects. Over a short distance the amplitude variation due to attenuation causes loss of signal modulation and therefore erroneous amplitude component computations as shown in Figure 5.

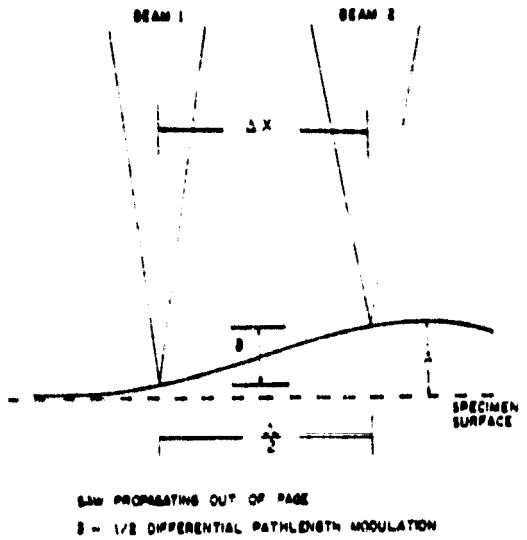

Figure 4. Edge Effect Modulation

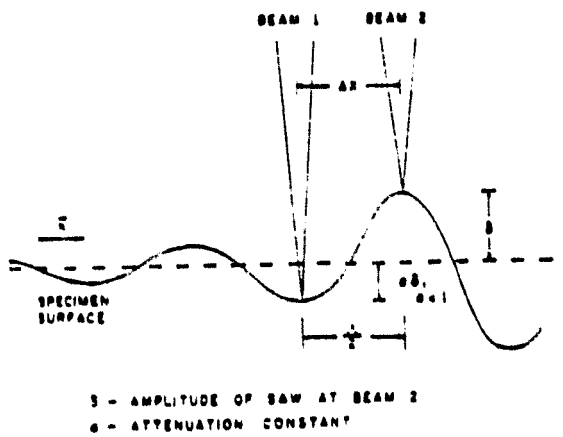

Figure 5. Loss of Modulation Due to Attenuation

5. Experiment

Confirmation of the angular relationships in amplitude for the dual differential interferometer was made by rotating a pulsed 2.25 MHz wedge transducer around the focus spot pairs. The interferometric signal was detected by a broadband optical detector and the resulting rf output signal filtered by a 2.25 MHz bandpass filter. The received signal was calibrated for detected SAW amplitude following the procedure outlined by Palmer, Claus and Fick [2]. By combining data from both output signal channels, a calibrated average of point displacements over the spot pattern may be obtained. Typical single-polarization wave amplitude system output data is shown in Figure 6. A complete description of system performance is in preparation.

6. Conclusion

An improvement of the SAW differential interferometric technique has been developed. The dual dual-differential interferometer has all the advantages of the differential interferometer but is not dependent on the incident angle of SAW. The dual dual-differential interferometer is well suited for the measurement of transient SAW in nondestructive testing and acoustic emission applications.

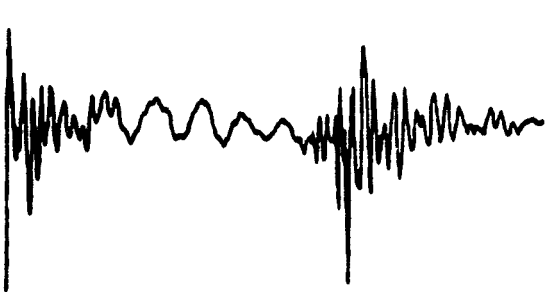

Figure 6. Interferometer Output for Pulsed SAW

Acknowledgements

Part of this research was supported by NASA Grant NAG-1-68 and National Science Foundation Grant ECS-79-25340. The authors thank C. H. Palmer and J. H. Cantrell for their helpful discussions.

References

[1] C. H. Palmer, "Ultrasonic surface wave detection by optical interferometry," J. Acoust. Soc. Am. 53, 948 (1973).

[2] C. H. Palmer, R. O. Claus, and S. E. Fick, "Ultrasonic wave measurements by differential interferometry," Appl. Opt. 16, 1849 (1977).

[3] R. O. Claus and C. H. Palmer, "Optical measurements of ultrasonic waves between bonded solids," IEEE Trans. Sonics Ultrason. SU-27, 97 (1980).

[4] D. P. Jablonowski, "Simple interferometer for monitoring Rayleigh waves," Appl. Opt. 17, 2064 (1978).

R. O. Claus and J. H. Cantrell, "Optical Probing of Pulsed Acoustic Surface Waves Using Wideband Differential Interferometry," Acoustics Letters, in press.

OMIT TO END

OPTICAL PROBING OF PULSED ACOUSTIC SURFACE WAVES USING WIDEBAND DIFFERENTIAL INTERFEROMETRY

Richard O. Claus[1] * and John H. Cantrell Jr[2]
[1] *Department of Electrical Engineering, Virginia Polytechnic Institute and State University, Blacksburg, Virginia 24061, USA.*
[2] *NASA-Langley Research Center, Hampton, Virginia 23665, USA.*

Abstract

Detection of acoustic surface wave pulses by a wideband differential interferometric optical technique which is insensitive to low frequency acoustical noise is described. System bandwidth is determined by the relationship between acoustical wavelength and the adjustable spacing between two optical probing beams focused on the surface which supports the waves. Sensitivity to surface displacement amplitude is equal to, or better than, that of other techniques.

Interferometric optical techniques offer excellent sensitivity for the measurement of ultrasonic surface waves. Several modifications of the Michelson interferometer with independent sample and reference arms have been used for acoustic wave detection [1] although the inherent pathlength sensitivity to ambient low frequency acoustical noise makes the Michelson design unsuitable in many applications [2]. Such low frequency acoustical vibrations may produce large changes in the optical pathlength of one arm, resulting in large shifts in the output fringe pattern. The large shifts mask small amplitude high frequency signals while slowly changing the operating point and gain of the interferometer. For those applications in which the acoustical signals and acoustical noise exist in separate frequency bands, vibration effects may be minimized by controlling the length of the reference arm with a feedback signal derived from the detector output [3, 4]. However, nonlinear stability criteria limit the effectiveness of such feedback systems.

By folding the arms of the Michelson interferometer so both sample and reference beams are parallel and reflect off the same surface, insensitivity to vibrations is greatly improved because induced low frequency changes in the optical path lengths of both beams are made nearly the same. Narrowband CW ultrasonic waves have been detected using such differential interferometric systems [5, 6]. In this paper, the application of a similar technique to the detection of wideband acoustic surface wave pulses is reported.

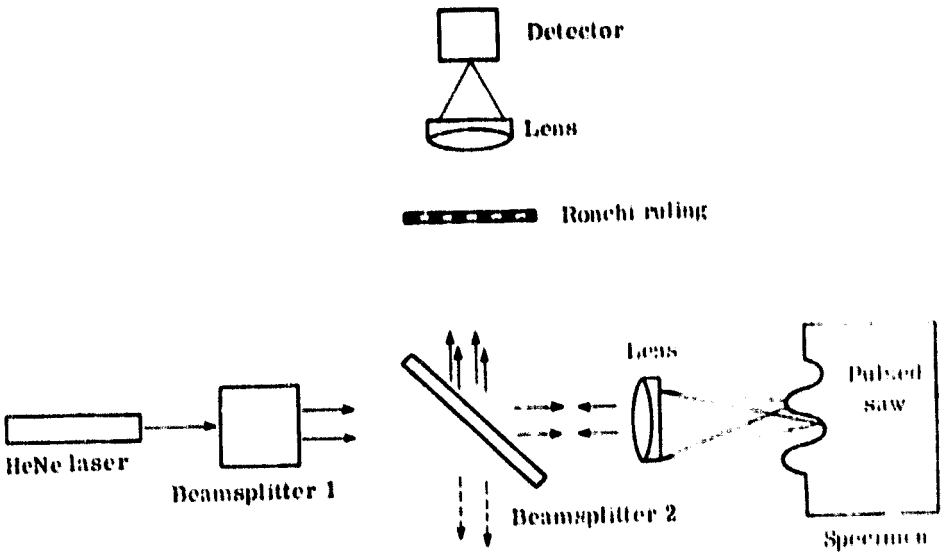

Figure 1. Differential interferometric system.

*Visiting Scientist, NASA-Langley Research Center, Hampton, VA 23665, USA

The basic optical system is shown in Figure 1. Light from a 2mW HeNe laser is divided into two parallel and slightly separated collimated beams of equal intensity by a fixed beamsplitter. The beams are partially transmitted by a second beamsplitter and focused to points separated by a distance d on the surface of the specimen. Upon reflection the beams are partially reflected by the second beamsplitter and superimposed to form a straight line interference pattern. This pattern is filtered using a stationary Ronchi ruling having the same spatial periodicity as the interference pattern. The transmitted light is focused on a wideband optical detector. Although half of the available light is lost by the second beamsplitter, this arrangement minimizes errors due to skewed reflections at the surface.

The interferometer is sensitive to differential changes in the optical pathlengths of the two beams which cause relative motions of the output fringe pattern with respect to the fixed spatial filter. To maximize sensitivity it is necessary to move the filter ¼ periods from perfect alignment [6]. Sensitivity to initial filter position may be eliminated using a rotating filter-beamsplitter [6].

Assume now that the differential pathlength changes are caused by an ultrasonic wave propagating in the $\hat{z}$ direction on the specimen surface. Assuming no variation in $\hat{x}$, we may express the normal component of particle displacement at the surface as

$$W(t) = 2A \sin(\omega_a t - Kz), \tag{1}$$

where A is the peak displacement from equilibrium, ω_a the acoustic radian frequency, and K the acoustic propagation constant. System response to this wave is maximized if (1) one focus point coincides with a local surface displacement minimum when the other coincides with a maximum, and (2) $\vec{d}' \parallel \hat{z}$. Thus, the required separation between the focus points, $d(=|\vec{d}'|)$, is

$$d = (2n + 1)\Lambda/2, \tag{2}$$

where $n = \{0, 1, 2, \ldots\}$ and $\Lambda = 2\pi/K$ is the acoustic wavelength. For d' and A constant, the system response decreases from this maximum if either A or the direction of K change. Response as a function of A may be calculated for different values of n in Eq. (2) and is shown in Figure 2 for n = 0 [6]. Plotted experimental data was measured for a probe

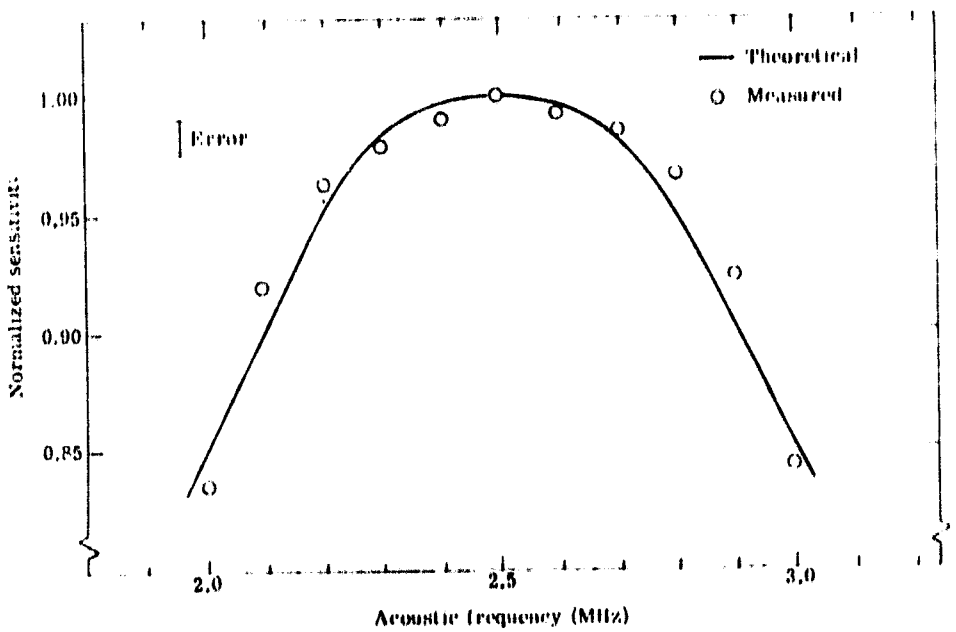

Figure 2. Interferometric frequency sensitivity. Theoretical and measured data for n = 0 in Eq. (2).

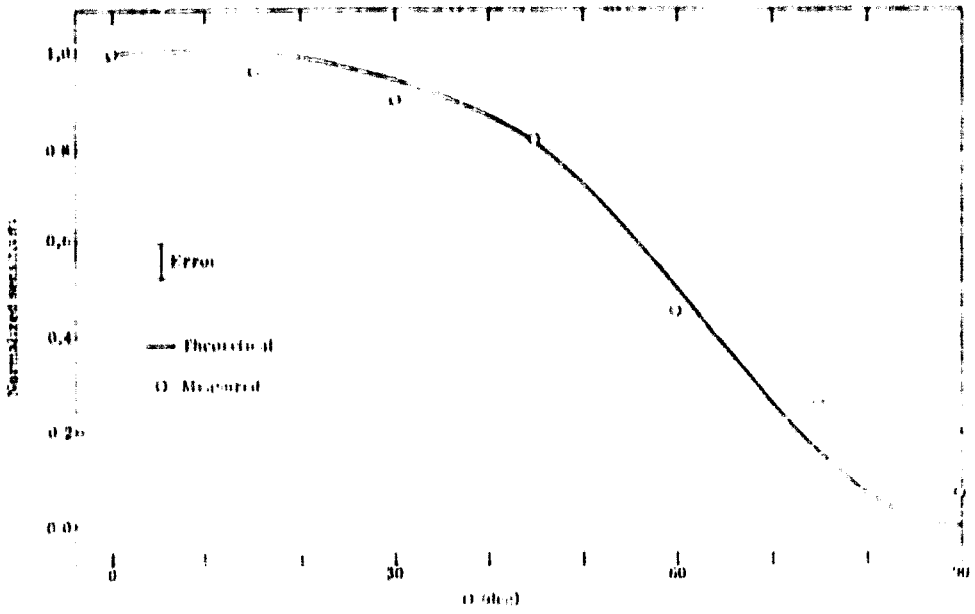

Figure 3. Interferometer response versus angle θ between d' and K' for 2.5MHz gated pulses and n = 0 in Eq. (2).

beam spacing of 0.5mm, approximately one half the wavelength of gated 2.5 MHz pulses generated on an aluminized pyrex plate. Variations in sensitivity as a function of K allow the direction of propagation of CW waves or repetitive pulsed signals of known frequency to be determined by rotating d for maximum output signal. Theoretical and measured sensitivity versus the angle θ between K' and d' is plotted for n = 0 in Figure 3. Theoretical response data in both Figure 2 and Figure 3 were calculated assuming that the focused optical beam waist is small compared to the acoustic wavelength. A detected 2.5 MHz gated pulse signal is shown in Figure 4.

Figure 4. Gated 2.5MHz surface wave pulses detected by wideband differential interferometry.

Response to the first half cycle of a gated acoustic wave pulse differs from the CW response. Let the time at which the leading edge of the pulse arrives at the location of one focus point be $t = t_1$. During the time interval $t_1 < t < t_1 + d/v = t_2$, where v is the velocity of the wave and $\theta = 0$, the output signal is only a function of the displacement at the first point independent of acoustic signal frequency. At $t = t_2$, the leading edge of the pulse arrives at the second point, and for $t > t_2$ response is identical to that for the CW case.

Now consider the case of an acoustic pulse travelling in an arbitrary direction and containing a wide bandwidth of frequency components. Such a pulse could be generated, for example, by acoustic emission in solids. During the interval $t_1 < t < t_1 + d(\cos\theta)/v = t_2$ the output signal is proportional to the instantaneous point displacement caused by the

wideband pulse. For $t > t_2$, frequency response is again limited by the differential gain function determined by n in Eq. (2). The center frequency of the differential passband may effectively be shifted by varying θ. A complete analysis of the generalized system response and the measurement of pulsed broadband ultrasonic signals is in preparation.

Acknowledgment

The authors wish to acknowledge useful conversations with C. H. Palmer and H. L. Ringermacher

References

[1] Stegeman, G.I., *IEEE Trans. Sonics. Ultrason.*, **SU-23**, 33 (1976).

[2] Whitman, R. L. and Korpel, A., *Appl. Opt.*, **8**, 1567 (1969).

[3] Deferrari, H. A., Darby, R. A. and Andrews, F. A., *J. Acoust. Soc. Am.*, **42**, 982 (1967).

[4] Palmer, C. H. and Green, R. E., *Materials Evaluation*, **35**, 107 (1977).

[5] Palmer, C. H., South, H. M. and Mak, T. H., *Ultrasonics*, **11**, 106 (1974).

[6] Jablonoski, D. P., *Appl. Opt.*, **13**, 2064 (1978).

(Received 1 July 1981)